

DEVELOPING MICROCOMPOSITE PHARMACEUTICAL MATERIALS USING  
DENSE GAS TECHNIQUE

by

KE WU

A Dissertation submitted to the  
Graduate School-New Brunswick  
Rutgers, The State University of New Jersey  
in partial fulfillment of the requirements

for the degree of

Doctor of Philosophy

Graduate Program in Chemistry and Chemical Biology

written under the direction of

Professor Jing Li

and approved by

---

---

---

---

New Brunswick, New Jersey

October, 2008

©2008

Ke Wu

ALL RIGHTS RESERVED

## ABSTRACT OF THE DISSERTATION

Developing Microcomposite Pharmaceutical Materials Using Dense Gas Technique

By KE WU

Dissertation Director:

Professor Jing Li

Micronized particulate pharmaceutical materials prepared using dense gas antisolvent precipitation is of great advantage over traditional micronization techniques in terms of particle size distribution and reproducibility. Our work shows that spherical particles with different degrees of agglomeration can be produced under mild operating conditions. These results stimulate further studies on the structure-property relationship of the precipitates.

Preliminarily, we performed dense gas antisolvent precipitation on a number of polymers of pharmaceutical interest, including poly(DTE carbonate) and polyvinylpyrrolidone (PVP) with different molecular weights. We explored the effect of experimental conditions on the particle size and morphology. For poly (desamino tyrosyl-tyrosine alkyl ester carbonate) [poly(DTE carbonate)], its microparticles with controlled size could be applied in the field of tissue engineering, which could facilitate better exertion of the biochemical functions of this biodegradable polymer. On the other hand, PVPs are common excipients widely used in pharmaceutical formulation development. Physicochemical properties of both types of polymers

provide flexibility of their application. Their precipitation by dense gas as antisolvent provided informative data for subsequent experiment of forming solid dispersions.

Solid dispersions were prepared by precipitation of PVP with several pharmaceutical compounds using dense gas carbon dioxide as antisolvent. We focused on the morphology and particle size control of the products for the first two model drugs, prednisolone and its acetate salt, and then we prepared solid dispersions of a nonsteroidal anti-inflammatory drug, piroxicam. Microcrystals or microspheres were formed where the drug was amorphaously dispersed in the polymeric matrix, with drug loadings dependent on initial drug-polymer weight ratios. The existence of interaction between the drug and polymer was confirmed through characterization of their physicochemical properties. The dissolution profiles of solid dispersions showed significant improvement in the dissolution rate of piroxicam compared with their corresponding physical mixtures and plain drug. These results manifest the great potential of this dense gas technique in improving bioavailability of water-insoluble pharmaceutical substances.

## ACKNOWLEDGEMENT

I would like to express my sincere gratitude to Prof. Jing Li for accepting me as a Ph.D. student in her group, and for her continuous guidance, advice, and support during the course of my research.

I am sincerely grateful to my committee members, Dr. Gene Hall, Dr. Ralf Warmuth, and Dr. Wayne Wang for serving on my thesis committee with their expertise of science. I'm also grateful to Dr. Laurence Romsted, who served as a member of my proposal defense committee two years ago.

I am grateful to Dr. David Olson for his help during the course of my study. His assistance in building apparatus and in my daily experiments has significantly improved my work skill and I have learned a great deal from him about mechanical and engineering concepts.

I would like to thank Dr. Joachim Kohn for providing poly(DTE carbonate) samples for part of this study.

Many thanks to Mr. Valentin Starovoytov at the Department of Cell Biology and Neuroscience for his continuous assistance in providing access to the SEM facilities.

I am also thankful to the staffs at the machine shop in the Department of Physics and Astronomy, whose expertise was very helpful in facilitating the maintenance of our apparatus.

I am very grateful to Dr. Denita Winstead for allowing me to carry out part of my thesis work at the research facilities of Johnson and Johnson Pharm. Res. and Development, L.L.C. at Raritan, NJ. I also want to express my special thanks to the scientists there with whom I had interacted.

Many thanks to all former and current group members who made my time at Dr. Li's group such a great experience.

I am deeply grateful to Prof. Jiacheng Zhong for his advice during my pursuit of Master's degree at Wuhan University. I will never forget the years I spent in his group with our group members.

I would like to thank my parents, especially my mother, Ms. Derong Zhang, who has made my life and education possible throughout these past almost thirty years.

Finally, I am grateful to Xiaojie Huang, my endeared wife, for her constant encouragement and support over the past years of our marriage.

## TABLE OF CONTENTS

ABSTRACT OF THE DISSERTATION .....	ii
ACKNOWLEDGEMENT .....	iv
TABLE OF CONTENTS.....	vi
LIST OF TABLES.....	x
LIST OF ILLUSTRATIONS.....	xi
LIST OF ABBREVIATIONS.....	xvii
LIST OF SYMBOLS .....	xx
CHAPTER 1 INTRODUCTION .....	1
1.1 Background.....	1
1.1.1 Micronization (Particle size reduction).....	2
1.1.2 Composite particles.....	4
1.2 Dense Gas Technique .....	6
1.2.1 Properties of dense gas carbon dioxide.....	9
1.2.2 Dense gas as solvent: Rapid Expansion of Supercritical Solutions (RESS) .....	12
1.2.3 Dense gas as solute: Particles from Gas-Saturated Solutions (PGSS).....	14
1.2.4 Dense gas as antisolvent .....	15
1.3 Particle Design Using Dense Gas Antisolvent Technique.....	18
1.4 Fundamentals of Dense Gas Antisolvent Technique.....	18
1.4.1 Thermodynamics.....	19
1.4.2 Mass transfer.....	20
1.4.3 Hydrodynamics .....	20
1.5 Motivation and Objective .....	21
CHAPTER 2 EXPERIMENTALS .....	24

2.1 Dense Gas Antisolvent Precipitation .....	24
2.1.1 Experimental setup.....	24
2.1.2 Experimental procedure of dense gas antisolvent precipitation .....	26
2.2 Spray Drying.....	26
2.3 Preparation of Physical Mixture .....	27
2.4 Morphological and Dimensional Characterization .....	27
2.4.1 Scanning electron microscope (SEM) experiment .....	27
2.4.2 Image analysis.....	27
2.4.3 Laser diffraction particle size analysis.....	27
2.5 Physicochemical Characterization .....	28
2.5.1 Powder x-ray diffraction (PXRD).....	28
2.5.2 Fourier-transform infrared spectroscopy (FT-IR).....	29
2.5.3 Differential scanning calorimetry (DSC).....	29
2.6 <i>In Vitro</i> Dissolution.....	30
2.6.1 Assay of drug loading .....	30
2.6.2 Dissolution studies .....	30
2.7 Preliminary Experiments on Micronization of Polyvinylpyrrolidone (PVP) ....	31
2.7.1 Effect of temperature .....	31
2.7.2 Effect of pressure .....	33
2.7.3 Effect of concentration.....	34
2.7.4 Effect of molecular weight.....	34
2.8 Summary of preliminary study .....	37
CHAPTER 3 PRECIPITATION OF A BIODEGRADABLE POLYMER USING	
DENSE GAS CARBON DIOXIDE AS ANTISOLVENT .....	38
3.1 Introduction.....	38

3.2 Materials .....	40
3.3 Results and Discussion .....	40
3.3.1 Effects of pressure on the particle size .....	42
3.3.2 Effects of temperature on the particle size.....	42
3.3.3 Effects of solution concentration and the solution flow rate. ....	44
3.3.4 Physicochemical properties of the DGA-processed polymer .....	46
3.4 Conclusions.....	46
CHAPTER 4 PREPARATION OF MICROCOMPOSITES OF PREDNISOLONE	
PREPARED WITH CONTROLLED DIMENSIONS.....	48
4.1 Introduction.....	48
4.2 Materials .....	50
4.3 Results and Discussion .....	50
4.3.1 Preliminary studies on antisolvent processing of drug .....	50
4.3.2 Coprecipitation of drug and polymer.....	52
4.3.3 Dependence of particle size and morphology on concentration of organic solutions .....	53
4.3.4 Dependence of particle size and morphology on pressure.....	54
4.3.5 Effect of molecular weight of carrier.....	56
4.3.6 Physicochemical characterization of the coprecipitates .....	57
4.4 Conclusion .....	60
CHAPTER 5 SIZE CONTROL OF PARTICULATE SOLID DISPERSION	
SYSTEMS .....	61
5.1 Introduction.....	61
5.2 Materials .....	63
5.3 Results and Discussion .....	63

5.3.1 Preliminary study on operating conditions .....	63
5.3.2 Dependence of particle morphology on solvent composition.....	66
5.3.3 Effect of concentration of solutions on particle size distribution .....	68
5.3.4 Effect of pressure on particle morphology.....	69
5.3.5 Effect of weight ratio of drug to polymer on particle size distribution .....	71
5.3.6 Physicochemical properties of coprecipitates from antisolvent processing	71
5.4 Conclusion .....	76
CHAPTER 6 PREPARATION OF SOLID DISPERSIONS OF PIROXICAM USING DENSE GAS TECHNIQUE .....	77
6.1 Introduction.....	77
6.2 Materials .....	78
6.3 Results and Discussion .....	79
6.3.1 Preliminary studies.....	79
6.3.2 Effect of Px/PVP weight ratio on the morphology of products .....	81
6.3.3 Crystallinity and polymorphic purity.....	83
6.3.4 Thermal analysis .....	85
6.3.5 FT-IR analysis.....	87
6.3.6 Drug loading .....	89
6.3.7 Dissolution studies .....	89
6.4 Conclusion .....	91
CHAPTER 7 CONCLUSION REMARKS .....	93
REFERENCES .....	94
APPENDICES .....	114
CURRICULUM VITAE.....	137

## LIST OF TABLES

<b>Table 1</b>	Common dense gas techniques for particle design.....	8
<b>Table 2</b>	Review articles on the dense gas antisolvent processes. ....	11
<b>Table 3</b>	Experimental conditions of DGA treatment on neat prednisolone.....	51
<b>Table 4</b>	Drug loadings of DGA-prepared solid dispersions. ....	91
<b>Table A-1</b>	Pharmaceutical substances micronized with the dense gas antisolvent process (1999 - present). ....	115
<b>Table A-2</b>	Polymeric materials prepared with the dense gas antisolvent process (2000 – present). ....	120
<b>Table A-3</b>	Composite particles prepared using dense gas antisolvent processes (1999 - present).....	123
<b>Table A-4</b>	Vendor information of dense gas antisolvent equipment and accessories. ....	127
<b>Table A-5</b>	Summary of dense gas antisolvent precipitation of PVP. ....	128
<b>Table A-6</b>	Summary of dense gas antisolvent precipitation of poly(DTE carbonate). ....	129
<b>Table A-7</b>	Summary of dense gas antisolvent precipitation of PVP and Prd from solutions of methylene chloride. ....	130
<b>Table A-8</b>	Summary of dense gas antisolvent precipitation of PVP and PrAc. ..	131
<b>Table A-9</b>	Summary of dense gas antisolvent precipitation of PVP and Px. ....	132

## LIST OF ILLUSTRATIONS

<b>Figure 1-1</b>	Schematics of composite particles. (a) microcapsule, (b) intermediate, and (c) microsphere.....	4
<b>Figure 1-2</b>	Typical phase diagram of carbon dioxide.....	7
<b>Figure 1-3</b>	Schematic representation of a RESS processing set-up. ....	12
<b>Figure 1-4</b>	Schematic representation of a PGSS processing set-up. ....	14
<b>Figure 1-5</b>	Schematic representation of a GAS setup. ....	16
<b>Figure 2-1</b>	Schematics of (a) the dense gas antisolvent precipitation setup. 1, High pressure precipitation chamber; 2, HPLC syringe pump; 3, air driven pump; 4, heat exchanger; 5, injection nozzle; 6, metal sinter filter; 7, back pressure regulator; 8, cyclone separator. (b) photograph of the DGA apparatus, and (c) coaxial nozzle.....	25
<b>Figure 2-2</b>	Repeat unit of polyvinylpyrrolidone (PVP).....	31
<b>Figure 2-3</b>	SEM micrographs of (a) as-received PVP K29/32, and PVP K29/32 particles precipitated at (b) 293 K, (c) 298 K, and (d) 303 K from methylene chloride. Pressure: 9.66 MPa, concentration: 3.0 % (w/v). 32	32
<b>Figure 2-4</b>	Temperature effect on size of PVP K25 after DGA: (a) as-received PVP K25, (b) 293 K, (c) 298 K, and (d) 308 K with solutions of 3.0 % (w/v) in DCM and 9.66 MPa.....	32
<b>Figure 2-5</b>	Pressure effect on size of PVP after DGA: (a) 9.66 MPa, (b) 11.0 MPa, (c) 12.4 MPa, and (d) 13.8 MPa with solutions of 3.0 % (w/v) in DCM and 298 K. ....	33
<b>Figure 2-6</b>	Concentration effect on size of PVP K29/32 after DGA: (a) 1.0 % (w/v), (b) 3.0 % (w/v), (c) 5.0% (w/v), and (d) 8.0% (w/v) with solutions in DCM at 9.66 MPa and 298 K. ....	36

<b>Figure 2-7</b>	Molecular weight of PVP 3.0 % (w/v) in methylene chloride (DCM) at 9.66 MPa and 298 K. (a) K90 (MW = 1300,000) and (b) MW = 360,000. ....	36
<b>Figure 3-1</b>	Repeat unit of poly(DTE carbonate). ....	41
<b>Figure 3-2</b>	SEM of poly(DTE carbonate) before (a) and after (b) dense gas antisolvent processing.....	41
<b>Figure 3-3</b>	SEM images of poly(DTE carbonate) microspheres precipitated from DCM at 10.3 MPa and (a) 293 K; (b) 308 K, and (c) comparison of particle size distribution at the two temperatures. ....	43
<b>Figure 3-4</b>	SEM image of poly(DTE carbonate) microspheres precipitated from DCM at 10.3 MPa and 306 K. (a) 5.0 % (w/v); (b) 0.5 % (w/v), and (c) comparison of particle size distribution at the two concentrations.....	45
<b>Figure 3-5</b>	DSC curves of (a) as-received and (b) a typical DGA-processed poly(DTE carbonate) .....	47
<b>Figure 3-6</b>	PXRD patterns of (a) as-received and (b) a typical DGA-processed poly(DTE carbonate) .....	47
<b>Figure 4-1</b>	Molecular structure of prednisolone (Prd).....	51
<b>Figure 4-2</b>	SEM micrographs of prednisolone before (a) and after dense gas antisolvent precipitation from (b) DCM/Ace (v/v = 4:1), (c) DCM/Ace (v/v = 40:3), and (d) EtAc/Ace (v/v = 1:1). ....	51
<b>Figure 4-3</b>	SEM micrographs of coprecipitates from solutions with concentration of (a) 1.5 % (w/v), (b) 3.0 % (w/v), (c) 5.0 % (w/v), and (d) 8.0 % (w/v) at 298 K and 9.66 MPa.....	53

<b>Figure 4-4</b>	SEM micrographs of coprecipitated prepared solution with concentration of (a) 9.66 MPa, (b) 11.0 MPa, (c) 12.4 MPa, (d) 13.8 % MPa, and (e) number particle size distribution of coprecipitates at 298 K using solution of 3.0 % (w/v) and drug/polymer ratio of 1:5.....	55
<b>Figure 4-5</b>	SEM micrographs of coprecipitates (w/w = 1:4) using (a) PVP K25 and (b) PVP K29/32 from solutions with concentration of 3.0 % (w/v) at temperature of 298 K and pressure of 9.66 MPa. ....	56
<b>Figure 4-6</b>	PXRD patterns of (a) as-received prednisolone, (b) dense gas treated drug, (c) physical mixture of drug and PVP K29/32, (d) coprecipitate of drug and PVP, and (e) neat PVP K29/32.....	57
<b>Figure 4-7</b>	FT-IR spectra of (a) as-received PVP K29/32, (b) neat prednisolone, (c) physical mixture of drug and PVP K29/32, (d) coprecipitate of drug and PVP.....	58
<b>Figure 4-8</b>	DSC curves of (a) as-received prednisolone, (b) physical mixture of drug and PVP K29/32, (c) coprecipitate of drug and PVP, and (d) neat PVP K29/32. ....	59
<b>Figure 5-1</b>	Molecular structure of prednisolone acetate (PrAc).....	65
<b>Figure 5-2</b>	SEM micrographs of prednisolone acetate before (a) and after antisolvent treatment from solution of (b) DCM + Ace (v/v = 1:4) at 298 K, (c) Ace at 298 K, and (d) Ace at 313 K. Pressure = 9.66 MPa.....	65
<b>Figure 5-3</b>	Particle size distributions of the samples prepared from mixture of methylene chloride and acetone with varying volume ratios. (a) VDCM:VAce = 4:6, 2:8, 1:9; (b) VDCM:VAce = 9:1, 8:2, 5:5. ....	66

<b>Figure 5-4</b>	SEM micrographs of coprecipitates prepared from mixture of methylene chloride and acetone with volume ratio of (a) 9:1, (b) 8:2, (c) 4:6, (d) 5:5, (e) 2:8, (f) 1:9. ....	67
<b>Figure 5-5</b>	SEM micrographs of coprecipitated prepared solution with concentration of (a) 1.2 % (w/v), (b) 2.4 % (w/v), (c) 3.6 % (w/v), and (d) 4.8 % (w/v).....	68
<b>Figure 5-6</b>	SEM micrographs of coprecipitates prepared at pressure of (a) 9.66 MPa, (b) 11.0 MPa, (c) 12.4 MPa, and (d) 13.8 MPa. ....	70
<b>Figure 5-7</b>	Particle size distributions of coprecipitates prepared at pressure of (a) 9.66 MPa, (b) 11.0 MPa, (c) 12.4 MPa, and (d) 13.8 MPa; (e) particle size distributions of the products. ....	70
<b>Figure 5-8</b>	SEM micrographs of coprecipitates prepared with starting drug to polymer weight ratio of (a) 1:2, (b) 1:3, (c) 1:5, and (d) 1:9.....	71
<b>Figure 5-9</b>	PXRD patterns of (a) as-received prednisolone acetate, (b) antisolvent processed drug, (c) physical mixture (w/w = 1:5), (d) coprecipitate, (e) as-received PVP K29/32.....	72
<b>Figure 5-10</b>	FT-IR spectra of (a) as-received prednisolone acetate, (b) physical mixture (m/m = 1:5), (c) coprecipitate, (d) as-received PVP K29/32..	74
<b>Figure 5-11</b>	DSC curves of (a) as-received prednisolone acetate, (b) physical mixture (w/w = 1:5), (c) coprecipitate, (d) as-received PVP K29/32...	75
<b>Figure 6-1</b>	Molecular structure of piroxicam (Px). ....	80
<b>Figure 6-2</b>	SEM micrographs of piroxicam before (a) and after dense gas antisolvent precipitation from (b) dichloromethane, (c) ethanol/acetone mixture (v/v=4:1), and (d) acetone.....	80

<b>Figure 6-3</b>	SEM micrographs of DGA precipitate of (a) pure Px, and coprecipitate of Px and PVP with a D/P of (b) 2:1, (c) 1:1, (d) 1:2, (e) 1:4, and (f) 1:9. ....	82
<b>Figure 6-4</b>	PXRD patterns of (a) simulated form I piroxicam (Px), (b) Raw Px, (c) simulated form II Px, (d) DGA-processed Px, (e) spray-dried (SD) Px, (f) physical mixture (PM) with drug-to-polymer weight ratio of 1:4, (g) DGA coprecipitate (starting drug to polymer weight ratio = 1:4), (h) spray-dried solid dispersion (starting drug to polymer weight ratio = 1:4), and (i) as-received PVP K25. ....	84
<b>Figure 6-5</b>	DSC curves of (a) as-received Px, (b) DGA-processed Px, (c) spray-dried Px, (d) PM, (e) DGA coprecipitate, (f) spray-dried solid dispersion, and (g) as-received PVP K25. ....	86
<b>Figure 6-6</b>	FT-IR spectra of (a) as-received Px, (b) DGA-processed Px, (c) spray-dried Px, (d) PM, (e) DGA coprecipitate, (f) spray-dried solid dispersion, and (g) as-received PVP K25. ....	88
<b>Figure 6-7</b>	Percent drug release profiles of (a) as-received Px, (b) DGA-processed Px, (c) spray-dried Px, (d) PM, (e) DGA coprecipitate, and (f) spray-dried solid dispersion at 37°C. ....	90
<b>Figure 6-8</b>	Particle size distribution of solid dispersions with drug to polymer weight ratio of 1:4 prepared by DGA and SD process. ....	91
<b>Figure A-1</b>	PXRD patterns of piroxicam before (a) and after (b) spray drying and spray-dried solid dispersions with drug/polymer weight ratio of (c) 2:1, (d) 1:1, (e) 1:2, (f) 1:4, (g) 1:9; PVP K25 before (h) and after (i) spray drying. ....	133

<b>Figure A-2</b>	PXRD patterns of piroxicam before (a) and after (b) DGA processing and DGA-processed solid dispersions with drug/polymer weight ratio of. (c) 2:1, (d) 1:1, (e) 1:2, (f) 1:4, (g) 1:9.....	133
<b>Figure A-3</b>	FT-IR spectra of piroxicam before (a) and after (b) spray drying and spray-dried solid dispersions with drug/polymer weight ratio of. (c) 2:1, (d) 1:1, (e) 1:2, (f) 1:4, (g) 1:9; PVP K25 before (h) and after (i) spray drying. ....	134
<b>Figure A-4</b>	FT-IR spectra of piroxicam before (a) and after (b) DGA processing and DGA-processed solid dispersions with drug/polymer weight ratio of. (c) 2:1, (d) 1:1, (e) 1:2, (f) 1:4, (g) 1:9; PVP K25 before (h) and after (i) DGA processing.....	134
<b>Figure A-5</b>	DSC curves of piroxicam before (a) and after (b) spray drying and spray-dried solid dispersions with drug/polymer weight ratio of. (c) 2:1, (d) 1:1, (e) 1:2, (f) 1:4, (g) 1:9; PVP K25 before (h) and after (i) spray drying. ....	135
<b>Figure A-6</b>	DSC curves of piroxicam before (a) and after (b) DGA processing and DGA-processed solid dispersions with drug/polymer weight ratio of. (c) 2:1, (d) 1:1, (e) 1:2, (f) 1:4, (g) 1:9; PVP K25 before (h) and after (i) DGA processing.....	135
<b>Figure A-7</b>	Dissolution profiles of spray-dried solid dispersion systems. Ratio behind SD is the starting drug/polymer weight ratio.....	136
<b>Figure A-8</b>	Dissolution profiles of DGA prepared solid dispersion systems. Ratio behind DGA is the starting drug/polymer weight ratio. ....	136

## LIST OF ABBREVIATIONS

Ace	Acetone
ACN	Acetonitrile
API	Active pharmaceutical ingredients
ASES	Aerosol enhanced extraction system
BCS	Biopharmaceutical classification systems
CAN-BD	Carbon dioxide-assisted nebulization in a bubble dryer
CO <sub>2</sub>	Carbon dioxide
DCM	Dichloromethane
DELOS	Depressurization of expanded liquid organic solution
DG	Dense gas
DMF	Dimethyl formamide
DMSO	Dimethyl sulfoxide
DSC	Differential Scanning Calorimetry
EtAc	Ethyl acetate
EtOH	Ethanol
GAS	Gas antisolvent recrystallization
GC	Gas chromatography
HPBCD	hydroxypropyl- $\beta$ -cyclodextrin
HPLC	High performance liquid chromatography
HPMC	hydroxypropyl methylcellulose
i-PrOH	isopropanol
MeOH	Methanol
MW	Molecular weight
NMP	n-methyl propyl pyrrolidone

DGA	Precipitation with compressed antisolvent
PCL	Poly( $\epsilon$ -caprolactone)
PEG	Poly(ethylene glycol)
PEO	Poly(ethylene oxide)
PGSS	Particles from gas-saturated solutions
PLA	Poly(lactide)
PLGA	Poly(lactic-co-glycolic acid)
PMMA	Poly(methyl methacrylate)
Poly(DTE carbonate)	Poly (desamino tyrosyl-tyrosine alkyl ester carbonate)
PSA	Poly(sebacic acid)
PSD	Particle size distribution
PVP	Polyvinylpyrrolidone
Prd	Prednisolone
PrAc	Prednisolone acetate
Px	Piroxicam
PVP	Polyvinylpyrrolidone
PXRD	Power X-Ray Diffraction
RESS	Rapid expansion of supercritical solutions
RESS-SC	Rapid Expansion of a Supercritical Solution-Solid Cosolvent
RESOLV	Rapid expansion of a supercritical solution into a liquid solvent
SAA	Supercritical assisted atomization
SAS	Supercritical antisolvent precipitation
SAS	Supercritical antisolvent with enhanced mass transfer
SCF	Supercritical fluid
SCF-drying	Supercritical fluid drying

ScMM	Supercritical Melting Micronization
SFL	Spray into freezing liquid
SEDS	Solution enhanced dispersion with supercritical fluids
SEM	Scanning electron microscopy
SFEE	Supercritical fluid extraction of emulsion
THF	Tetrahydrofuran

## LIST OF SYMBOLS

$A$	surface area of the particle
$c$ or $C$	concentration of drug in the bulk solvent
$c_0$	equilibrium concentration
$C_s$	concentration of drug (equal to solubility of drug) in the stagnant layer
$\gamma$	interfacial tension
$d$	spacing between the planes in the atomic lattice
$D$	diffusion rate constant
$h$	thickness of the stagnant layer
$\theta$	angle between the incident ray and the scattering planes
$\lambda$	wavelength of x-rays, and moving electrons, protons and neutrons
$n$	integer (1, 2, 3, ...)
$P$	pressure
$P_c$	critical pressure
$Q$	solution flow rate
$Q_{CO_2}$	CO <sub>2</sub> flow rate
$r$	radius of crystal
$s$	supersaturation ratio
$t$	time
$T$	temperature
$T_c$	critical temperature
$T_g$	Glass transition temperature
$V_c$	molar volume
$x_{eq}$	solubility
$\rho$	density

## CHAPTER 1

### INTRODUCTION

#### 1.1 Background

The field of Pharm. Res. and development witnesses increasing application of combinatorial chemistry and, high-throughput screening technology to the discovery and design of materials with improved therapeutic performance. While numerous compounds are being created continuously, the chances of these material candidates being developed into marketable products are often slim because of the poorly-understood and under-controlled structure-properties relationship. Therefore, decades of research and development have been focusing on designing and modifying formulation techniques.

Among various formulations, particulate pharmaceutical materials with specific size and structures are of great interest. First of all, particles with low aspect ratios are often more desirable than their irregular-shaped counterparts with respect to manipulation during industrial processing. Secondly, particles with controlled dimensions and structures are able to exert maximum therapeutic efficacy. For instance, dry powders used in pulmonary and intranasal delivery need to have a size distribution between 1-5  $\mu\text{m}$ .<sup>1</sup> Insufficient deposition of drugs will result if the particle size falls outside this range.<sup>2</sup> Another example is the paclitaxel-loaded poly(lactic-co-glycolic acid) (PLGA) microspheres. The degradation of the carrier material modulates the release the active pharmaceutical ingredient (API), and causes sustained in vivo release at targeted locations.

To meet the increasingly strict drug administration requirement on the quality of the particulate pharmaceutical substances, the concept of “particle design” attracts

more and more interests, and efforts are progressively made in this area. Among a range of aspects on particle design of pharmaceutical materials, particle size reduction (or micronization) and composite particles receive the most attention, because they both provide possibility of improving the bioavailability of poorly water-soluble drug substances. As a measurement of the extent of a therapeutically active drug that reaches the systemic circulation and is available at the site of action,<sup>3</sup> bioavailability is the key to evaluate the success of pharmaceutical formulation.

### 1.1.1 Micronization (Particle size reduction)

Dissolution of pharmaceuticals is affected by a number of factors, such as particle size,<sup>4</sup> morphology, defects, polymorphism, impurities, and physicochemical properties (e.g., density, viscosity, and wettability).<sup>5</sup> Our interest herein focuses on morphology and size control of pharmaceutical materials because they are critical to both the primary and bulk powder properties.

According to Ostwald-Freundlich equation (Eqn. 1), micronization (or sometimes referred to particle size reduction) of pharmaceutical substances can lead to exponential increase in their solubility as a function of particle size:.

$$x_{eq}(r) / x_{eq}(\infty) = \exp(2\gamma V_c / rRT) \quad \text{Eqn. 1}$$

Where

$r$  = radius of crystal,

$x_{eq}$  = solubility,

$\gamma$  = interfacial tension,

$V_c$  = molar volume.

In addition, according to the Noyes–Whitney equation (Eqn. 2), micronization of a drug is also possible to improve the bioavailability of poorly soluble substances due to the increased effective surface area.

$$\frac{dC}{dt} = \frac{D \cdot A}{h} (C_s - C) \quad \text{Eqn. 2}$$

Where

$dC/dt$  = rate of drug dissolution at time  $t$ ,

$D$  = diffusion rate constant,

$A$  = surface area of the particle,

$C_s$  = concentration of drug (equal to solubility of drug) in the stagnant layer,

$C$  = concentration of drug in the bulk solvent,

$h$  = thickness of the stagnant layer.

Moreover, the dissolved drug molecules can be distributed more rapidly with thinner diffusion layer around small particles (esp.  $<5 \mu\text{m}$ ). Furthermore, the hydrodynamics of drug particles in the gastrointestinal tract will have minimal impact on the absorption rate so the thickness of the diffusion layer is also affected. More specifically, poorly soluble drugs (solubility  $<1 \text{ mg/mL}$ ) given in low doses are absorbed under more influence of the particle size because of correlation between the bioavailability and dissolution rate in these cases.

Pharmaceutical substances are normally micronized by either top-down or bottom-up methods. The first group includes milling, grinding, and crushing, etc; while the second group contains chemical precipitation, spray drying, and freeze drying, and so on. These micronization techniques are often associated with such limitations as excessive solvent involvement, thermal and chemical degradation of products, residual solvents, and poor reproducibility, etc. Therefore, it is highly

desirable to generate microparticles with controlled particle size, desired morphology, and low environmental impact.

### 1.1.2 Composite particles

Particles with composite structures, besides particle size reduction, provide an alternative opportunity of controlled drug delivery, including sustained release, fast (or immediate) release, delayed release, etc.<sup>6</sup> As a result, desirable dissolution profiles can be achieved, which benefits selection suitable routes of drug delivery such as oral, intravenous, and respiratory administration.

Composite particles generally include microcapsules [Fig. 1-1(a)] and microspheres [Fig. 1-1(c)], according to Jung and Perrut.<sup>7</sup> As shown in Fig. 1-1, microcapsule are core-shell structured with excipients usually coating around the active ingredients; while in the case of microspheres, the active ingredients are dispersed within the matrix composed by the excipients. There are various intermediate cases between the two extreme situations, and these intermediate-structured particles are sometimes more practical.

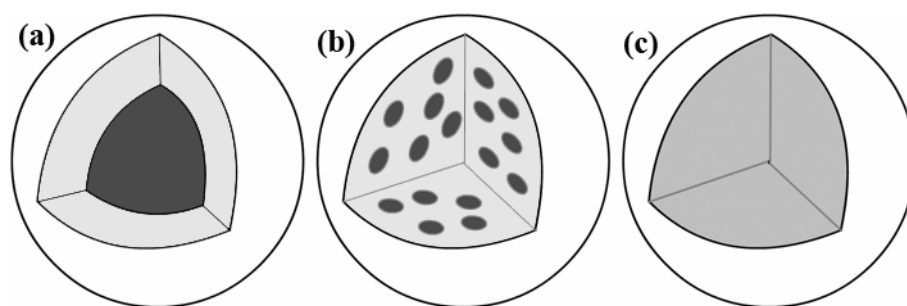


Figure 1-1. Schematics of composite particles. (a) microcapsule, (b) intermediate, and (c) microsphere.

Solid dispersions, an appealing branch of composites, have been progressively designed because solid dispersion systems are shown to be able to enhance the

bioavailability superior to that of other formulations.<sup>8,9</sup> In terms of structure, solid dispersion systems lie between Fig. 1-1(b) and Fig. 1-1(c), ranging from drug cluster-dispersed mixture to solid solution. There are several advantages using solid dispersions over other strategies, rendering this technique attractive for bioavailability improvement.<sup>10</sup> Firstly, solid dispersions are easier to prepare compared to chemical approaches such as prodrug or salt formation. Secondly, solid dispersions are more acceptable to patients than solubilization products. In addition, in terms of particle size, wettability, porosity, crystallinity of drugs, etc., solid dispersions provide more opportunity of improving drug bioavailability.<sup>11</sup>

So far, only a few solid dispersion systems have been marketed, among which are: Gris-PEG (griseofulvin in PEG) developed by Novartis, Cesamet (nabilone in PVP) by Lily, and Sporanox (itraconazole in HPMC and PEG 20000 sprayed on sugar spheres) by Janssen Pharmaceutica of Johnson & Johnson. This is because the development of solid dispersion systems entails raw materials with scrutinized physicochemical properties, product reproducibility and stability, as well as cost and intellectual property concerns. Currently, techniques such as hot melt extrusion and spray drying have been employed to develop solid dispersion systems. However, challenges such as in-processing stress and post-processing treatment are still hindering wider application of the solid dispersion systems. Furthermore, the quality of their products is not always satisfying. To overcome these disadvantages, more efficient and productive formulation techniques are of great demand as the evolution of drugs from bench- to bed-side is increasingly bottlenecked by their limited bioavailability.

## 1.2 Dense Gas Technique

After the discovery of the existence of supercritical fluid by Hannay and Hogarth<sup>12</sup> more than a century ago, researchers began to explore the properties and applications of supercritical fluids. Starting from the late 1980s, more and more supercritical fluid techniques were developed utilizing special physicochemical properties of these fluids. By the end of the twentieth century, people began to realize the potential of these techniques in designing particulate systems with composite structures. During these progresses, liquid CO<sub>2</sub>, especially those in the vicinity of critical point of CO<sub>2</sub>, were found having similar properties that can be used for process engineering. Different definitions regarding supercritical fluid techniques have arisen over the years, and often they cause confusions as to the operation conditions with regards to the relative location to critical point of binary, ternary, and multiple component systems. Therefore, it is more appropriate to refer the technique in this study as dense gas technique, because we use supercritical as well as liquid carbon dioxide as processing medium.

By definition, dense gas (DG) refers to a fluid close to, but not necessarily above, its critical point.<sup>13</sup> As presented in Fig. 1-2, at critical point, the vapor-liquid equilibrium curve ends and the dissimilarity between gaseous phase and liquid phase vanishes. Depending on the role it plays, dense gas can be used as a processing medium for chemical and physical transformation process, or reaction medium.<sup>14</sup> Playing roles either as solutes, solvents or antisolvents (or nonsolvent) in a physical process, dense gas techniques have been actively applied in the field of pharmaceutical development because of the aforementioned features of dense gases.

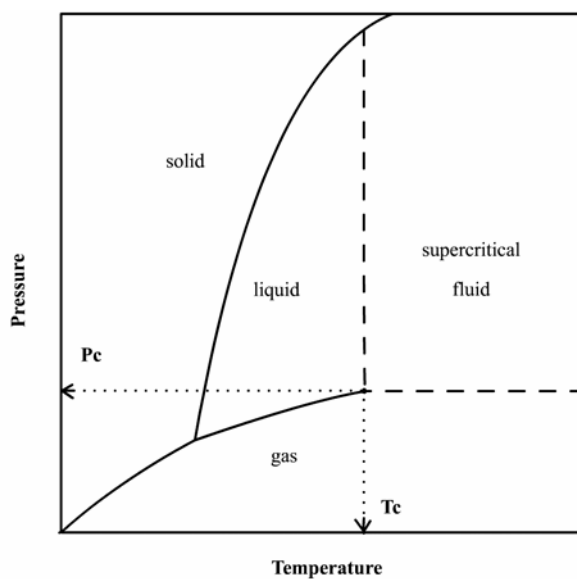


Figure 1-2. Typical phase diagram of carbon dioxide.

Dense gas carbon dioxide is of special interest as a processing medium because it offers such bonuses as mild operating temperature and ease of solvent separation, as well as environmental benignity.

So far, various dense gas techniques have been developed, including rapid expansion of supercritical solutions (RESS), particles from gas-saturated solutions (PGSS), and antisolvent precipitation. These techniques differ in the role of dense gas, whether or not organic solvent is involved, and experimental conditions. Typically, they are able to yield particles ranging from  $10^{-2}$ - $10^2 \mu\text{m}$ . Their features have been reviewed in details and summarized in Table 1.

Table 1. Common dense gas techniques for particle design.

Acronym	Process	Role of CO <sub>2</sub>	Typical pressure (MPa)	Typical temperature (K)	Typical particle size (μm)	Derivative
RESS	Rapid Expansion of Supercritical Solutions	solvent	20-30	310-400	0.2-3	RESS-SC RESOLV
GAS	Gas AntiSolvent precipitation	antisolvent	6-10	298-333	0.1-100	N/A
PCA	Precipitation with Compressed Antisolvent	antisolvent	7-15	298-333	0.2-10	SAS-EM
SAS	Supercritical AntiSolvent precipitation					
ASES	Aerosol Solvent Extraction System					
SEDS	Solution Enhanced Dispersion of Supercritical Fluids	antisolvent	10-30	308-363	0.05-10	SEDS-PA
PGSS	Particles from Gas-Saturated Solutions	Solute	8-20	323-460	15-50	ScMM

### 1.2.1 Properties of dense gas carbon dioxide

Among many dense gases studied, carbon dioxide ( $\text{CO}_2$ ) is of greatest interest, because of the location of its critical point ( $T_c = 304.1 \text{ K}$ ,  $P_c = 7.38 \text{ MPa}$ ), high compressibility, and nonpolar properties.<sup>15</sup> There are many physicochemical features of dense gas  $\text{CO}_2$  that make it attractive as process medium in processing pharmaceutical materials.

First of all, dense gas  $\text{CO}_2$  is found to be completely or partially miscible with various ordinary organic solvents,<sup>16</sup> this affinity with organic solvents may facilitate efficient removal of residual solvents and monomers. Therefore, dense gas  $\text{CO}_2$  can be used to extract small organic molecules from polymers or pharmaceutical substances under relatively mild conditions.

Secondly, near the critical point, their liquid-like density and solvation power, along with their gas-like mass transfer properties such as diffusivity and viscosity can be tuned by changing the temperature and pressure. These adjustable mass transfer and penetration ability render the dense gas a powerful extraction and cleaning medium.

Thirdly,  $\text{CO}_2$  usually can not solubilize polar molecules by itself because of its nonpolar nature. As a result, most pharmaceutical materials are practically insoluble in dense gas  $\text{CO}_2$ . Though this fact limits the application of dense gas in extraction of these substances, it provides an opportunity for utilizing  $\text{CO}_2$  as antisolvent (nonsolvent), which itself makes a much more flexible, versatile, and controllable choice of precipitation and crystallization.

Finally, dense gas, such as  $\text{CO}_2$ , is also capable of reducing the glass transition temperature ( $T_g$ ) of a variety of polymers by acting as plasticizers. In fact, the extent of  $T_g$  depression is a function of pressure and temperature, and the temperature

difference can reach as high as 100 K. This property of dense gas CO<sub>2</sub> offers a basis for foaming, particle formation, and impregnation of polymeric materials with bioactive substances, etc.

In addition, CO<sub>2</sub> itself is relatively inexpensive, inert, and safe with regard to current status of process engineering. Thus, dense gas CO<sub>2</sub> holds great promise as a versatile processing and synthesis medium.

Over the past two decades, growing attentions have been paid to the application of dense gas techniques in drug delivery, controlled release and tissue engineering, etc.<sup>17-</sup>

<sup>21</sup> Extensive reviews have been made on these processes and are summarized in Table 2. These techniques are complementary to each other and can provide an operation system for processing or formulation of polymers and pharmaceuticals. Among various dense gas techniques, RESS, PGSS, and antisolvent precipitation are the most typical processes that employ basic physicochemical properties of dense gas carbon dioxide. Therefore, more details of each technique will be described in the following sections.

Table 2. Review articles on the dense gas antisolvent processes.

Processes	Subject	Year	Reference
RESS, GAS, SAS	pharmaceuticals	1997	J. Pharm. Sci. <sup>22</sup>
GAS, SAS	general	1999	J. Supercrit. Fluids <sup>23</sup>
RESS, SAS, SEDS, PGSS	phase behavior	1999	Pharm. Res. <sup>24</sup>
RESS, GAS, PGSS	general	2000	Chem. Eng. Process. <sup>25</sup>
RESS, SAS, SEDS	polymers	2000	J. Mater. Chem. <sup>26</sup>
RESS, SAS, SEDS, PGSS	general	2001	J. Supercrit. Fluids <sup>7</sup>
RESS, GAS, SAS	drug delivery	2001	Crit. Rev. Ther. Drug Carrier Syst. <sup>18</sup>
RESS, GAS, SAS, SEDS	pharmaceuticals	2001	Drug Dev. Ind. Pharm. <sup>27</sup>
RESS, SAS, SEDS, PGSS	pharmaceuticals	2001	Expert. Opin. Ther. Pat. <sup>28</sup>
RESS, GAS, SAS, PGSS	drug delivery	2002	Aust. J. Chem. <sup>21</sup>
RESS, SAS	polymers		
	nanomaterials	2003	J. Chem. Edu. <sup>29</sup>
RESS, GAS, SAS, SEDS, PGSS	polymers	2005	J. Supercrit. Fluids <sup>30</sup>
RESS, GAS, SAS, SEDS, PGSS	experimental	2005	Int. J. Pharm. <sup>31,32</sup>
RESS, GAS, SAS, SEDS, SAA	general	2006	Eur. J. Pharm. Sci. <sup>33]</sup>
RESS, SAS, SAA	nanomaterials	2006	J. Supercrit. Fluids <sup>34</sup>
RESS, SAS, PGSS	composite	2007	J. Supercrit. Fluids <sup>14</sup>
RESS, GAS, SAS, PGSS	drug delivery	2007	Int. J. Pharm. <sup>35</sup>
	polymers		
RESS, GAS, SAS, PGSS, SFEE	nanoparticles	2008	Adv. Drug Deliv. Rev. <sup>36</sup>
RESS, SAS, PGSS	drug delivery	2008	Adv. Drug Deliv. Rev. <sup>37</sup>
	polymers		
RESS, GAS, SAS, PGSS	mechanisms	2008	Adv. Drug Deliv. Rev. <sup>38</sup>
RESS, GAS, SAS, PGSS	biodegradable particles	2008	Adv. Drug Deliv. Rev. <sup>39</sup>
RESS, GAS, SAS, SEDS, PGSS	proteins	2008	Adv. Drug Deliv. Rev. <sup>40</sup>
RESS, SAS, PGSS	pharmaceuticals	2008	Adv. Drug Deliv. Rev. <sup>41-43</sup>
	composite		

### 1.2.2 Dense gas as solvent: Rapid Expansion of Supercritical Solutions (RESS)

In some cases, dense gas  $\text{CO}_2$  is capable of solvating nonpolar molecules and interacts with slightly polar molecules or molecules containing certain functional groups. This interaction is often enhanced with the presence of cosolvent, for example polar small-molecule solvents such as methanol or ethanol, etc. By manipulating such parameters as temperature and pressure, substance-of-interest can be dissolved in a dense gas, fast nucleation then results upon sudden depressurization of the mixture through a throttling device. Consequently, nano- or microparticles will be produced.<sup>44-54</sup> Besides aforementioned operating variables, geometry of the equipment,<sup>55</sup> nozzle configuration,<sup>56</sup> and the nature of the material-of-interest all affect the quality of final products.

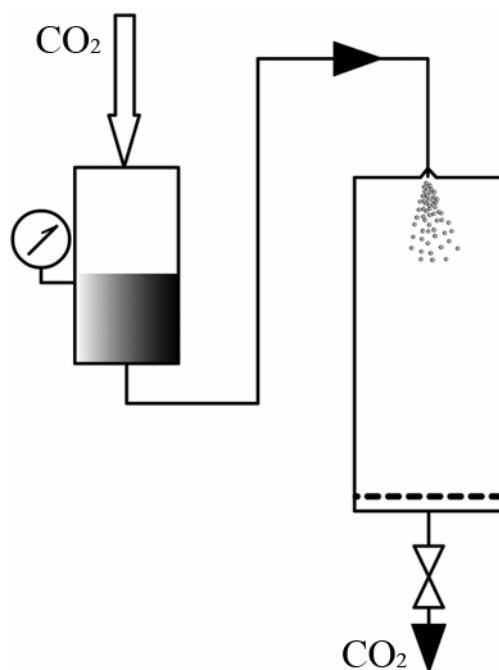


Figure 1-3. Schematic representation of a RESS processing set-up.

Fig. 1-3 shows a typical configuration of a RESS setup. The solvation of solute by dense gas  $\text{CO}_2$  takes place in pre-expansion chamber 1, where temperature and

pressure are controlled. Then the mixture is introduced into the expansion chamber 2 via a throttling device 3. Because of the pressure difference, solvation power of dense gas CO<sub>2</sub> dropped quickly so that solute originally dissolved will precipitate out as fine particle, fibers, and other morphologies, depending operating conditions.

When two or more compounds are solubilized in a dense gas with or without cosolvent, composite particles can be generated. Depending on the difference in the crystallization thermodynamics and kinetics of the components, along with their interaction, it is possible to obtain particles in forms of encapsulation or coating. These studies have been widely conducted using the RESS process.<sup>31,57-61</sup>

Because it's simple and less expensive in nature, RESS is the first choice whenever applicable. However, the solubility of most compounds of interest often limits the application regime of the RESS technique; therefore sometimes cosolvents are added to enhance the solvation power of CO<sub>2</sub>, which compromises the original advantage of solvent-free process.

In fact, a couple of derivatives of RESS process have been developed to further control the quality and stability of final products. For example, Sun and co-workers<sup>62-65</sup> employed rapid expansion of a supercritical solution into a liquid solvent (RESOLV) to produce nanoparticles. They modified the traditional RESS by expanding the supercritical solution into a liquid solvent instead of ambient air to produce nanoparticles. In this way, the particle growth in the expansion jet is retarded by the liquid at the receiving end of the rapid expansion. As a result, a variety of materials have been micronized, including metals, semiconductors, pharmaceuticals, and polymers. On the other hand, Thakur and Gupta invented Rapid Expansion of Supercritical Solution with Solid Cosolvent (RESS-SC) process to produce nanoparticles of narrow size distribution.<sup>45,66,67</sup> According to these researchers, the

involvement of menthol as solid cosolvent (SC) improves the solubility of the drug in dense gas CO<sub>2</sub> and inhibits the in- and post-expansion coagulation.

### 1.2.3 Dense gas as solute: Particles from Gas-Saturated Solutions (PGSS)

In a PGSS, or otherwise referred to as supercritical melt micronization (ScMM) process,<sup>68</sup> compound-of-interest and dense gas CO<sub>2</sub> switch their role as opposed to what they play in a RESS process.<sup>69</sup> Typically, dense gas CO<sub>2</sub> is dissolved into a solution of a solute in a solvent or into a melted material. Under appropriate pressure and temperature conditions, this liquid mixture is further depressurized through a nozzle producing particles. Mechanistically, this process utilizes the fact that solubility of CO<sub>2</sub> in a liquid is often higher than that of the liquid in CO<sub>2</sub>. Therefore, PGSS is receiving lots of attention on the application of processing materials with low melting point. Also, the CO<sub>2</sub> consumption is much lower than any other dense gas techniques. In addition, production of composite particle is also possible with careful selection of compounds and operating conditions.

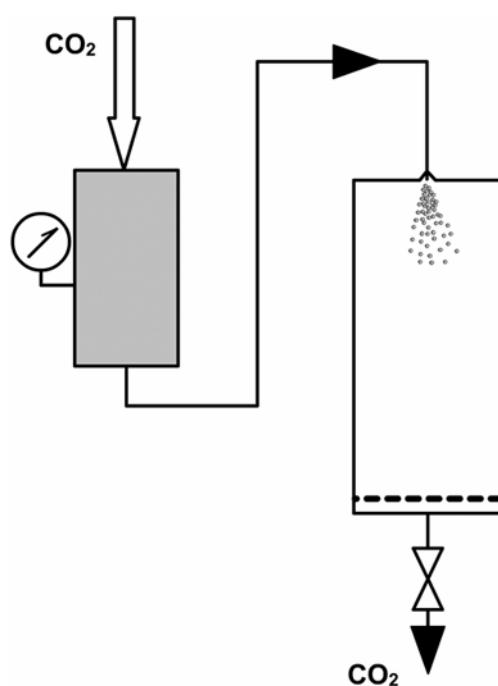


Figure 1-4. Schematic representation of a PGSS processing set-up.

Nonetheless, there are still many disadvantages challenging the applicability of PGSS process. For example, to-be-processed substances need to possess sufficient thermal stability under liquefaction conditions. This places a great barrier that limits the flexibility of PGSS method. Moreover, the micronization of this process is not as powerful as other dense gas techniques in terms of particle morphology, smallest obtainable size, and particle size distribution, which is undesirable for applications in drug encapsulation processes. Unless its mechanism can be deduced to adequately describe and model the particle formation, the PGSS process is far from a reliable particle engineering technique in terms of “particle design”.

#### **1.2.4 Dense gas as antisolvent**

In reality, many substances of interest are polar molecules, so the nonpolar nature of CO<sub>2</sub> molecule greatly limits its application for processing macromolecules and pharmaceutical molecules possessing polar functional groups. While many pharmaceutical substances usually do not have solubility high enough to be suitable for RESS processing, they may be suitable as subjects for dense gas antisolvent processing where their low solubility necessitates the success of antisolvent precipitation. We focus on the dense gas antisolvent technique because it provides wider applicability on substance-of-interest and greater possibility of continuous operation which is clearly more attractive for industrial-scale applications.<sup>23</sup>

In dense gas antisolvent processing, dense gas CO<sub>2</sub> is used to decrease the solubility of a solute (or multiple solutes) in a solvent (or solvent mixture). Consequently, the substance(s)-of-interest can precipitate out in different morphologies. Because the physical and mass transfer properties of dense gases can be manipulated between those of gases and liquids, operating conditions can be

chosen to reach high supersaturation rapidly. This way favors the formation of micro- or nano-particles.

Dense gas antisolvent processing can be operated in two major modes, namely batch mode and semi-continuous mode. In the first mode (usually referred to as GAS process), a dense gas is programmed to induce the expansion of a static solution until the solute precipitates upon reach the critical supersaturation ratio. Afterwards, dense gas is further added to extract the residual solvent and yield dry product after depressurization. Fig. 1-5 gives a schematic representation of a typical batch-mode dense gas antisolvent process.

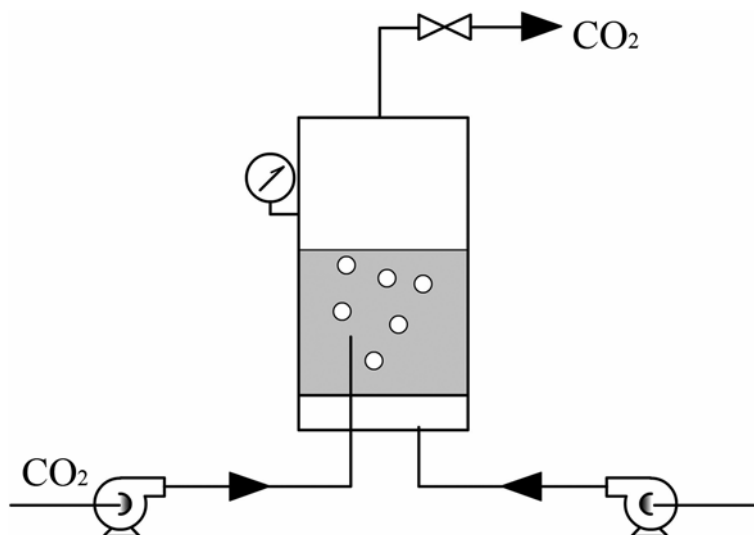


Figure 1-5. Schematic representation of a GAS setup.

However, because the kinetics of a GAS is often limited by the mixing process, products with poorly-controlled particle size distribution often result. In order to exert better control on the product quality in terms of morphology, yield, particle size, and particle size distribution, contact mode of solvent with antisolvent is modified in the way that solution and antisolvent flow and contact simultaneously. Meanwhile, steady ratio of solution to antisolvent flow can be established and hence better reproducibility of the processing is achieved.

There are several variants of semi-continuous dense gas antisolvent techniques, such as precipitated with compressed antisolvent (PCA), supercritical antisolvent precipitation (SAS), aerosol solvent extraction system (ASES), solution enhanced dispersions system (SEDS), etc. Although mechanistically all these processes involve introducing an organic solution via an atomization device into a flowing or static dense gas or vice versa, experimentally they differ in such factors as nozzle design and operating condition, etc. However, these differences are not strictly defined, so these acronyms should be interpreted with cautions.. For example, coaxial nozzles are employed in SEDS and sometimes in PCA processes, though in the former method a premixing chamber in the nozzle helped further breakup of the solution into finer droplets. There is no clear distinction in terms of operating conditions between PCA and SAS processes. When the experiment is conducted in supercritical conditions, i.e., above critical point of both solvent and CO<sub>2</sub> and their mixture, SAS is often employed, as indicated by its full name. Nonetheless, it is not uncommon that PCA was used for the same conditions.

In spite of the mixed uses of acronyms, there have been continuous renovations in the nozzle design, high-pressure precipitation vessel, and product-collecting medium, etc., to improve product quality, increase recovery, design specific particulate structures, and minimize particle agglomeration, etc.<sup>70</sup>

Our primary interest is concentrated on dense gas antisolvent precipitation operated in semi-continuous mode, because this mode is more suitable and desirable for large-scaled production, as well as the reproducibility of product quality. Therefore, more fundamentals of semi-continuous antisolvent precipitation with dense gas are detailed in the next section.

### 1.3 Particle Design Using Dense Gas Antisolvent Technique

Precipitation with dense gas as antisolvent is extensively studied as a promising particle formation technique. Over the past several decades, studies on micronization have covered a broad range of materials, including dye and pigments, energetic materials, pharmaceuticals, nutraceuticals, cosmetic and specialty chemicals, and so on.<sup>2,7,14,19,23,24,27,28,30-33,36,39,41,70-86</sup> Table A-1 summarizes the pharmaceutical compounds treated with dense gas antisolvent process over the last nine years or so. Additional excellent reviews summarizing this area of study from various different perspectives are also available in the literature.

### 1.4 Fundamentals of Dense Gas Antisolvent Technique

Similar to regular liquid nonsolvent induced phase separation, a solution of a solid substance in a primary solvent is expanded with a compressed gas which induces the precipitation of the dissolved substance according to the phase equilibrium of the ternary system at given temperature and pressure. A dense gas acts as an antisolvent which reduces the solvent power of the primary solvent and causes the precipitation of the solid. The fluid mixture is then removed through a filter and the precipitates are dried in a flush of pure compressed gas. The fluid mixture is separated by releasing the pressure and each of the components can be recycled within the process.

However, there are also dramatic differences between conventional nonsolvent precipitation and dense gas antisolvent process because of special physicochemical properties of dense gases. Let us take dense gas CO<sub>2</sub> as an example. Though CO<sub>2</sub> is similar to hexane in terms of density, the mass transfer in dense gas CO<sub>2</sub> is much faster. As a result, supersaturation of the solute can be reached within a very short period of time.

Over the years, the antisolvent applications of dense gas carbon dioxide have been studied extensively both experimentally and theoretically.<sup>87-91</sup> It has been widely agreed that thermodynamics, mass transfer, hydrodynamics of mixing, particle precipitation kinetics, as well as the natures of solvent and substrate, generally play roles in the sizing and shaping of final precipitates<sup>87,92,93</sup>, although there are still discrepancies of claims as to how these factors interplay together.

#### 1.4.1 Thermodynamics

The driving force for any equilibrium-based separation process is the departure from the phase equilibrium conditions. More specifically, the essential driving force for precipitation is supersaturation, defined as:

$$s = \ln \frac{\gamma c}{\gamma_0 c_0(P, T)} \quad \text{Eqn. 3}$$

Where  $c$  and  $c_0$  are the real and equilibrium concentrations of the substrate at a given pressure ( $P$ ) and temperature ( $T$ ),  $\gamma$  and  $\gamma_0$  are the correspondent fugacity coefficients.

First of all, choice of solvent is critical because it affects the equilibrium concentration of the substrate-of-interest by interacting with substrate and CO<sub>2</sub>. As a matter of fact, solvent mixtures were sometimes employed for control of crystallization to yield products of desired size, polymorphic form, and structure, etc.

In the substrate-solvent-CO<sub>2</sub> system, the fugacity coefficient is a function of pressure and temperature. Therefore, temperature, pressure, and concentration of solution all possibly affect the nucleation and growth. In addition, flow ratio of solution to CO<sub>2</sub> determines the initial composition of the three components. A lower flow ratio implies higher mass flow of CO<sub>2</sub>, which facilitates faster buildup of supersaturation ratio high enough to initiate nucleation, and in turn the size, size

distribution and morphology of the particles formed, provided growth and agglomeration can be controlled.

#### **1.4.2 Mass transfer**

Depending on the operating condition, there are two distinct thermodynamic states: subcritical (below the mixture critical pressure) and supercritical.<sup>88,89,94</sup> Precipitation mechanisms are different at subcritical and supercritical conditions. At subcritical conditions, an interface between the solution and CO<sub>2</sub> exists with the CO<sub>2</sub> in the gaseous or in the supercritical state, thus distinct droplets form with heat and mass being exchanged between the drops and their environment; at supercritical conditions, i.e., when the pressure is above the solvent-CO<sub>2</sub> mixture critical pressure, a homogenous phase forms upon equilibrium, where the surface tension becomes negligible. Consequently, gaseous plume instead of jet breakup takes place. Therefore, particles with different morphologies and sizes are produced because of the dissimilar mechanisms associated with the operating location relevant to the critical point of the system.<sup>95,96</sup>

In addition, the presence of solute sometimes can modify the phase behavior of the binary mixture;<sup>97</sup> but in many cases, it can be considered negligible, when low concentrations of solute are used.

#### **1.4.3 Hydrodynamics**

Normally, the investigations on hydrodynamics of the antisolvent precipitation are conducted through correlating the direct visualization of the jet dispersion with the observations of the product morphologies. The hydrodynamics of the dense gas antisolvent process depends on the physicochemical factors, including the geometry

of the precipitation chamber and the configuration of the fluid injection devices, as well as the scale of mixing.<sup>98</sup>

To help better atomization and hence more sufficient mixing of the solution with CO<sub>2</sub>, the solution is sprayed through a nozzle into droplets with different degrees of visibility. As the droplets contact the CO<sub>2</sub>, a two-way mass transfer takes place: CO<sub>2</sub> diffuses into the solution and the solvent evaporates from the droplet surface. A fast and uniform supersaturation is required for the proceeding of this two-way process, which causes the formation of small particles.

There have been considerable efforts modifying the injection devices with the aim of obtaining nanoparticles, maximizing control, and improving reproducibility. Coaxial, jet-swirl, ultrasonication-agitated, and prefilming nozzles<sup>99-102</sup> are designed and employed with various degree of success.

The development of high-pressure characterization system will allow us to obtain a clear picture of the role of hydrodynamics during the antisolvent precipitation with dense gas carbon dioxide.

## **1.5 Motivation and Objective**

Because of their potentials in particle design in an environmentally-benign way, dense gas antisolvent techniques have attracted increasing attention from chemists and engineers in medical and pharmaceutical applications. However, studies on size reduction and formation of solid dispersion systems by dense gas antisolvent precipitation are still inadequate to lay a sustainable groundwork to provide products with controllable quality and further understanding the performance-structure relationship. Therefore, more efforts should be aimed at developing micro-particles and nano-particles using these techniques, as well as preparation of composite

particles incorporating double or multiple components. Specifically, the endeavor of current work focuses on:

- Contribution to the development of dense gas antisolvent technology for the optimal design of structured particulate pharmaceutical materials.
- Development of science-based methods for optimizing and controlling the processes involved in preparing structured organic particulate systems.
- Understanding of structure-property relationships through analyzing the physicochemical and functional characterizations of the products.

Chapter 2 describes the experimental details of this work, including apparatus used and characterization techniques. Trial experiments on a series of water-soluble polymers, polyvinylpyrrolidone (PVP), were conducted and the influence of the experimental conditions on the morphology and size of the polymeric particles were described. These results demonstrated the validity of our apparatus on treating polymeric materials and also provided preliminary data for further studies on formation of solid dispersion systems.

In Chapter 3, poly(DTE carbonate), a rationally designed biodegradable polymer for tissue engineering, was precipitated from its organic solution using dense gas carbon dioxide as antisolvent. The effects of the main process parameters, namely antisolvent addition rate, temperature, pressure, initial solute concentration, on product quality are discussed. The degree of agglomeration and particle size distribution are evaluated. The processing of this polymer into particulate states holds potential in extending its medical applications.

Chapter 4 and Chapter 5 elaborate on the formation of solid dispersion systems of prednisolone and its acetate salt using dense gas antisolvent technique. Spherical particles with controlled size distributions were generated and their physicochemical

properties substantiated the formation of amorphous drug in the solid dispersion. From FT-IR spectra, the interaction of the drug with the carrier was found responsible for the disappearance of the melting peaks of the drug in the DSC curve of the solid dispersion.

Chapter 6 further addresses the dense antisolvent processing on another poorly water-soluble drug, piroxicam, and the polymorphic transformation is addressed. In addition, the drug-polymer interaction was substantiated by spectroscopy. Finally, the dissolution performance of the solid dispersion was evaluated in comparison with corresponding physical mixture and that prepared by spray drying. The robustness of the dense gas antisolvent techniques was once more demonstrated.

Finally, the work concludes itself by summarizing the systems processed and pointing out the challenges currently bottlenecking the advancement of this technique, which will be the direction for future efforts.

## CHAPTER 2

### EXPERIMENTALS

#### 2.1 Dense Gas Antisolvent Precipitation

##### 2.1.1 Experimental setup

Dense gas antisolvent precipitation experiments were performed in semi-continuously on the apparatus shown in Fig. 2-1. The precipitation vessel consisted of a Jerguson gage (1, Northeast Controls, Upper Saddle River, NJ) with two borosilicate windows allowing a visual monitoring of the precipitation process. A high-pressure syringe pump (2, Teledyne, Thousand Oaks, CA) was employed to deliver organic solutions of API or its mixture with polymer into the precipitation vessel. Liquid carbon dioxide was pressurized using an air driven pump (Haskel, Costa Mesa, CA). Heat exchanger (4) was used to heat the CO<sub>2</sub> to desired temperature before entering the precipitation chamber. The operating pressure inside the precipitation chamber was controlled by manually manipulating a backpressure regulator (7, Tescom, Elk River, MN). A co-axial nozzle (5, Sonotek, Milton, NY) with inner and outer nozzle of 152  $\mu\text{m}$  and 800  $\mu\text{m}$  respectively was used to introduce organic solutions of polymer and compressed CO<sub>2</sub> cocurrently into the precipitation chamber. Downstream to the bottom of the vessel, precipitated products were trapped onto a 0.5  $\mu\text{m}$  stainless steel sinter filter (6, Swagelok, Mountainside, NJ) unit. After the precipitation, CO<sub>2</sub> and organic solvent separated in the cyclone separator (8, homemade).

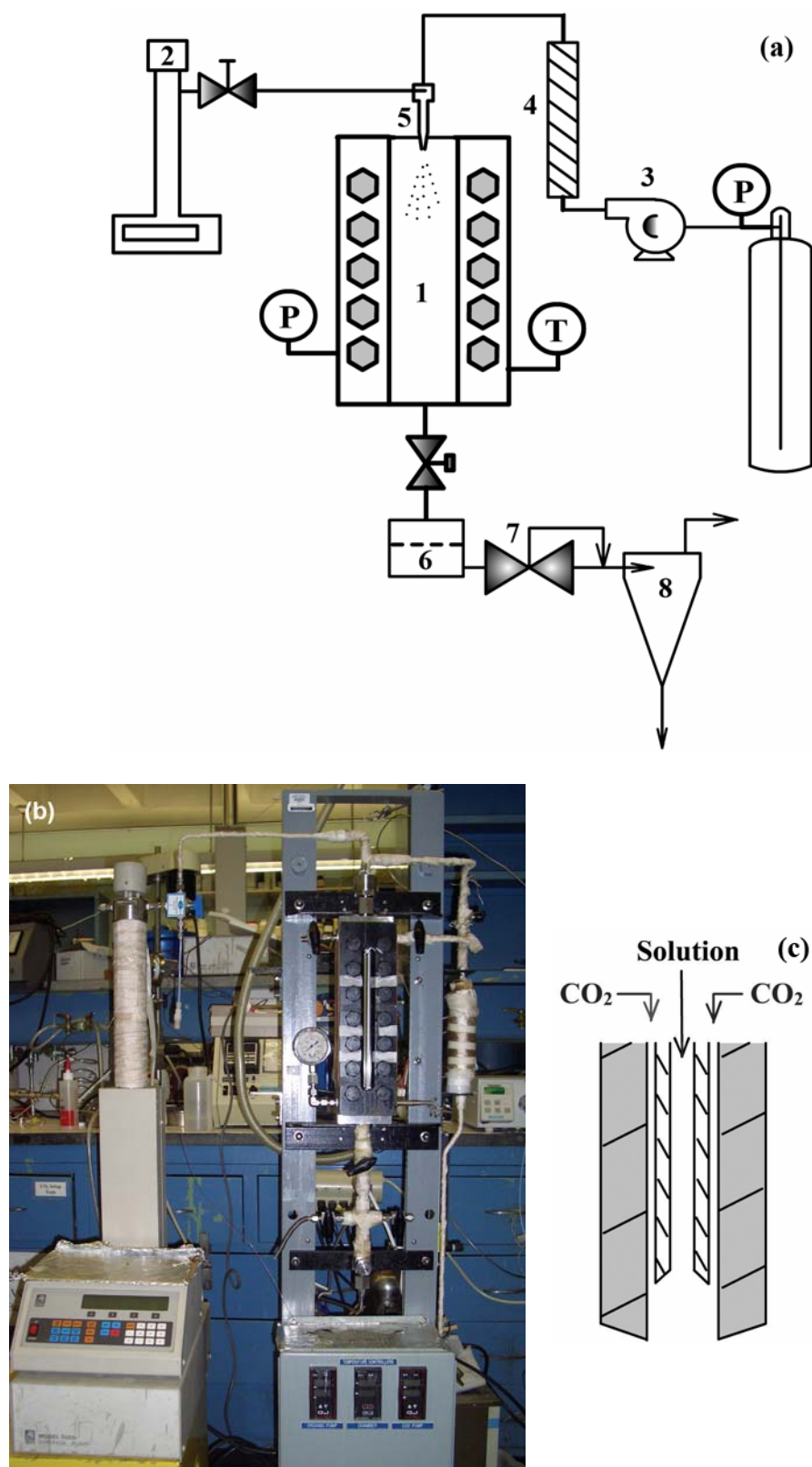


Figure 2-1. Schematics of (a) the dense gas antisolvent precipitation setup. 1, High pressure precipitation chamber; 2, HPLC syringe pump; 3, air driven pump; 4, heat exchanger; 5, injection nozzle; 6, metal sinter filter; 7, back pressure regulator; 8, cyclone separator. (b) photograph of the DGA apparatus, and (c) coaxial nozzle.

### **2.1.2 Experimental procedure of dense gas antisolvent precipitation**

The precipitation process proceeds as follows: We first prepared organic solutions containing either neat solute or mixture of solutes, and the solutions were loaded into the preheated HPLC syringe pump; on the other hand, liquid CO<sub>2</sub> from the tank was pressurized and heated to desired temperature in a heat exchanger and then pumped into the thermostated high-pressure precipitation chamber. After the whole system was equilibrated at desired conditions for 15-30 minutes, solutions and CO<sub>2</sub> were introduced into the precipitation chamber via a co-axial nozzle, with solutions flowing through the central capillary and CO<sub>2</sub> through the collar nozzle. The flow rate ratio of solution to CO<sub>2</sub> flow was set to maintain a CO<sub>2</sub> molar fraction. After the injection, compressed CO<sub>2</sub> flushed through the precipitation chamber for another 40-60 minutes to extract the residual organic solvent from the product. Then the system was slowly depressurized at the experimental temperature. Final products were collected from the filter element and kept in a desiccator. After CO<sub>2</sub> and organic solvent separated, finally gaseous CO<sub>2</sub> was vented into fuming hood. During the entire process, tubing and valves after the vessel were isolated to prevent freezing because of Joule-Thompson effect during the CO<sub>2</sub> expansion.

## **2.2 Spray Drying**

Solutions of piroxicam and its mixtures with PVP K25 in mixture of ethanol and acetone were fed into a mini spray-dryer Büchi Mini Spray Dryer 290 (Flawil, Switzerland) with a co-axial nozzle with co-current flow. The total concentration of the solutions was 5.0 % (w/v). The inlet temperature at the drying chamber was maintained between 363-383 K and outlet temperature was 333±5 K. The aspirator

setting was 35 m<sup>3</sup>/hr. The spray feed rate was 5.5 mL/min. The spray-dried powders were prepared in duplicate.

## **2.3 Preparation of Physical Mixture**

In some cases, physical mixtures (PM) of the API and polymer with varying mass ratios were prepared by mixing the two components until a homogenous mixture was obtained.

## **2.4 Morphological and Dimensional Characterization**

### **2.4.1 Scanning electron microscope (SEM) experiment**

The samples were fixed by double-sided conductive adhesive tape on aluminum stubs and covered with a 250 Å film of gold-palladium using a sputter coater. Then a scanning electron microscope (SEM, model AMRAY 1830I, Bedford, MA) was used to examine the morphology of samples at 20 kV accelerating voltage.

### **2.4.2 Image analysis**

The mean particle size (PS) and the particle size distribution (PSD) were measured using an image analysis performed using ImageJ program (a public domain Java image processing software provided by National Institutes of Health).<sup>103</sup> About 500-600 particles were randomly selected in each PSD calculation.

### **2.4.3 Laser diffraction particle size analysis**

In some cases, particle size distribution of samples was measured with a laser diffraction size analyzer (LS 13 320, Beckman, Fullerton, CA). Samples were suspended in deionized water with ultrasonication for 60 seconds. Dispersed samples

were then fed into the analyzer. Number size distributions were estimated based on the data collected.

## 2.5 Physicochemical Characterization

### 2.5.1 Powder x-ray diffraction (PXRD)

X-ray powder diffraction (PXRD) is a robust, non-destructive technique for identifying phases and probing crystallographic structures of materials. Typically, an X-ray diffractometer consists of an X-ray source, a sample holder, and a detector for the diffracted X-rays. Copper is the most common target material for single-crystal diffraction, with  $\text{CuK}_\alpha$  radiation =  $0.5418\text{\AA}$ . When the incident X-rays are directed onto the samples, the intensity of the reflected X-rays is recorded. When the geometry of the incident X-rays impinging the sample satisfies the Bragg Equation (Eqn. 4), constructive interference occurs and results in a peak in intensity. A detector tracks and converts the signal to a count rate which is then output to a computer.

$$n\lambda = 2d \cdot \sin(\theta) \quad \text{Eqn. 4}$$

Where

$n$  is an integer determined by the order given,

$\lambda$  is the wavelength of the X-ray,

$d$  is the spacing between the planes in the crystal lattice, and

$\theta$  is the angle between the incident ray and the scattering planes.

The X-ray diffraction patterns of samples were obtained on a Rigaku D/M-2200T automated diffraction system (Ultima+, The Woodlands, TX). Measurements were made under exposure of  $\text{Cu-K}\alpha$  radiation ( $\lambda=1.5418\text{\AA}$ ) in the range of  $2\theta = 3\text{--}50^\circ$ . The data were collected at room temperature with a step size of  $0.015^\circ$  and a counting time of 0.15 s/step at the operating power of 40 kV/40 mA.

### **2.5.2 Fourier-transform infrared spectroscopy (FT-IR)**

Infrared spectrometer is a versatile analytical instrument for identification and quantification of materials. A normal FT-IR spectrometer usually consists of a source, an interferometer, a sample compartment, and a detector. The IR beam from a glowing black-body source is "spectral encoded" in the interferometer. The resulting beam then interacts with the sample body or surface with specific frequencies of energy being absorbed. The detector measures the resulting special interferogram signal. This captured signal is then Fourier-transformed and processed into infrared spectrum.

In this work, infrared spectra were collected on a Thermo Nicolet FT-IR spectrometer (Avatar 360, Madison, WI). KBr pellets were prepared by first grinding mixture of sample and IR grade KBr (Sigma) with a weight ratio of 1:50-1:100 using agate pestle and mortar. Then this mixture was pressed into a pellet with a diameter of 12 mm. Then the samples were scanned over  $400\text{--}4000\text{ cm}^{-1}$ . The spectra were obtained by averaging 32 scans at a resolution of  $2\text{ cm}^{-1}$ . OMNIC 6.0 program was used to analyze the obtained spectra.

### **2.5.3 Differential scanning calorimetry (DSC)**

DSC is a common thermoanalytical technique to detect the difference in the amount of heat flow between a sample and reference when the sample undergoes a physical or chemical transformation. This difference is measured as a function of temperature with both the sample and reference maintained at the same temperature during the thermal program. This technique is very powerful to obtain many characteristic properties of a sample, such as melting temperature, crystallization temperature, and glass transition temperature, etc.

Our thermal analyses were performed on a DSC (TA instruments, Q 100, New Castle, DE) with nitrogen flow rate of 20 mL/min. Typically, about 2-5 mg of samples were placed in non-hermetic aluminum pans and underwent a heating procedure by preconfigured program at a scanning rate of 10°C/min. All the obtained curves were evaluated by the TA program

## **2.6 *In Vitro* Dissolution**

### **2.6.1 Assay of drug loading**

The content of piroxicam in the solid dispersion samples was determined using a SHIMADZU UV-Vis spectrophotometer (UV-2401PC, Columbia, MD). A 10 mg sample was dissolved in 100 mL methanol, and then 1 mL of the stock solution was diluted to 50 mL with simulated gastric fluid (SGF) without pepsin. Drug content was calculated from the absorbance measured at 334.0 nm.

### **2.6.2 Dissolution studies**

The dissolution rate of piroxicam samples was measured in a Distek 2100C dissolution test system (Distek, North Brunswick, NJ) using SGF at pH 1.2. In each dissolution vessel, quantities of samples equivalent of 10 mg  $\pm$  0.1 mg piroxicam were added to 500 ml dissolution medium. Bath temperature and paddle rotation speed were set at 37  $\pm$  0.5°C and 50 rpm, respectively. Regularly, the amount of dissolved drug was assayed using UV-Vis spectrometry at 334.0 nm. The dissolution tests were performed in duplicate.

## 2.7 Preliminary Experiments on Micronization of Polyvinylpyrrolidone (PVP)

We processed neat PVP of different molecular weights with pure methylene chloride (DCM) and then mixtures of DCM and acetone (Ace). With DCM as solvent, non-connected spherical particles were obtained, while agglomerated particles were collected with the solvent mixture (DCM/Ace). In addition, when precipitation was induced from solvent mixture of methylene chloride and acetone, smaller particles were obtained. Similar observations have been reported by Gokhale, et al.,<sup>104</sup> where mixture of methylene chloride and acetone was employed to reduce the particle size of polyvinylpyrrolidone.

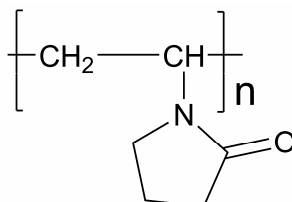


Figure 2-2. Repeat unit of polyvinylpyrrolidone (PVP).

Operating variables such temperature, pressure, concentration, flow rate, etc. were evaluated on their influence on the product morphology and particle size distribution.

### 2.7.1 Effect of temperature

We started our study by conducting test runs at various temperatures on neat PVP K25 (MW = 20,000) and PVP K29/32 (MW = 50,000). From Fig. 2-3(b)-(d), it is apparent that primary particle size of neat PVP K29/32 particles precipitated from methylene chloride slightly increases with higher temperature when the operating temperature was raised from 293 K to 308 K. More apparent phenomena were observed with PVP K25, as shown in Fig. 2-4(b)-(d), indicating the influence of the properties of the polymer on the final products.

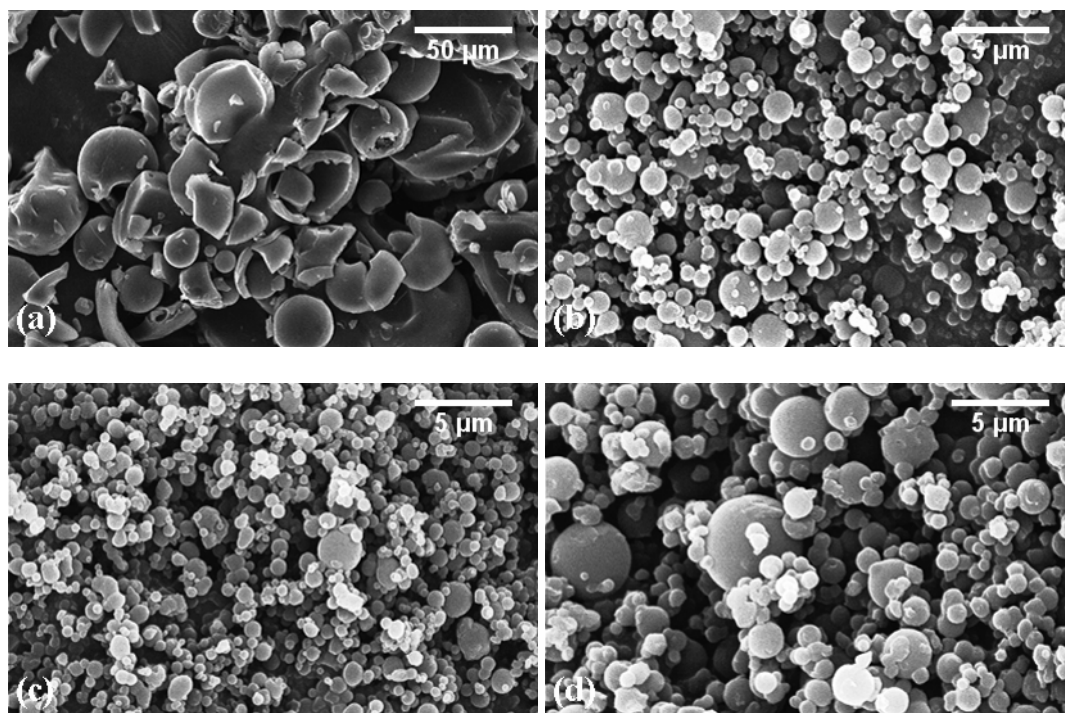


Figure 2-3. SEM micrographs of (a) as-received PVP K29/32, and PVP K29/32 particles precipitated at (b) 293 K, (c) 298 K, and (d) 303 K from methylene chloride. Pressure: 9.66 MPa, concentration: 3.0 % (w/v).

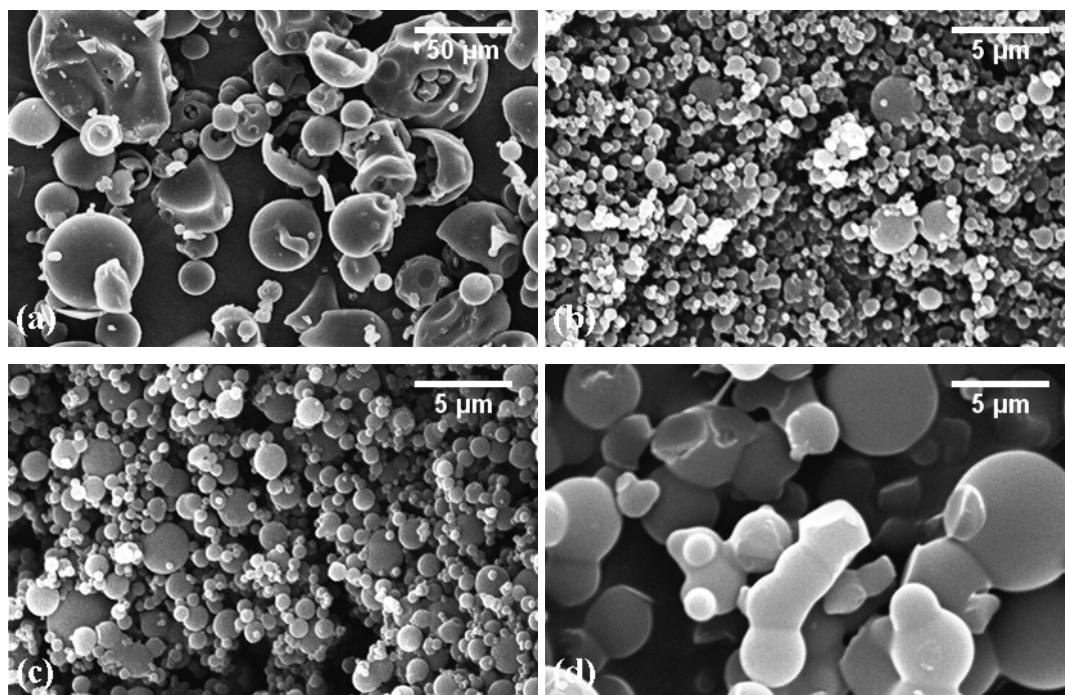


Figure 2-4. Temperature effect on size of PVP K25 after DGA: (a) as-received PVP K25, (b) 293 K, (c) 298 K, and (d) 308 K with solutions of 3.0 % (w/v) in DCM and 9.66 MPa.

In summary, temperature is an important factor in controlling the particle size of this specific family of polymers. Moreover, particles were more agglomerated with higher temperature as shown in products of both PVP K25 and PVP K29/32, leading to decreased surface area of the particular products. Consequently, ensuing coprecipitation experiments were performed at lower temperatures to minimize agglomeration of particles.

### 2.7.2 Effect of pressure

The dependence of particle size on the pressure at 298 K was assessed by varying pressure between 9.66-13.8 MPa. The pressure levels were maintained to ensure complete miscibility to carbon dioxide and the solvent. Within the pressure range studied, there was clear difference both in particle size and size distribution, as shown in Fig. 2-5. This can be explained in terms of density effect of liquid carbon dioxide.

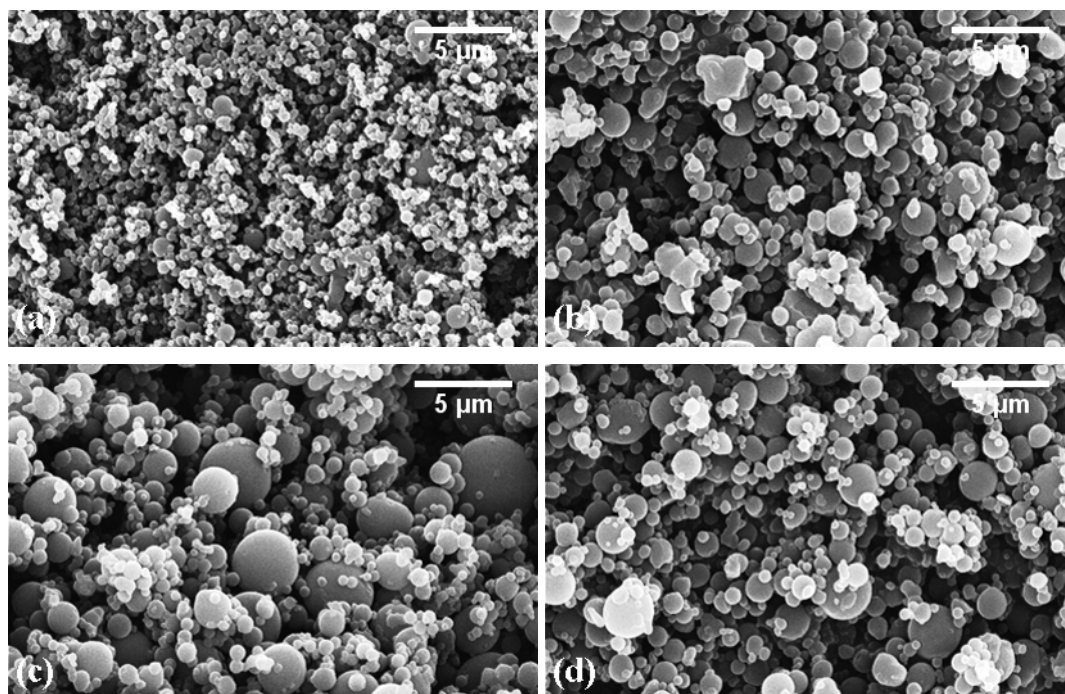


Figure 2-5. Pressure effect on size of PVP after DGA: (a) 9.66 MPa, (b) 11.0 MPa, (c) 12.4 MPa, and (d) 13.8 MPa with solutions of 3.0 % (w/v) in DCM and 298 K.

By graphing the density-pressure plot, it is clear that the difference in the density of the antisolvent is small. Because this precipitation experiments took place at subcritical conditions, the jet break-up played a critical role, especially since the substrate of interest is a macromolecular substance. Therefore, the Raleigh number will be determining factor to control the particle size.

### **2.7.3 Effect of concentration**

Concentration of the polymer solutions were changed from 1.0-8.0 % (w/v), and it is apparent from Fig. 2-6 that concentration were affecting the particle size, with smaller particles produced using 1.0 % (w/v) solution.

However, when the concentration of the solution was 1.0 % (w/v), the recovery of the final product was relatively low, which is because supersaturation could not be efficiently built up. On the other hand, however, products precipitated from 8.0 % (w/v) solution often caused clogging of the injection nozzle because of high viscosity of the solution. As a result, solutions with medium concentration range were adopted in our later studies.

### **2.7.4 Effect of molecular weight**

We also examined the influence of the molecular weights of the polymers on the particle size. However, the difference in the molecular weights could result in different phase behavior and glass transition temperature and lead to variation in yield and extend of agglomeration. This is compatible with our SEM observations of the products shown in Fig. 2-7, where PVP of different molecular weights were processed using dense gas antisolvent methods at same operating conditions.

As demonstrated in Fig. 2-7, particles were more agglomerated than those prepared with PVP of higher molecular weight. The smaller size of the primary particles was probably due to higher supersaturation ratio of the precipitation process because PVP of higher molecular weight have lower solubility in methylene chloride. In addition, with the same concentration, the viscosity of solutions with PVP of higher MW is higher, therefore, the solvent within the precipitates was more difficult to be extracted out, which facilitates the bridging of primary particles into agglomerated products.

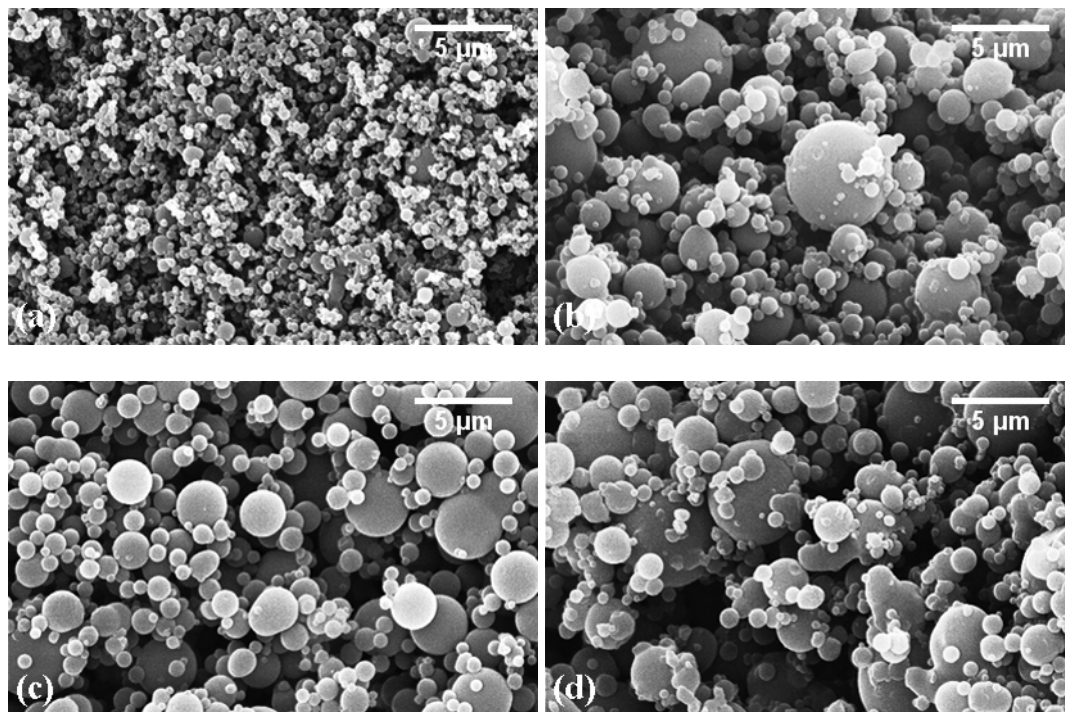


Figure 2-6. Concentration effect on size of PVP K29/32 after DGA: (a) 1.0 % (w/v), (b) 3.0 % (w/v), (c) 5.0% (w/v), and (d) 8.0% (w/v) with solutions in DCM at 9.66 MPa and 298 K.

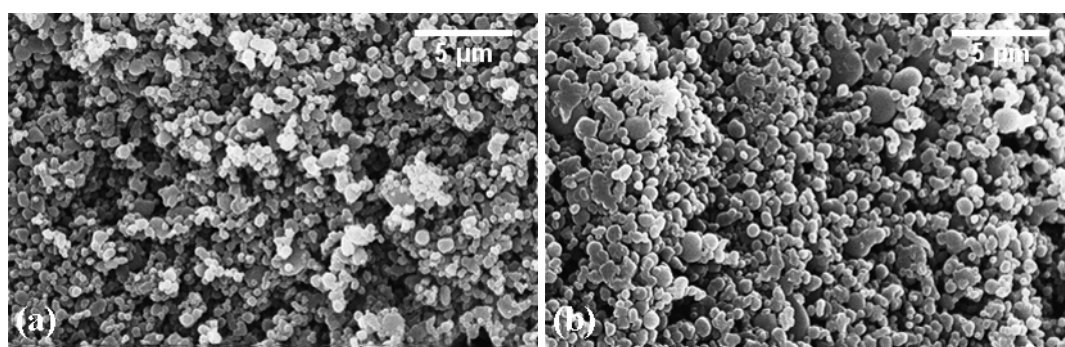


Figure 2-7. Molecular weight of PVP 3.0 % (w/v) in methylene chloride (DCM) at 9.66 MPa and 298 K. (a) K90 (MW = 1300,000) and (b) MW = 360,000.

## **2.8 Summary of preliminary study**

As demonstrated in these preliminary experiments, the morphology and particle size of the precipitated PVP particles were affected by a variety of factors including solvent, temperature, pressure, concentration, and molecular weight of the polymer, etc. We found that non-agglomerated micronic and submicronic particles were obtained at 298 K and 9.66 MPa with concentrations around 3.0-5.0 % (w/v) in methylene chloride. At the same time, the concentration of the polymeric solution and the molecular weight of PVP were also responsible for the morphology and degree of agglomeration of the products. Consequently, all the aforementioned operating variables will be cautiously manipulated in our study.

## CHAPTER 3

### PRECIPITATION OF A BIODEGRADABLE POLYMER USING DENSE GAS CARBON DIOXIDE AS ANTISOLVENT

#### 3.1 Introduction

Polymers performing biological functions are playing more and more important roles in pharmaceutical areas such as tissue engineering and drug delivery.<sup>105-107</sup> These polymers can either function by themselves or serve as matrix for the active pharmaceutical ingredients. Some biocompatible polymers are robust raw materials for medical devices with their special molecular structure and properties. For example, Poly(2-hydroxyethyl methacrylate) (PHEMA) was employed for manufacturing soft contact lenses. On the other hand, biodegradable polymers with controlled degradation profiles provide opportunities for time- and space-targeted drug release. For instance, polyanhydrides are a big family of biodegradable polymers synthesized as drug precursors and carriers, the degradation of which will produce or promote therapeutic efficacy with suppressed side products;<sup>108</sup> another example is poly(lactic-co-glycolic acid) (PLGA), which can be formulated with pharmaceuticals to prepare microencapsulates with controlled release of the active ingredient.<sup>109</sup>

To fully exert their functions, it is critical to process these polymers into physical forms with appropriate dimension and morphologies. An especially interesting form is spherical particle with well-defined size distribution, which improves the functionality of the polymeric materials. For instance, by micronizing the biologically active polymer, the degradation profile may be adjusted up to several folds; also, the drug-loaded polymeric matrix may offer modified release. Depending on the time and

extend of erosion or swelling of the polymer, drug release can be accelerated, delayed, or retarded.

Moreover, particle size and shape play important roles in pharmaceutical formulation by affecting the safety, stability and efficiency of product. Therefore, formulating these pharmaceuticals with polymers becomes increasingly crucial. Conventionally, the quality of micronized products is often jeopardized by mechanical or heat stress while the processing often brings about environmental issues. As “green” science and techniques are becoming more and more imperative, great efforts have been made to find milder and healthier solvents than volatile organic solvent (VOC).

Tyrosine-derived polycarbonates are a series of polymers that are of special interest in their physicomachanical properties, surface chemistry, degradation, and biocompatibility.<sup>110,111</sup> Among this series of biodegradable polymers, poly(DTE carbonate) (see Fig. 3-1) is the most suitable candidate to construct scaffolds for guided bone regeneration.<sup>112</sup> Conventional processing techniques have been used to shape it into spherical particles but only with partial success, especially in terms of organic residues. As was introduced in previous section, CO<sub>2</sub> is a poor solvent for many macromolecules such as polymers and proteins due to its low polarizability per unit volume and low cohesive energy density, which lays the ground for quite a few antisolvent methods based on similar principle as in a liquid antisolvent precipitation. Formations of polymeric particles with low organic residue and good reproducibility using DGA have been reported in number studies.<sup>113-116</sup> Therefore, it is our interest to resize this polymer using precipitation with dense gas antisolvent precipitation (DGA) process.

The work explores the relationship between processing conditions and the properties of final products through antisolvent precipitation or coprecipitation of structurally related and unrelated polymers, which in turn helps the understanding of the underlying mechanism of the DGA process. We utilized the DGA technique to explore the feasibility of processing the polymer poly(DTE carbonate) with the aim of preparing spherical, non-agglomerated particles. We studied effect of temperature, pressure, concentration of the polymer solution in organic solvent on the morphology of the precipitates. In addition, modification of thermal and solid state properties of the polymer after DGA treatment was also discussed.

### **3.2 Materials**

Polymer samples (MW = 84,000) were supplied by our collaborator and were synthesized according to published procedures.<sup>117</sup> Methylene chloride (99.5%), was purchased from VWR and used without further purification. CO<sub>2</sub> (99.9%) was supplied by Welco-CGI Gas Technology.

### **3.3 Results and Discussion**

Our preliminary studies indicated that solubility of the polymer in the carbon dioxide/methylene chloride mixture was sufficiently low to conduct antisolvent precipitation. Then, we investigated the morphology control of precipitates by testing the precipitation of polymer solutions under various conditions in order to reveal the relationship between the operating conditions and final products. In all experiments, the CO<sub>2</sub> flow rate was maintained at around 30 g/min and the molar fractions of CO<sub>2</sub> in CO<sub>2</sub>/methylene chloride mixtures during the precipitation varied from 0.90-0.99. Spherical particles were obtained at various pressure and temperature. An example comparison of poly(DTE carbonate) particles before and after DGA treatment is

shown in Fig. 3-2. DGA processing yielded spherical particles as opposed to the irregular shape of the raw material.

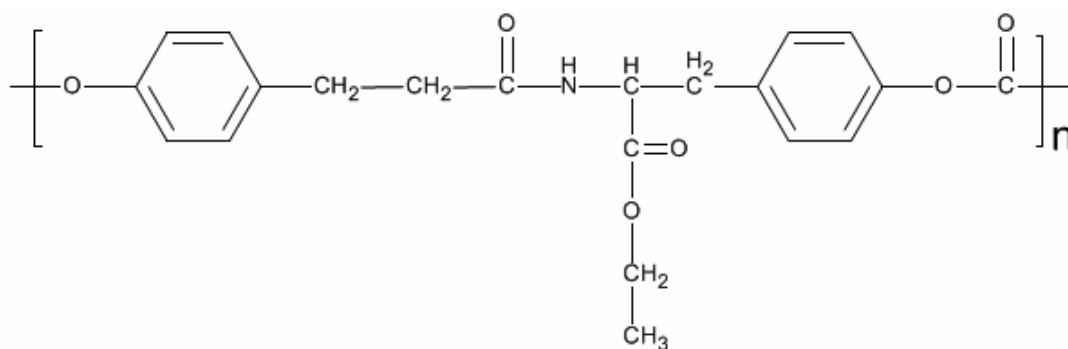


Figure 3-1. Repeat unit of poly(DTE carbonate).

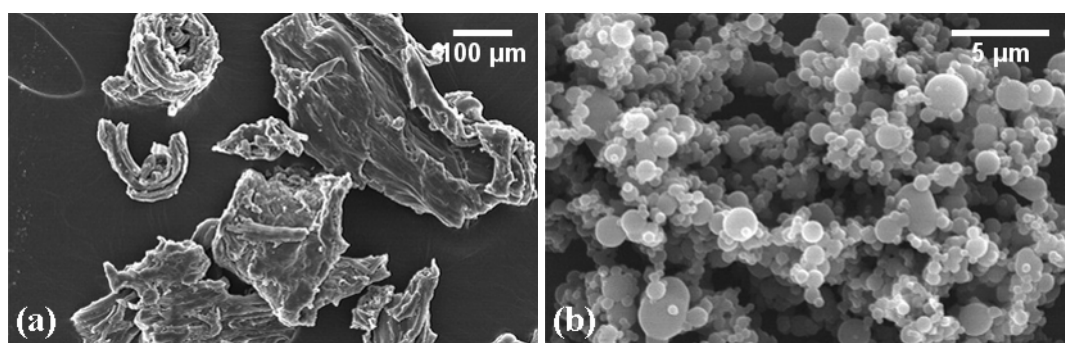


Figure 3-2. SEM of poly(DTE carbonate) before (a) and after (b) dense gas antisolvent processing.

### 3.3.1 Effects of pressure on the particle size

Similar to our preliminary studies on polyvinylpyrrolidone, we did not observe a clear correlation between the pressure and size of the particles in this study, although these two families of polymers are remarkably different in their structures. There have been diverse observations as to how pressure influences the size and morphology of the precipitates during dense gas antisolvent precipitation process, which is qualitatively explainable through phase behavior study.

### 3.3.2 Effects of temperature on the particle size

The effect of temperature on the products was more apparent than that of pressure with higher temperature favoring bigger primary particle size; in addition, the extent of agglomeration of resulted particles increased with higher operating temperature, as indicated in Fig. 3-3(c). The glass transition temperature ( $T_g$ ) of poly(DTE carbonate) is around 373 K at ambient condition. Because of the amorphous nature of the polymer, CO<sub>2</sub> molecules could slip into its interstitial spaces and act as lubricant. Therefore, the polymer could be partially plasticized, so the temperature was chosen to be appropriately below the  $T_g$  of polymer. As can be seen from the SEM images in Fig. 3-3(a) and (b), higher temperature seems to affect the size of primary particles, but the degree of agglomeration also increases. This is probably due to partial plasticization of polymer by CO<sub>2</sub> at elevated temperature and pressure, as the amorphous nature of this polymer and the carbonyl group in its molecular structure maybe favors the interaction of the polymer with carbon dioxide.

In addition, particles having a similar size range were obtained using both supercritical and near-critical carbon dioxide as antisolvent; this indicates that in this two-way mass transfer process, the inward diffusion of CO<sub>2</sub> is much faster than the

vaporization of the organic solvent. Moreover, the macromolecular nature of the polymer seems to weaken the dependence of the size and morphology of the product on the processing condition such as temperature and pressure.

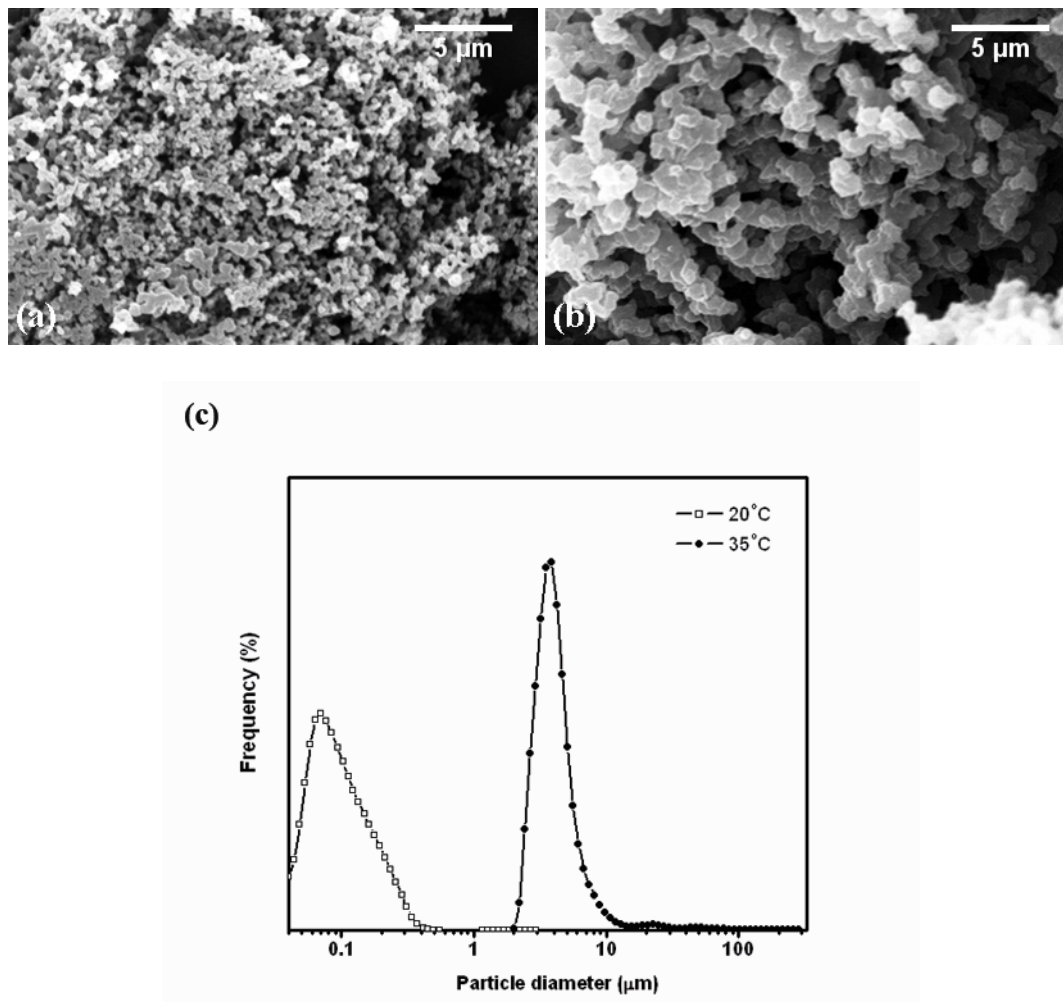


Figure 3-3. SEM images of poly(DTE carbonate) microspheres precipitated from DCM at 10.3 MPa and (a) 293 K; (b) 308 K, and (c) comparison of particle size distribution at the two temperatures.

### 3.3.3 Effects of solution concentration and the solution flow rate

The concentration of the poly(DTE carbonate) solution in methylene chloride varied from 0.5 to 5.0 % (w/v). The SEM micrographs of the products are shown in Fig. 3-4(a) and (b). Primary particle sizes are similar in spite of the difference in the solution to CO<sub>2</sub> flow ratio; however, higher initial solution concentration favored the formation of non-agglomerated particles. This is because the initial solvent content was lower so that the solvent could be extracted more readily. In addition, more uniformly distributed particles were obtained at higher concentrations, since higher initial supersaturation was reached which led to homogeneous nucleation. With solution concentration higher than 5.0 % (w/v), atomization of the solution became difficult due to increasing viscosity and fibrils formed as a result.

The flow rate of the solution injection affected the products in the similar way as the concentration did, which suggested the influence of phase equilibrium during the precipitation. However, flow rates higher than 5 mL/min often caused binary phases in the precipitation chamber and films were found on the filter instead.

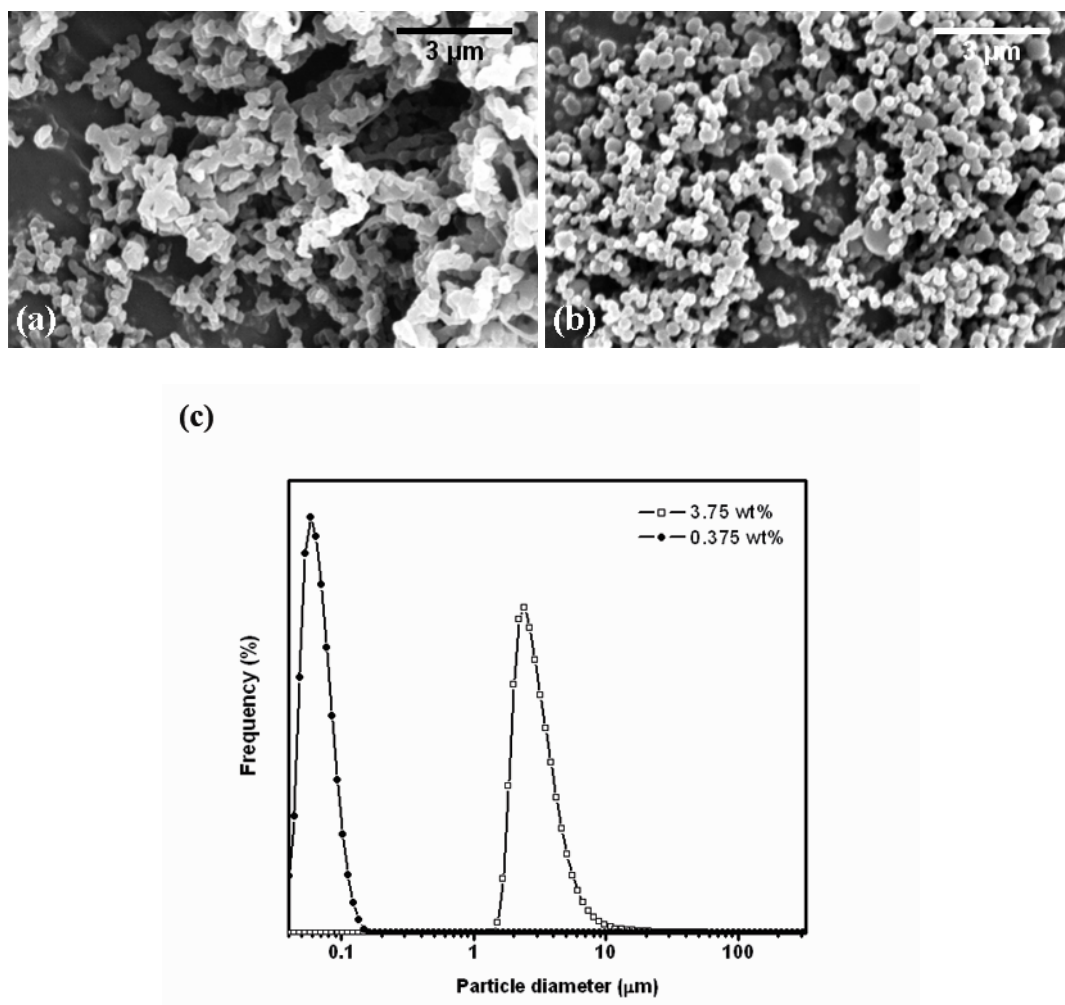


Figure 3-4. SEM image of poly(DTE carbonate) microspheres precipitated from DCM at 10.3 MPa and 306 K. (a) 5.0 % (w/v); (b) 0.5 % (w/v), and (c) comparison of particle size distribution at the two concentrations.

### 3.3.4 Physicochemical properties of the DGA-processed polymer

The glass transition temperature of some polymers, especially semicrystalline and amorphous polymers, may be depressed when pressurized with CO<sub>2</sub>. Because the antisolvent precipitation process takes place on a very short timescale, combined with the relatively slow crystallization kinetics of the polymers, this change is possibly locked in permanently. DSC curves of the polymer (Fig. 3-5) show the shift of the  $T_g$  to lower temperature upon DGA processing. This change in the thermal properties may have some mild impact on the mechanical and physical properties of the processed polymer. The rapid precipitation process decreases the crystallinity of the polymer, which can be confirmed by a comparison of the PXRD patterns before and after the CO<sub>2</sub> processing, as depicted in Fig. 3-6.

## 3.4 Conclusions

This study presents the precipitation of a biodegradable polymer with compressed carbon dioxide as antisolvent. The dense gas antisolvent technique is shown to be effective to micronize poly(DTE carbonate) into particles of sizes between 50nm to 10 $\mu$ m. The temperature, initial concentration and flow rate of polymer solution play a significant role in affecting the degree of agglomeration of the precipitates, which may be important for future applications in the field of tissue engineering. The thermal and solid state properties of the polymer were less affected by the pressure within the range chosen for this study, revealing that the intrinsic property of this polymer was the determining factor during the antisolvent precipitation.

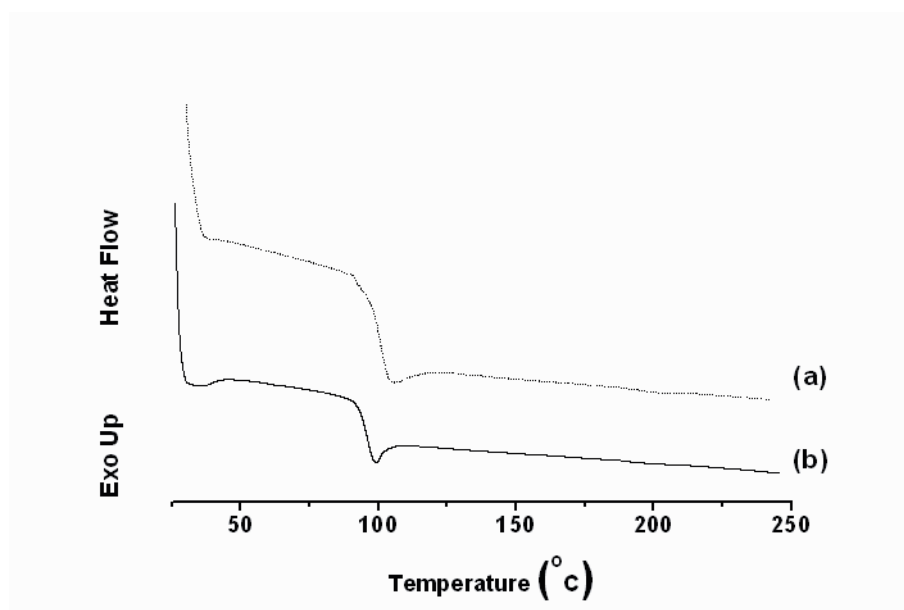


Figure 3-5. DSC curves of (a) as-received and (b) a typical DGA-processed poly(DTE carbonate)

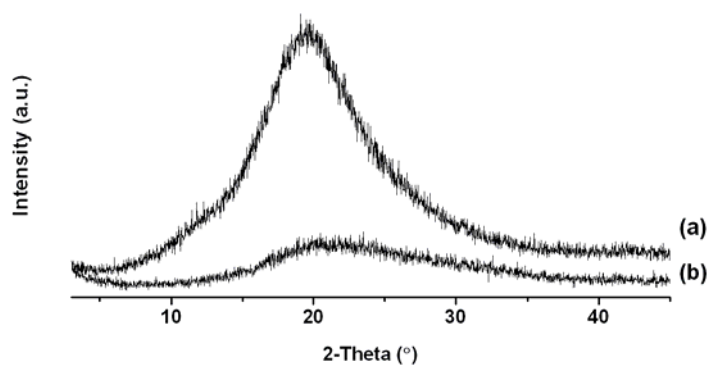


Figure 3-6. PXRD patterns of (a) as-received and (b) a typical DGA-processed poly(DTE carbonate)

## CHAPTER 4

# PREPARATION OF MICROCOMPOSITES OF PREDNISOLONE PREPARED WITH CONTROLLED DIMENSIONS

### 4.1 Introduction

Dense gas techniques are showing great potential for material engineering and processing because of the reduced environmental impacts and improved product qualities concomitant with these techniques.<sup>118</sup> Our interest focuses on the dense gas antisolvent processing because this technique provides flexible choice of solute-solvent couple and possibility of continuous operation, which are desirable for forming coprecipitates of multiple components.

The derivatives of dense gas antisolvent precipitation techniques, such as SAS, PCA, ASES, and SEDS, etc., differ in such aspects as location of experimental conditions relevant to the critical point of solute-solvent-CO<sub>2</sub> system, contact mode of solvent to antisolvent, and configuration of liquid atomization device, etc. In this work, we use the acronym DGA to represent the semi-continuous processes where liquid carbon dioxide, instead of supercritical CO<sub>2</sub>, was mostly used as antisolvent in our experiments.

Over the past several decades, numerous studies have been reported on DGA micronization of energetic materials, organic compounds, dyes and pigments, catalysts, macromolecules, and pharmaceuticals, etc.<sup>20,23,41,75,82,83,119,120</sup> The work in Chapter 3 serves as another example of its robustness. Currently (or Additionally), interests are being developed in formation of composite structures using this technique.<sup>14,19,32,37,77,121,122</sup>

As a branch of composite structures, solid dispersion systems have been frequently designed using dense gas antisolvent techniques to improve the

bioavailability of water-insoluble drugs.<sup>32,123-127</sup> This is because the intrinsic disadvantages of the preparation methods still hinder the development of solid dispersion techniques to attract wider commercial interest. Specifically, it is difficult to address stability issues and reproducibility of the physicochemical properties of products with conventional melting method and solvent evaporation method. For example, the application of melting methods is frequently limited by thermostabilities of active pharmaceutical ingredients (API) and excipients. On the other hand, usage of organic solvents in the solvent evaporation processes often jeopardizes the qualities of products, let alone the concomitant economic and environmental problems. Therefore, alternative solid dispersion techniques are critical for their advance towards commercialization. In fact, many technologies such as spray drying and freeze drying, etc. have been developed to alleviate the challenges associated with conventional methods. In terms of particle size and size distribution control, however, antisolvent precipitation with dense gas offers unparalleled advantages. Therefore, solid dispersion systems prepared with antisolvent dense gas techniques are highly desirable to lay further experimental groundwork for better understanding of the release mechanism and for products of satisfying quality.

In this work, we selected prednisolone (Fig. 4-1), an anti-inflammatory agent, as the model drug to form solid dispersions because of its pharmacological interest in anti-inflammatory and analgesic activities.<sup>128</sup> Solid dispersions of prednisolone with different formulations have been studied by traditional methods.<sup>129-131</sup> Therefore it is interesting to evaluate the feasibility of dense gas antisolvent precipitation processing to prepare microspherical solid dispersion systems with controlled size, smooth surface, and better flowability. Physicochemical properties of the products were

characterized and the comparative evaluation shows the efficacy of the dense gas antisolvent technique in formation of solid dispersion systems.

## **4.2 Materials**

Prednisolone was purchased from Sigma, inc. (99%); PVP with different K values were obtained from ISP Chemical Products Inc.; "bone dry" grade carbon dioxide (99.9%) was supplied by GTS-Welco, inc.; dichloromethane (99.95%) and acetone (99.8%) from VWR. All chemicals and reagents were used as-received.

## **4.3 Results and Discussion**

We started our preliminary studies by conducting antisolvent precipitation experiments on neat prednisolone. Then this drug and PVP K29/32 were coprecipitated using same method. Effect of solvent choice, temperature, pressure, and concentration of solution on the morphology of the products was evaluated.

### **4.3.1 Preliminary studies on antisolvent processing of drug**

Solubility of prednisolone in compressed carbon dioxide at different temperatures had been reported by Dean et al.<sup>132</sup> By extrapolating their data of prednisolone we were able to conduct dense gas antisolvent precipitation on this drug with proper selection of solvent systems. Though the presence of organic solvent might complicate the phase behavior of system,<sup>97</sup> this complicated situation was assumed negligible because of low concentrations of the solutes.

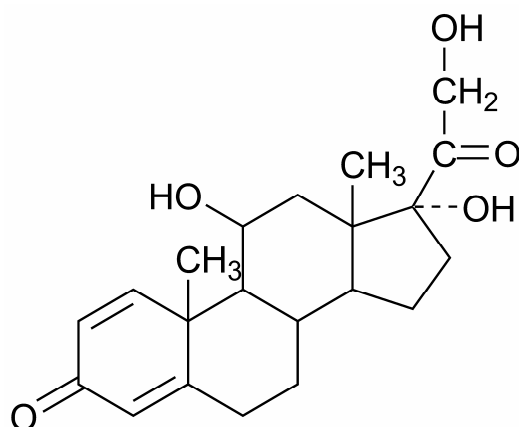


Figure 4-1. Molecular structure of prednisolone (Prd).

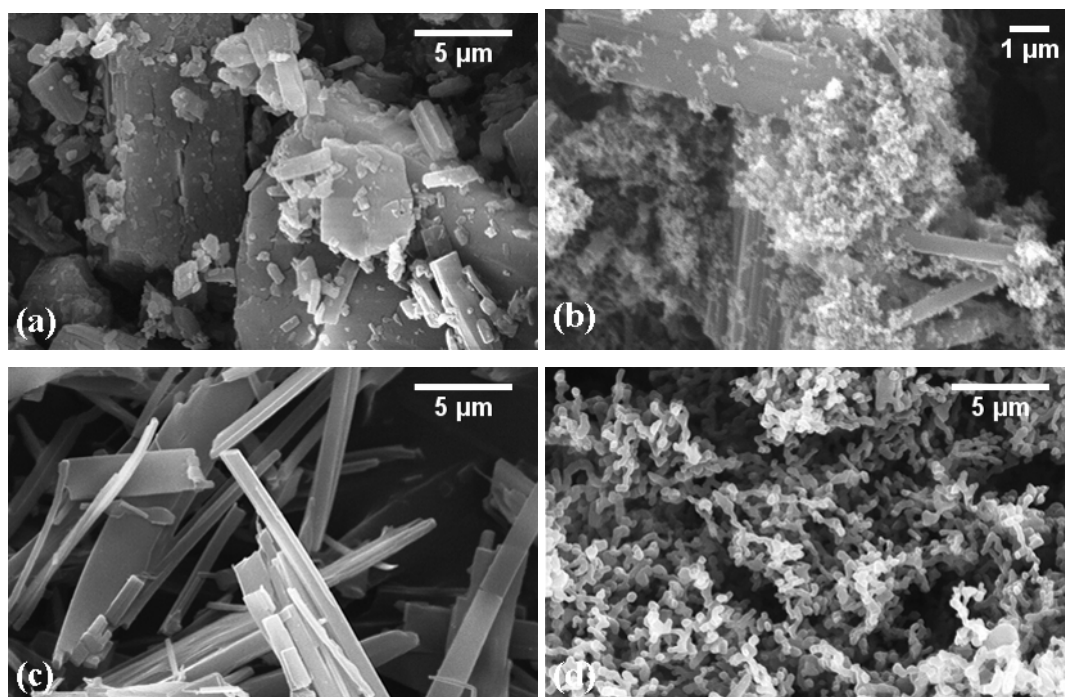


Figure 4-2. SEM micrographs of prednisolone before (a) and after dense gas antisolvent precipitation from (b) DCM/Ace ( $v/v = 4:1$ ), (c) DCM/Ace ( $v/v = 40:3$ ), and (d) EtAc/Ace ( $v/v = 1:1$ ).

Table 3. Experimental conditions of DGA treatment on neat prednisolone.

Substance	Solvent (s)	$C_{total}$ [% (w/v)]	$T$ (K)	$P$ (MPa)	SEM
Prd	DCM + Ace ( $v/v = 4:1$ )	0.4	298	9.66	Fig. 4-2(b)
Prd	DCM + Ace ( $v/v = 40:30$ )	0.5	298	9.31	Fig. 4-2(c)
Prd	EtAc + Ace ( $v/v = 1:1$ )	0.5	308	9.66	Fig. 4-2(d)

SEM micrograph of as-received prednisolone appeared irregular-shaped powder [Fig. 4-2(a)]. After the antisolvent precipitation from solvent mixture of methylene chloride and acetone with a volume ratio of 4:1, however, prednisolone particles appeared two different morphologies: spherical particles with diameters smaller than 200 nm and crystals with at least one dimension over 10  $\mu\text{m}$ , as shown in Fig. 4-2(b). Partial miscibility of solvent mixture and carbon dioxide at the studied experimental condition could be responsible for this heterogeneous product morphology. When methylene chloride and acetone ( $v/v = 40:3$ ) was employed as solvent, needle like crystals with aspect ratio greater than 10 were generally observed. Meanwhile, agglomerated nanoparticles were prepared when mixture of ethyl acetate and acetone were adopted. Therefore, choice of solvent is critical in controlling the crystal habit of the precipitates. Similar observation that choice of solvent or solvent mixtures were able to affect the crystal habit and polymorphic form of the precipitates had been reported in supercritical antisolvent precipitation of pharmaceuticals.<sup>133</sup> Because neither ethyl acetate nor acetone is good solvent for PVP, we skipped their mixture for further study.

#### **4.3.2 Coprecipitation of drug and polymer**

We used methylene chloride to dissolve mixture of prednisolone and PVP with a weight ratio of the drug to the polymer of 1:5. On the basis of the preliminary study, we further explored the effect of operating pressure, concentration and flow rate of the organic solution on the morphology and particle size of the coprecipitates. Because carbon dioxide is possible to extract more drugs at higher pressures, a moderate pressure range of 9-12.4 MPa was selected for study. In addition, solutions with total concentrations between 1.5–8.0 % (w/v) were tested considering that significant

supersaturation ratio during precipitation could be reached and meanwhile avoiding formation of fibrils at higher concentrations. Moreover, coprecipitates with polymers of different molecular weights were also compared in terms of product morphology and particle size distribution.

#### 4.3.3 Dependence of particle size and morphology on concentration of organic solutions

SEM analyses of the powders precipitated in these experiments showed that coprecipitates were spherical microparticles in spite of different concentrations in methylene chloride (Fig. 4-1). When the total concentration of the drug and polymer in DCM were increased from 1.5 to 8.0 % (w/v), there was subtle difference among the mean particle size of products while their particle size distributions were more uniform at medium concentration levels.

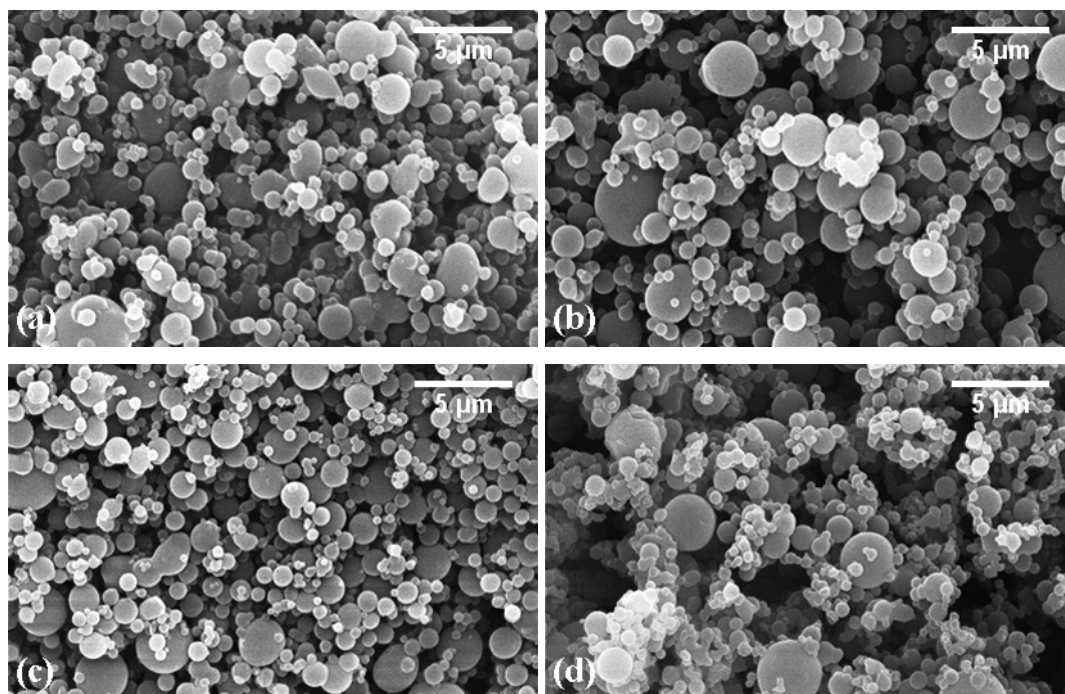


Figure 4-3. SEM micrographs of coprecipitates from solutions with concentration of (a) 1.5 % (w/v), (b) 3.0 % (w/v), (c) 5.0 % (w/v), and (d) 8.0 % (w/v) at 298 K and 9.66 MPa.

#### 4.3.4 Dependence of particle size and morphology on pressure

With the effect of the concentration in the liquid solution evaluated and optimized, the temperature was set at 298 K, the concentration of the organic solution at 3.0 % (w/v) and the pressure was varied from 9.66 to 13.8 MPa.

The effect of pressure was studied at 298 K with solution flow rate of 1.0 mL/min. The increase of pressure from 9.66 to 13.8 MPa did not affect the morphology of the particles when the concentration was 0.5 % (w/v). However, an increase of particle size and enlargement of particle size distribution (PSD) was noted with solution of 3.0 % (w/v). In Fig. 4-4(e), the PSDs of the powders obtained varying the pressure between 9.66-13.8 MPa are represented. All particle size distributions are similar with the mean particle size less than 1.0  $\mu\text{m}$ .

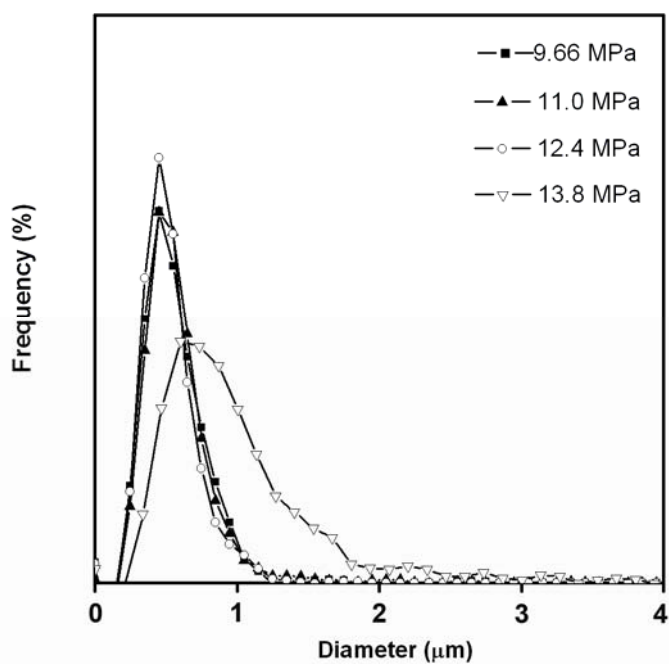
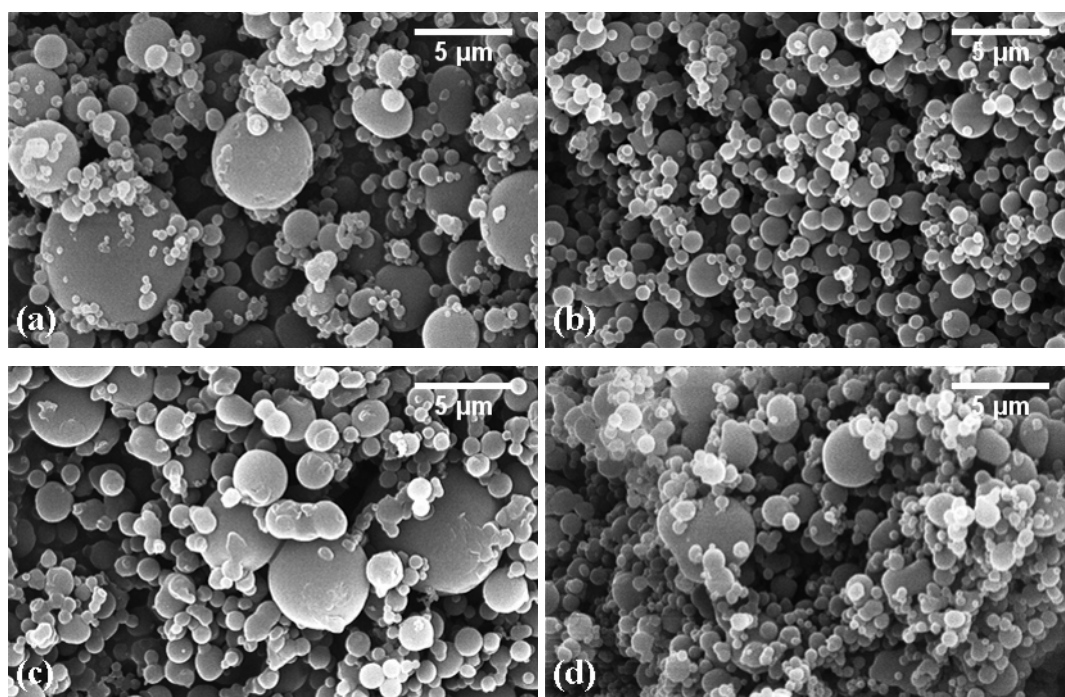


Figure 4-4. SEM micrographs of coprecipitated prepared solution with concentration of (a) 9.66 MPa, (b) 11.0 MPa, (c) 12.4MPa, (d) 13.8 % MPa, and (e) number particle size distribution of coprecipitates at 298 K using solution of 3.0 % (w/v) and drug/polymer ratio of 1:5.

#### 4.3.5 Effect of molecular weight of carrier

Polyvinylpyrrolidone with different molecular weights were tested using solutions with total concentration of 3.0 % (w/v) and drug to polymer weight ratio of 1:5. With increasing of molecular weight, particle size decreases (Fig. 4-5).

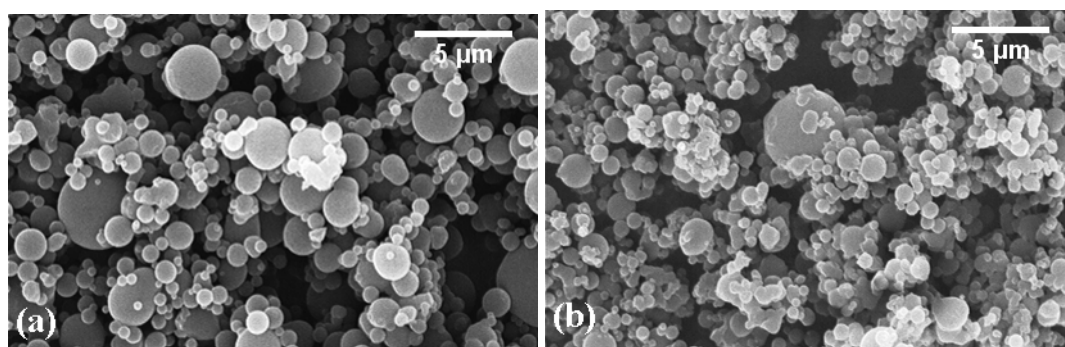


Figure 4-5. SEM micrographs of coprecipitates (w/w = 1:4) using (a) PVP K25 and (b) PVP K29/32 from solutions with concentration of 3.0 % (w/v) at temperature of 298 K and pressure of 9.66 MPa.

This observation seems to disagree with the mechanism from hydrodynamics of the antisolvent precipitation process, because atomization of solutions would be more difficult under same operating condition due to greater viscosity of the solution increased with higher molecular weight of the solute. Therefore, kinetics of precipitation process probably played more important role in this specific situation. Primary polymeric particles processed by dense gas antisolvent are often similar because of their relatively slower crystallization as opposed to smaller molecules, and thus particle growth would dominate. Effective collision of primary particles would produce bigger particles, which could be facilitated with lower viscosity of starting solutions.

#### 4.3.6 Physicochemical characterization of the coprecipitates

PXRD measurements were carried out to analyze the crystallinity of the drug in solid dispersion samples. For comparison, PXRD patterns of PVP K29/32, as well as their solid dispersions and physical mixtures are also shown in Fig. 4-6.

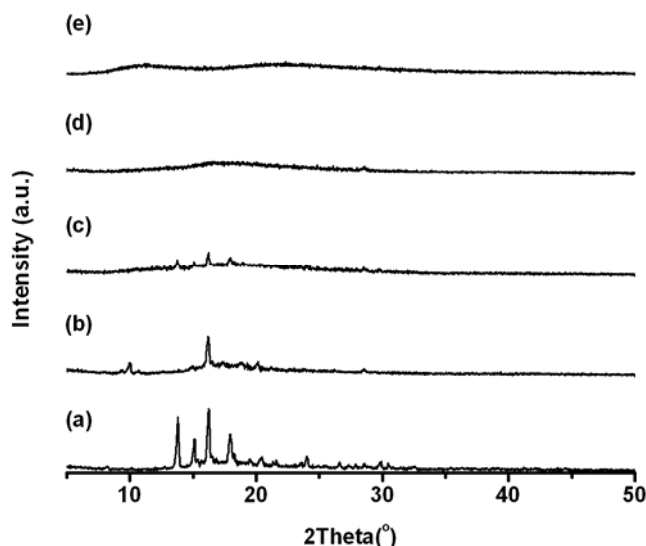


Figure 4-6. PXRD patterns of (a) as-received prednisolone, (b) dense gas treated drug, (c) physical mixture of drug and PVP K29/32, (d) coprecipitate of drug and PVP, and (e) neat PVP K29/32.

As-received prednisolone shows characteristic peaks between  $12.5\text{--}20^\circ$  corresponding to form II of prednisolone, according to Veiga et al.<sup>134</sup> After dense gas antisolvent treatment, crystallinity of the drug was significantly reduced. The fast antisolvent precipitation process could be responsible for these observations.<sup>135</sup> In addition, small peaks at around  $10^\circ$  indicated emerging of another polymorphic form. In fact, polymorphism as well as crystal habit could be adjusted by varying the composition of the solvent mixtures, as compatible with our SEM observations.

It is not surprising that the diffractograms of the physical mixtures were simply summation of the pattern of drug and that of the amorphous polymer because of the absence of drug-polymer interaction with mere physical contact. However, almost no

peak could be found in the diffraction pattern of the coprecipitate, showing loss of crystallinity after the dense gas antisolvent treatment. Because neat drug could retain certain degree of crystallinity after antisolvent treatment, it is our speculation that presence of PVP is possible leading to the loss of characteristic peaks of the drug. It has been reported that the interaction of drug with polymer molecules could prevent the drug molecules from packing in their preferable orientation.<sup>136</sup> On the other hand, selective adsorption of the polymer on certain growing faces of the drug crystals could also modify the crystallization of the drug.<sup>137,138</sup> Consequently, diffusion of drug molecules onto the growing surfaces was interrupted. Therefore, we further conducted spectroscopic study to probe the possibility of drug-polymer interaction.

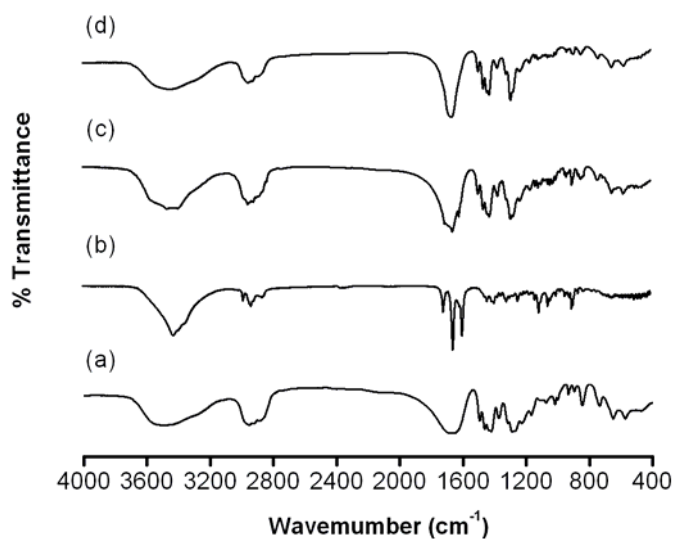


Figure 4-7. FT-IR spectra of (a) as-received PVP K29/32, (b) neat prednisolone, (c) physical mixture of drug and PVP K29/32, (d) coprecipitate of drug and PVP.

It is known that interactions at molecular level between the drug and the polymer could be reflected by specific band shifts and broadening in the FT-IR spectrum. In this case, each prednisolone molecule contains three hydroxyl groups which can form hydrogen bonds. Thus, theoretically, hydrogen bonding is possible between the drug

molecule and the polymer because there are carbonyl groups in the PVP molecules. In the FT-IR spectrum of its coprecipitate with PVP [Fig. 4-7(d)], the drug lost its characteristic carbonyl and hydroxyl group bands. As seen in Fig. 4-8, there is clear difference between coprecipitate of the drug with polymer and their physical mixture, which often indicates the existence of drug-carrier interaction. This kind of interaction is relatively weak according to Raghavan et al.,<sup>137</sup> because there is only one hydrogen bonding site per monomer unit with PVP molecules. We then performed DSC analysis on the coprecipitates to further detect the drug-polymer interaction.

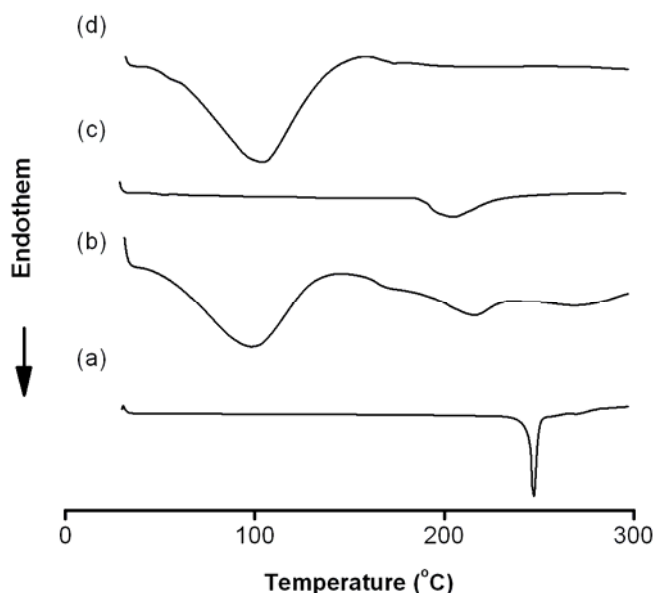


Figure 4-8. DSC curves of (a) as-received prednisolone, (b) physical mixture of drug and PVP K29/32, (c) coprecipitate of drug and PVP, and (d) neat PVP K29/32.

It was obvious from the DSC curves (Fig. 4-8) that the existence of PVP affected the melting peak of the drug either with or without drug-polymer interaction. Moreover, it is as suggested by the discrepancies of melting point of prednisolone in both samples that solid dispersion was formed after dense gas antisolvent precipitation. In this case, the melting endotherm of prednisolone in the coprecipitates appeared at much lower temperature than its corresponding physical mixture.

Combined with other PXRD patterns that we obtained, prednisolone is amorphously dispersed in the coprecipitate with hydrogen bonding between the drug and the polymer.

According to Sahin and Arslan<sup>130</sup>, performance superior to the physical mixture and the neat drug is desirable with the solid dispersion in terms of solubility. It is our next step to evaluate the solubility and dissolution behavior of the coprecipitates. Moreover, it is also interesting to further study the correlation of the physicochemical stability of the composite particles with the drug-polymer interaction. Data collected from these studies will facilitate the progress of optimizing formulations with dense gas technique towards industrial applications.

#### **4.4 Conclusion**

Precipitation with dense gas carbon dioxide as antisolvent was investigated for their potential to prepare composite particles of prednisolone embedded by PVP K29/32. We fabricated microparticulate solid dispersions of this poorly water-soluble drug with dense gas as antisolvent. Results of physicochemical characterizations of the solid dispersion samples indicated that the drug was dispersed in the polymer with hydrogen bonding. Microparticles containing amorphous prednisolone might provide modified dissolution properties of the drug. Meanwhile, optimizing the operating conditions of this technique is still necessary for product of controllable performance.

## **CHAPTER 5**

### **SIZE CONTROL OF PARTICULATE SOLID DISPERSION SYSTEMS**

#### **5.1 Introduction**

The pharmaceutical field is in ever-increasing need of formulations with better dissolution performance and higher bioavailability. Pharmaceutical materials with controlled size provide wide opportunities of improved processability and therapeutic efficacy. Therefore, size reduction of these materials is of great interest as the evolution of drugs from bench- to bed-side is increasingly bottlenecked by their limited bioavailability.

Pharmaceutical substances are conventionally micronized by either top-down or bottom-up methods. The former includes milling, crushing, and so on; while the latter includes chemical precipitation, spray drying, and freeze drying, etc. All these methods find their applications all over the pharmaceutical industry. However, the products of these techniques often suffer from undesired quality or performance. Furthermore, the bottom-up methods mentioned above often impair the controllability of particle size distribution due to limitations in the mechanism and kinetics of these processes. To overcome these disadvantages, more and more interests are focusing on developing alternative methods for particle formation, especially those addressing solubility and dissolution issues.

Since their origination, dense gas techniques have been frequently directed towards studies delivering micro-and nano-particles with controlled product qualities. Among increasing efforts in developing composite structures using this dense gas technique, synthesis of micro-particles and nano-particles incorporating double or

multiple components is of particular interest to address difficulties faced in pharmaceutical industry.

One of the urgencies for pharmaceutical companies is to improve the bioavailability of poorly soluble drugs. Solid dispersions, with certain advantages over micronization and other methods, have been progressively designed to this end; however, in- and post-preparation stability of the products, as well as product quality are still problematic with conventional melting method and solvent evaporation method. This difficulty defers the progress of solid dispersion systems towards more commercialization. In fact, many technologies such as spray drying and freeze drying, etc. have alleviated the challenges associated with conventional methods, such as thermo-stability, etc. For particle size control and environmental benignity, antisolvent precipitation with dense gas offers incomparable advantages. Moneghini et al.<sup>125</sup> proposed it for the first time by combining carbamazepine and PEG 4000 with GAS, then Juppo et al.<sup>139</sup> further proved that SEDS could be used to form intimate blends and solid solutions for drug and excipients. Subsequently, Meure tried ASES on coprecipitation of Copper indomethacin and poly(vinylpyrrolidone) (PVP);<sup>140</sup> more recent studies by Majerik et al.<sup>126,127</sup> reported the feasibility of SAS on Oxeglitazar and several polymers. Despite of increasing interests, studies on solid dispersion systems by antisolvent precipitation using dense gas are still scarce to provide an informative picture for further understanding the release mechanism and providing products of better quality.

In this work, we intended to produce composite particles of prednisolone acetate and PVP by using dense gas as antisolvent. We tried manipulating the composition of solvent mixture, pressure, and flow rate and concentration of solution to control product size. These two pharmaceutical substances had been individually precipitated

using compressed CO<sub>2</sub> as antisolvent,<sup>104,141</sup> which preliminarily rationalizes their coprecipitation. Physicochemical properties of the products were analyzed in order to evaluate the efficacy of dense gas antisolvent technique in particle size control of solid dispersion systems.

## 5.2 Materials

Prednisolone acetate (Fig. 5-1) was bought from Sigma-Aldrich, inc.; PVP K29/32 was obtained from ISP Chemical Products Inc.; bone-dry carbon dioxide (99.9%) was supplied by GTS-Welco; dichloromethane (99.95%) and acetone (99.8%) from VWR. All chemicals and reagents were used as-received.

## 5.3 Results and Discussion

Based on our previous experience, we set the system temperature at 298 K to avoid agglomeration of product due to plasticization effect of CO<sub>2</sub> on the polymer. Mixtures of methylene chloride and acetone were used to dissolve both the API and PVP. We first mixed these two solvents with varying volume ratios, and these mixtures were used as solvents to prepare solutions, then the solutions were introduced to meet with dense gas carbon dioxide to produce coprecipitates. Effects of solvent mixture, pressure, and flow rate and concentration of solution on the morphology of coprecipitates were evaluated.

### 5.3.1 Preliminary study on operating conditions

SEM micrograph of as-received prednisolone acetate appeared irregular-shaped powder [Fig. 5-2(a)]. Precipitation of prednisolone acetate from mixture of methylene chloride and acetone produced irregular particles with similar size of the raw materials, as shown in Fig. 5-2(b). When acetone was used as solvent, however,

particles with two different morphologies resulted depending on the operating temperature: irregular particles were obtained at room temperature while connected microcrystals were produced when experiment was conducted at 313 K. The phase behavior of the drug in presence of solvent and CO<sub>2</sub> is possibly responsible for the observation. The density of CO<sub>2</sub> decreases with the temperature, therefore, the solubility of the API in solvent/CO<sub>2</sub> is lower at higher temperature, leading to faster precipitation and hence finer particles. Moreover, because carbon dioxide at higher pressure may extract a significant amount of drug, a moderate pressure range of 9-12.4 MPa was studied. In addition, solutions with concentrations of 1.2-4.8 % (w/v) were tested under the premise that significant supersaturation ratio during precipitation could be reached while avoiding formation of fibrils at higher concentrations. Moreover, flow rate of organic solution was fixed at 1.0 mL/min while the flow rate of carbon dioxide was kept constant at 30 L/min. Detailed information of the experimental conditions can be found in Table A-8 in the Appendix.

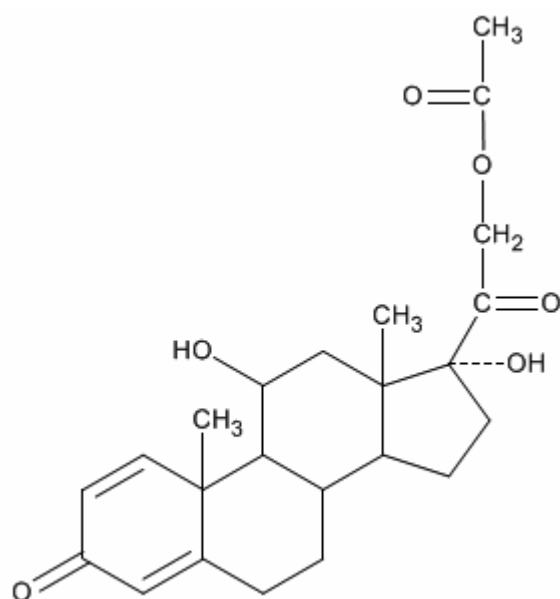


Figure 5-1. Molecular structure of prednisolone acetate (PrAc).

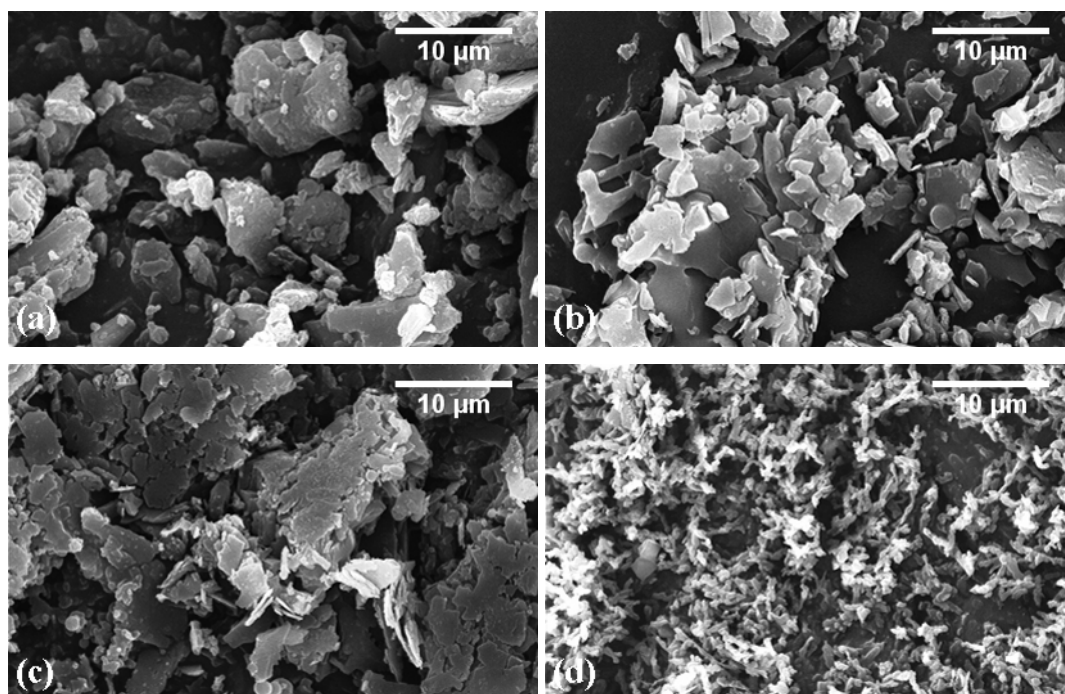


Figure 5-2. SEM micrographs of prednisolone acetate before (a) and after antisolvent treatment from solution of (b) DCM + Ace (v/v = 1:4) at 298 K, (c) Ace at 298 K, and (d) Ace at 313 K. Pressure = 9.66 MPa.

### 5.3.2 Dependence of particle morphology on solvent composition

Furthermore, we examined the influence of solvent strength on the particle morphology by mixing methylene chloride with varying proportion of acetone from 10-90 % (v/v). Co-existence of methylene chloride and acetone ensured the thorough solvation of both drug and polymer. This set of experiments were then carried out with a total concentration of 2.4 % (w/v) (D/P=1:5) and at a fixed pressure and temperature of 9.66 MPa and 298 K, respectively.

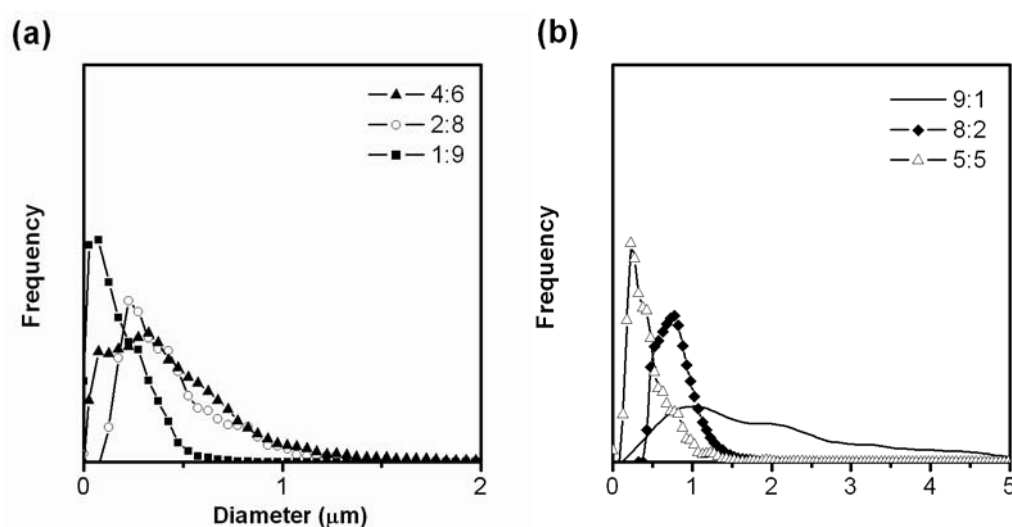


Figure 5-3. Particle size distributions of the samples prepared from mixture of methylene chloride and acetone with varying volume ratios. (a)  $V_{\text{DCM}}:V_{\text{Ace}} = 4:6, 2:8, 1:9$ ; (b)  $V_{\text{DCM}}:V_{\text{Ace}} = 9:1, 8:2, 5:5$ .

Varying the proportion of acetone in the solvent mixture changed the mean particle size, and shown in Fig. 5-3. With low acetone content of 10-30 % (v/v), mixtures of submicron- and microparticles were produced; meanwhile, nanoparticles with narrower particle size distribution were yielded when the content of acetone reached 80 % (v/v) and above. More complicated situations were seen when the acetone content was between 30-70 % (v/v). No monotonic relation of mean particle with volume percentage of acetone could be deduced. In addition, non-agglomerated

particles were produced with all the solvent mixtures, as opposed to the agglomerated particles formed when PVP K29/32 alone was treated under same experimental conditions.

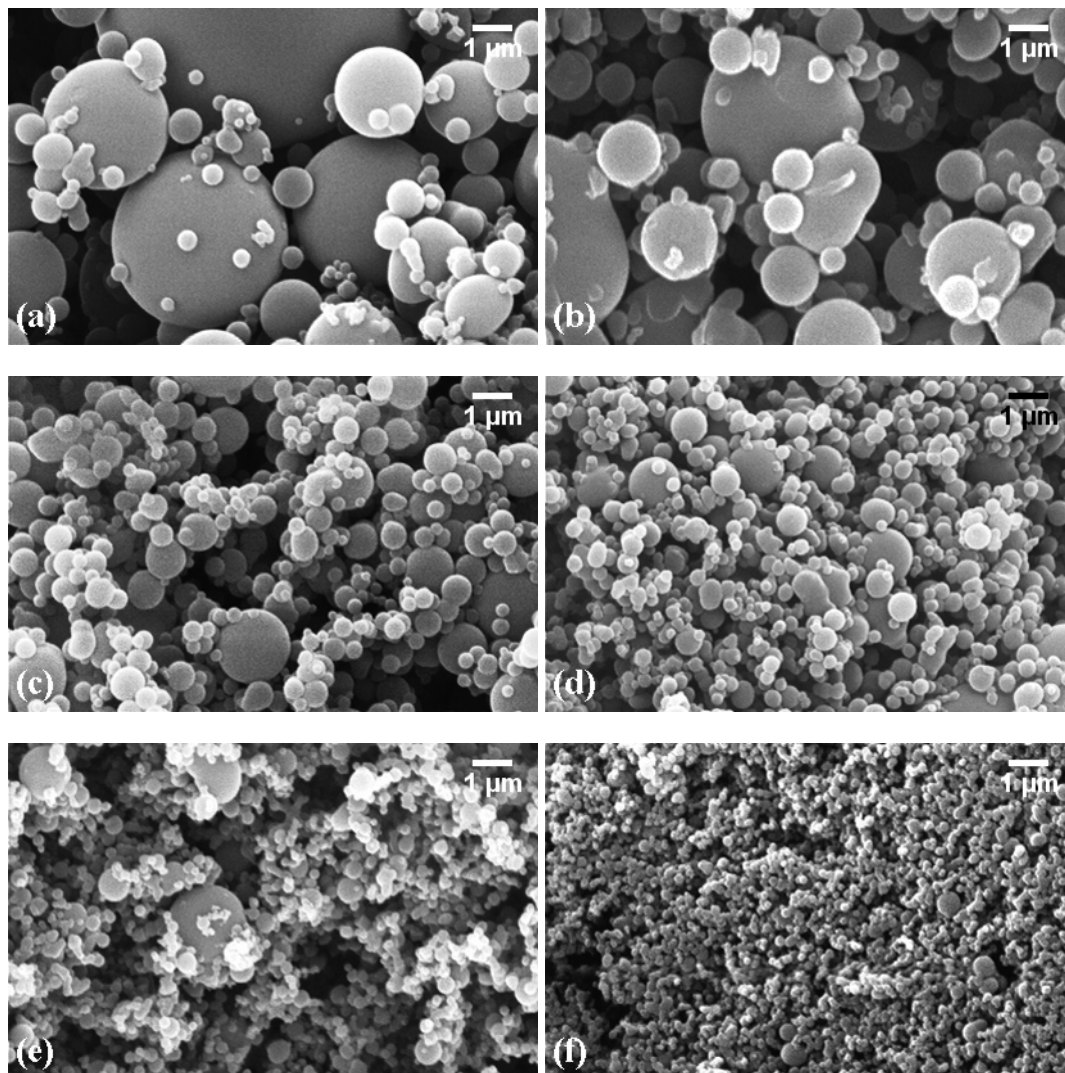


Figure 5-4. SEM micrographs of coprecipitates prepared from mixture of methylene chloride and acetone with volume ratio of (a) 9:1, (b) 8:2, (c) 4:6, (d) 5:5, (e) 2:8, (f) 1:9.

### 5.3.3 Effect of concentration of solutions on particle size distribution

The first set of runs was performed by varying the total concentration from 1.2 to 4.8 % (w/v), with drug/polymer ratio fixed at 1:5, at a pressure of 9.66 MPa and a flow rate of 1.0 mL/min. SEM images show that products precipitated as microparticles for concentrations up to 4.8 % (w/v) in DCM/Ace mixture (v/v=1:4). The products in Fig. 5-5 appear as spherical particles with smooth surface.

When the total concentration of the drug and polymer in DCM were increased from 1.2 to 4.8 % (w/v), there was subtle difference among the mean particle size of products while their particle size distributions showed more uniform at medium concentration levels.

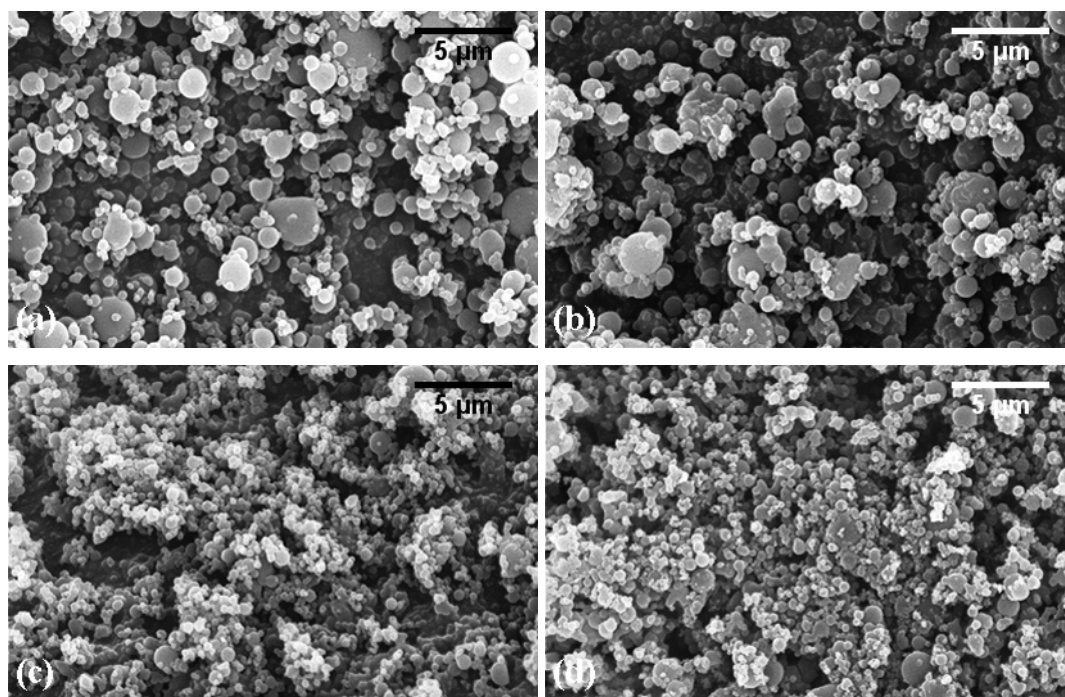


Figure 5-5. SEM micrographs of coprecipitated prepared solution with concentration of (a) 1.2 % (w/v), (b) 2.4 % (w/v), (c) 3.6 % (w/v), and (d) 4.8 % (w/v).

#### 5.3.4 Effect of pressure on particle morphology

After we studied the dependence of particle morphology on the concentration of solutions, we performed further experiments on the effect of pressure on product with same temperature and other working parameters. Considering the solvent-CO<sub>2</sub> phase behavior and the capacity of our apparatus, we tested the precipitation of solution [2.4 % (w/v)] with the pressure between 9.66-13.8 MPa.

The increase of pressure from 9.66 to 12.4 MPa did not have significant effect on the product size. However, higher pressure favored a more uniform particle size distribution, as shown in Fig. 5-7(a)-(c). At even higher pressure of 13.8 MPa, significantly larger particles were obtained. Fig. 5-7 shows the particle size distributions of the powders obtained varying the pressure from 9.66 to 13.8 MPa. It should be cautious to project the pressure effect beyond the range studied because we have examined only the medium pressure range. At lower pressures, complete miscibility of solvent mixture with CO<sub>2</sub> could be disturbed by the presence of solutes; while at higher pressures, increased solvation power of the CO<sub>2</sub> is no longer negligible which will complicate the precipitation process.

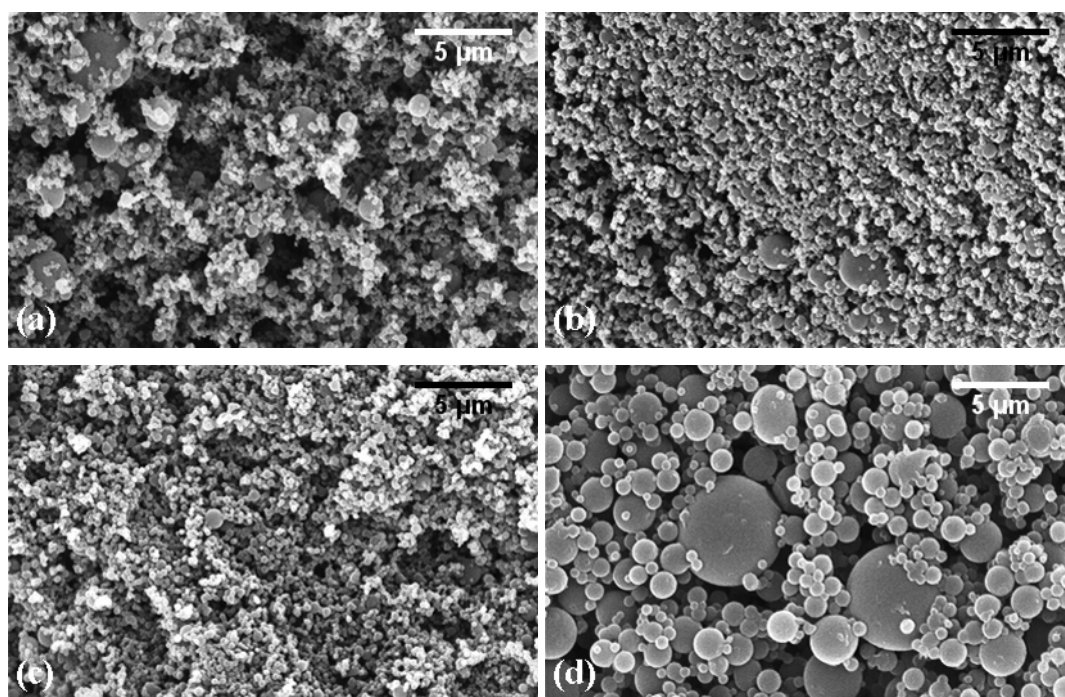


Figure 5-6. SEM micrographs of coprecipitates prepared at pressure of (a) 9.66 MPa, (b) 11.0 MPa, (c) 12.4 MPa, and (d) 13.8 MPa.

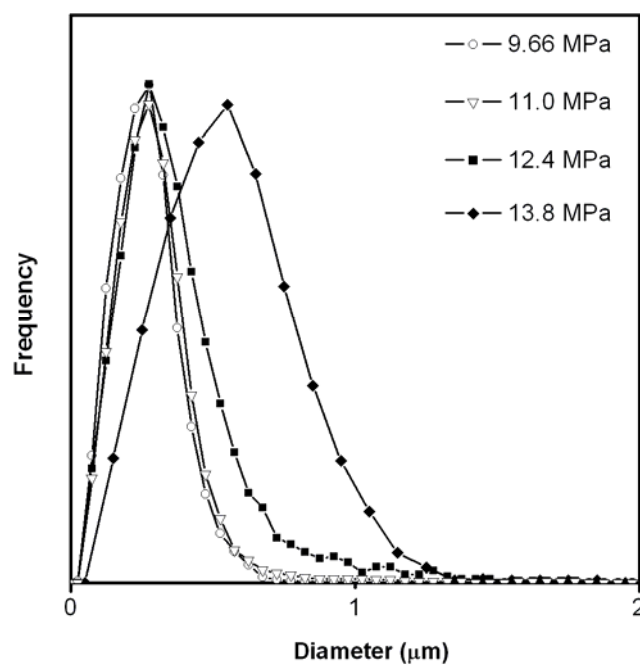


Figure 5-7. Particle size distributions of coprecipitates prepared at pressure of (a) 9.66 MPa, (b) 11.0 MPa, (c) 12.4 MPa, and (d) 13.8 MPa; (e) particle size distributions of the products.

### 5.3.5 Effect of weight ratio of drug to polymer on particle size distribution

Furthermore, we investigated the effect of concentration on particles size and size distribution by varying drug to polymer weight ratio, maintaining total concentration and other operating variables. As the proportion of polymer increased, coprecipitates evolved from mixtures of microcrystals and microparticles to spherical microparticles without subtle change in particle size, as displayed in Fig. 5-8.

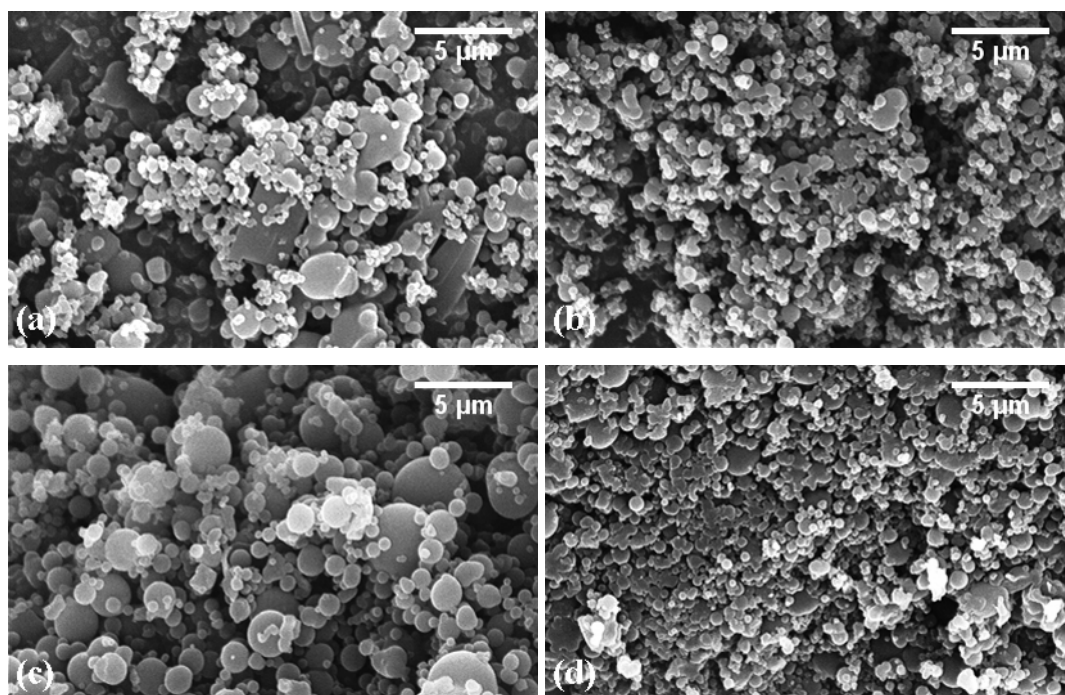


Figure 5-8. SEM micrographs of coprecipitates prepared with starting drug to polymer weight ratio of (a) 1:2, (b) 1:3, (c) 1:5, and (d) 1:9.

### 5.3.6 Physicochemical properties of coprecipitates from antisolvent processing

PXRD measurements were used to evaluate the crystallinity of the drug in solid dispersion samples. PXRD patterns of as-received drug and PVP K29/32, as well as their coprecipitate and physical mixture (D/P = 1:5, w/w) are paralleled in Fig. 5-9.

There was no clear change in the polymorphic form of prednisolone acetate in the physical mixture according to comparison of its PXRD pattern with that of neat drug.

This is not surprising because there is usually lack of drug-polymer interaction in physical mixtures. However, remarkable change in PXRD pattern was observed with DGA coprecipitates, suggesting modification of solid state properties after the antisolvent treatment.

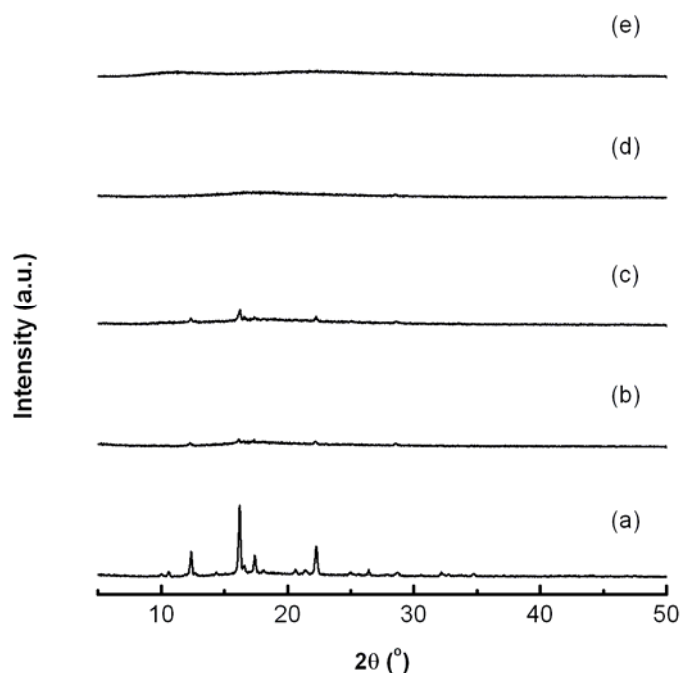


Figure 5-9. PXRD patterns of (a) as-received prednisolone acetate, (b) antisolvent processed drug, (c) physical mixture (w/w = 1:5), (d) coprecipitate, (e) as-received PVP K29/32.

There are three possible reasons for this observation. The first one involves the influence of the antisolvent processing on the drug molecules. Because the antisolvent precipitation process typically takes place within the timescale of  $10^{-6}$ - $10^{-4}$  s, the crystallization kinetics of the drug might not allow packing of molecules in their most stable form when the crystal growth rate is slower than the kinetics of antisolvent precipitation. This quenching process often leads to products with reduced crystallinity and disappearance of the PXRD peaks when amorphous product is formed. This speculation is partially supported by the PXRD pattern of antisolvent

processed neat drug. Therefore, the PXRD pattern of the coprecipitate of PrAc and PVP could be attributed to the antisolvent processing.

The second reason relates to the interference of polymer with the crystallization process of the drug when the crystal growth rate is significant faster than the kinetics of antisolvent precipitation. In this instance, the crystallization of drug is possible to be upset by the presence of polymer through different mechanisms. In some cases, structures of the drug and polymer molecules allow interactions such as hydrogen bonding through certain functional groups;<sup>136</sup> in other situations, however, the polymer molecules were selectively adsorbed on specific faces of the growing drug crystals, which prevents or retards the growth of the crystals in their inherent manners, resulting in modified crystalline properties.<sup>138</sup> Although there have been plenty of reports on the interaction of drug with polymer molecules in antisolvent processes, the loss of characteristic PXRD pattern of the drug doesn't necessarily results from the interaction as we discussed earlier.

To investigate the interactions between drug and polymeric, we collected FT-IR spectra of prednisolone acetate, PVP K29/32, their physical mixture, and coprecipitate. Prednisolone acetate contains a number of hydrogen donors (-OH) whose characteristic absorption bands are shown in Fig. 5-10(a). The spectra shown in Fig. 5-10(c) are simple summations of pure drug and PVP K29/32, suggesting no structure change of the polymer and drug and therefore absence of interaction. The FT-IR spectrum of the solid dispersions is significantly different from that of their physical mixture counterparts. This change was due to drug-polymer interaction and such interactions in drug-PVP solid dispersions were previously reported.<sup>142-146</sup>

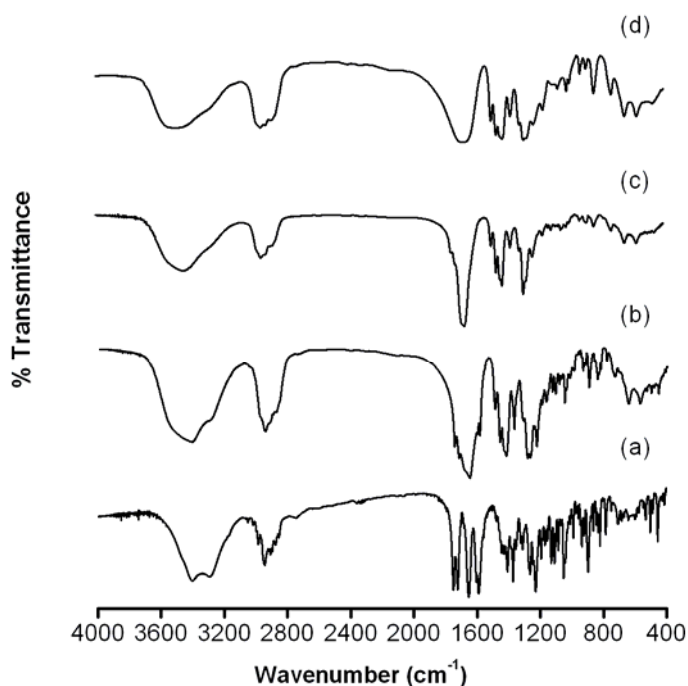


Figure 5-10. FT-IR spectra of (a) as-received prednisolone acetate, (b) physical mixture (m/m = 1:5), (c) coprecipitate, (d) as-received PVP K29/32.

Furthermore, we acquired the DSC endotherms of prednisolone acetate, PVP K29/32, their physical mixture, and coprecipitate to evaluate the thermal properties of the coprecipitate. In both physical mixture and DGA-prepared coprecipitates, the endotherm between 473-523 K was attributed to prednisolone acetate, as compared with the sharp endotherm with the as-received drug. And the melting peak shift of the drug indicates appearance of different phases in the physical mixture and the coprecipitate. Because the crystallinity of physical mixing with PVP could not change the crystallinity of the drug as confirmed the PXRD pattern, the lower melting point of the coprecipitate could be relevant to the amorphous state of the drug dispersed in the polymer.

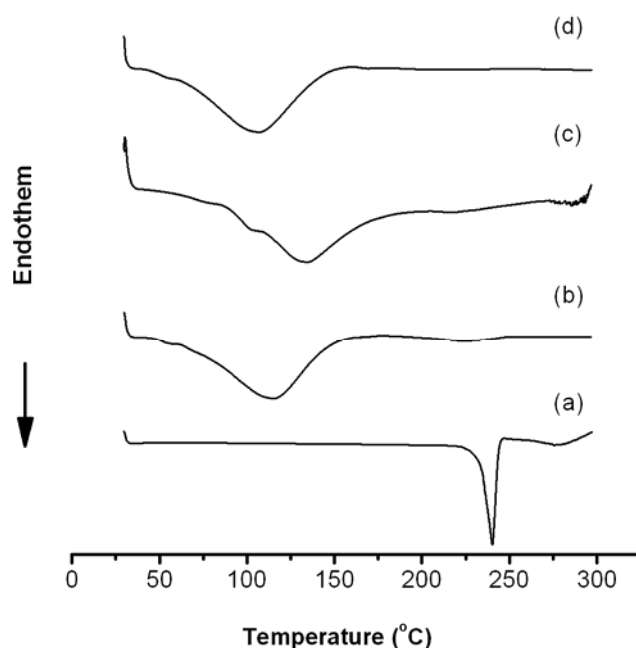


Figure 5-11. DSC curves of (a) as-received prednisolone acetate, (b) physical mixture (w/w = 1:5), (c) coprecipitate, (d) as-received PVP K29/32.

The third possibility is the combinatory effect of the polymer and the antisolvent processing with comparable kinetics of crystal growth and antisolvent precipitation. The addition of antisolvent triggers the crystallization of the drug molecules, the growing crystals can be frozen within the polymeric matrix because of the poorer crystallization tendency of the polymer. As a result, both crystal habits and crystalline properties can be modified, depending on the relative kinetics of the nucleation and growth rate of crystal with the interference of polymer.

Despite its preliminary character, this study shows the potential to control particle size of solid dispersions using dense gas technique. Because the size of solid dispersion systems have shown to affect their release profiles,<sup>130</sup> further studies on correlating the operating parameters with dissolution properties would enlighten us more about the structure-property relationship with the solid dispersions systems.

More systematic evaluation of dissolution of the coprecipitates will be included in our next study, which would provide more guidance on controlling the dissolution profiles of the products by changing of operating conditions.

#### **5.4 Conclusion**

This work presents our study on the control of particle size of the microcomposites of prednisolone acetate and polyvinylpyrrolidone using dense gas as antisolvent. The effect of total concentration of the solution, pressure and solvent composition on the particle size was investigated. It was found that the solvent composition had the most significant effect on the particle size and size distribution. Combined with physicochemical property characterizations, the interactions between the drug and polymer molecules were found responsible for the formation of composite structure. Further studies on the structure of the products will be conducted to understand the mechanism of dissolution.

## **CHAPTER 6**

### **PREPARATION OF SOLID DISPERSIONS OF PIROXICAM USING DENSE GAS TECHNIQUE**

#### **6.1 Introduction**

Solid dispersions have shown great potential to enhance the oral bioavailability of poor water-soluble drugs.<sup>8,9</sup> In typical solid dispersion systems, amorphous or low-crystalline drugs are embedded in hydrophilic carrier materials.

Over the last ten years or so, quite a number of attempts have been made to prepare solid dispersions of APIs in order to modify their release profile. Dissolution of the drug in its solid dispersion systems was often evaluated in comparison with that of its corresponding physical mixtures and drug alone. For example, the Won group formulated felodipine into solid dispersions with HPMC and surfactants by supercritical antisolvent precipitation method.<sup>123</sup> Later, Muhrer et al.<sup>124</sup> investigated solid dispersions of an anticonvulsant drug phenytoin with PVP K30 using compressed gas precipitation methods. In their study, precipitation with compressed carbon dioxide as antisolvent showed a promising method for development of solid dispersions. More recently, Majerik et al reported formation of solid dispersions of oxeglitazar with several water-soluble polymers using supercritical antisolvent (SAS) precipitation.<sup>126,127</sup> Comparing to raw drug, the resultant products exhibited significantly greater dissolution rate. As a technique of forming solid dispersions, antisolvent precipitation with dense gas is of increasing interest and more investigation will facilitate the development of pharmaceutical formulations with improved therapeutic performances.

In this work, piroxicam, a Biopharmaceutics Classification System (BCS) class II drug, was chosen as the model to form solid dispersions with PVP K25. This water-insoluble drug has been studied over years with the aim of improving its bioavailability; trials of its formulation using dense gas as antisolvent could provide us another opportunity of achieving desired dissolution profile. We used PVP K25 as carrier materials to form solid dispersions with piroxicam. Surface morphology and physicochemical properties of DGA-processed solid dispersions were characterized by scanning electron microscope (SEM), powder X-ray diffraction (PXRD), differential scanning calorimetry (DSC), and Fourier transform infrared spectroscopy (FT-IR), etc. In addition, dissolution profiles of the products were compared with those of corresponding physical mixtures. Comparative evaluation of the DGA products with their physical mixture counterparts demonstrates the efficacy of the DGA technique.

## **6.2 Materials**

Piroxicam (Fig. 6-1) was purchased from Sigma-Aldrich, Co., St. Louis, MO. Polyvinylpyrrolidone K25 (PVP) was obtained from International Specialty Products, Inc. (ISP), Wayne, NJ. Carbon dioxide (99.7%) was supplied by GT&S, inc., Allentown, PA. Ethanol (99.8%) was purchased from EMD Chemicals Inc. (Gibbstown, NJ) and dichloromethane (99.95%) and acetone (99.8%) from VWR International, West Chester, PA. All chemicals and reagents were used without further purification.

## 6.3 Results and Discussion

### 6.3.1 Preliminary studies

It is well-known that choice of solvents is critical for polymorph control of crystals during crystallization with SCF techniques.<sup>147,148</sup> In the current work, different solvent and solvent mixtures were compared under same operating conditions. SEM micrograph of as-received piroxicam appeared irregular-shaped powder [Fig. 6-2(a)]. After DGA treatment, microspheres were precipitated from mixture and ethanol and acetone compared with acicular particles from methylene chloride, as shown in Fig. 6-1(d). From their PXRD pattern, obviously form II was produced from methylene chloride while monohydrate from mixture of ethanol and acetone. For DGA treatment of PVP K25 at same conditions, little difference was observed with different solvents, however, higher yield was obtained with methylene chloride as primary solvent, probably because of minimal cosolvent effect under working conditions. Therefore, methylene chloride was chosen for production of solid dispersions in all following experimental runs.

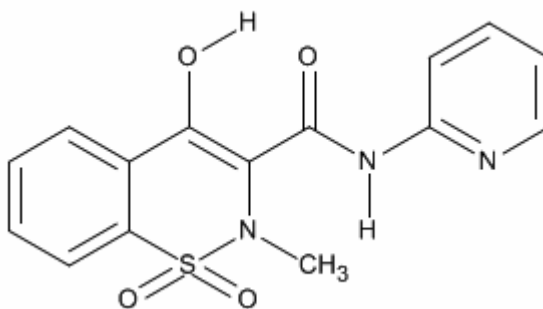


Figure 6-1. Molecular structure of piroxicam (Px).

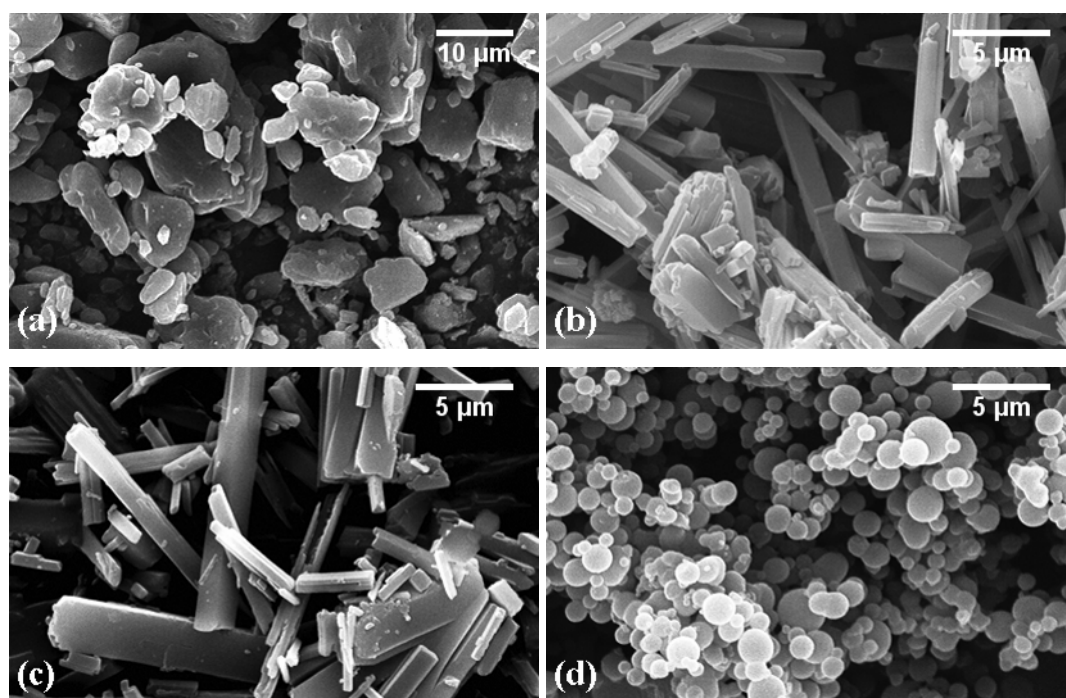


Figure 6-2. SEM micrographs of piroxicam before (a) and after dense gas antisolvent precipitation from (b) dichloromethane, (c) ethanol/acetone mixture (v/v=4:1), and (d) acetone.

Temperatures were varied from 298 K to 313 K. It turned out that higher temperature led to greater yield when precipitating piroxicam by itself, which confirms the solubility behavior of piroxicam in compressed carbon dioxide;<sup>149,150</sup> however, precipitation of PVP K25 was more successful at lower temperature. Therefore, liquid carbon dioxide ( $T = 298$  K) instead of supercritical carbon dioxide was chosen as antisolvent to avoid worse agglomeration of products with increasing temperature. A moderate pressure range of 8.0-11.0 MPa was studied.

Lower pressure yielded more particles of piroxicam but less PVP powder. To balance both yield and achieve complete miscibility of solvent with carbon dioxide, all experiments were conducted at 9.66 MPa. In addition, a total concentration of 5.0 % (w/v) ensured significant supersaturation ratio during precipitation while avoiding formation of fibrils at higher concentrations. Finally, flow rate ratio of liquid solution to carbon dioxide was set at 1:300 as a balance to the capacity of the apparatus and the working efficiency of the treatment. Effect of temperature, pressure, and concentration of solution on the morphology of precipitates and coprecipitates were evaluated.

### **6.3.2 Effect of Px/PVP weight ratio on the morphology of products**

Transition of morphologies of DGA-prepared solid dispersions with varied drug-polymer weight ratios (D/P) is clearly shown in Fig. 6-3. At lower PVP contents, acicular particles were still discernible, though the aspect ratio was decreasing with increasing amount of PVP K25; With D/P of 1:2 and above, microparticles were produced and there was only subtle difference in morphology and size, as displayed in Fig. 6-4. Under the same operating conditions, no correlation between the weight ratio and mean particle size could be deduced, which is not surprising because interplays

among mass transfer, hydrodynamics, and thermodynamics control the shape and size of precipitates during the DGA process.<sup>87</sup> Further exploration of the effect of working parameters on final products will facilitate the improvement of product quality.

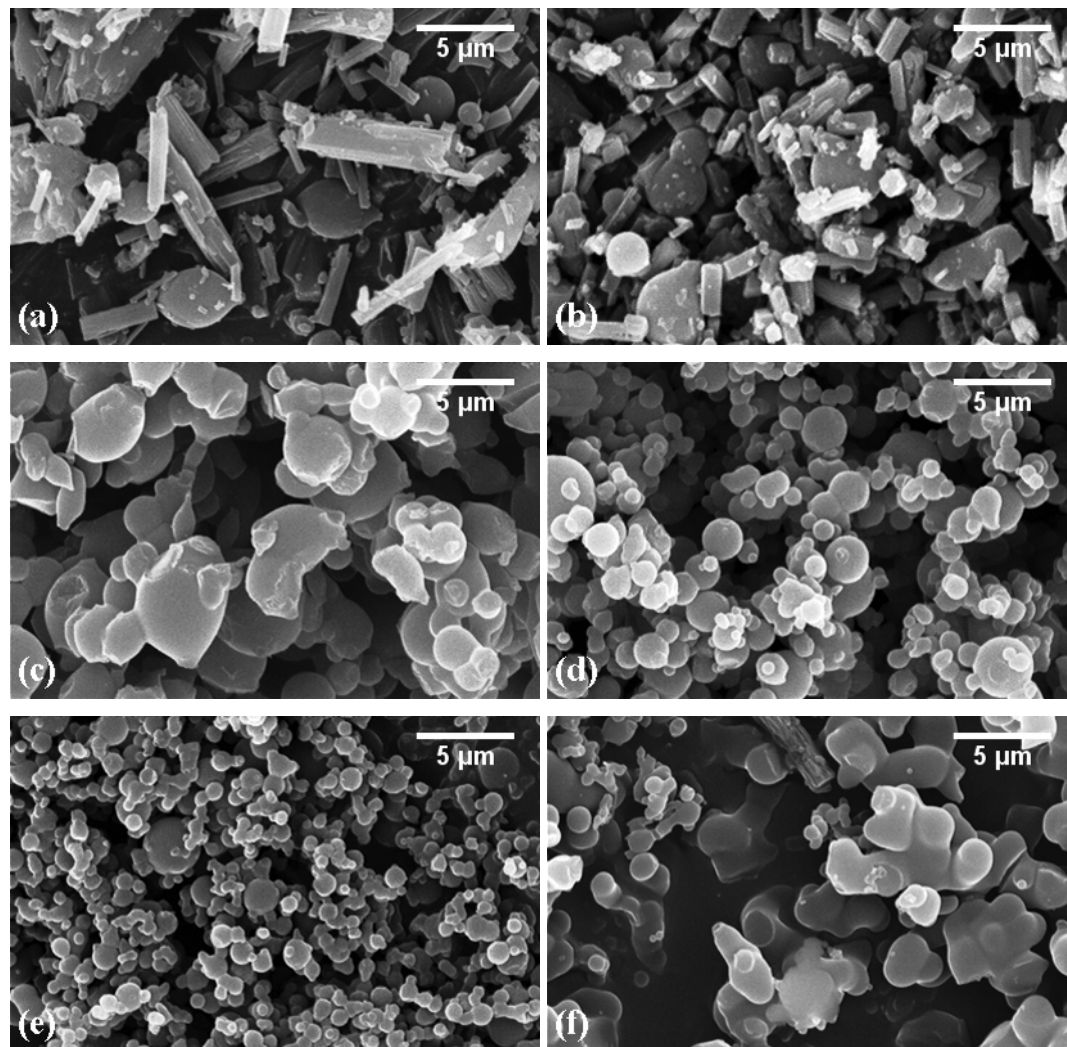


Figure 6-3. SEM micrographs of DGA precipitate of (a) pure Px, and coprecipitate of Px and PVP with a D/P of (b) 2:1, (c) 1:1, (d) 1:2, (e) 1:4, and (f) 1:9.

### 6.3.3 Crystallinity and polymorphic purity

PXRD experiments were performed to examine the crystallinity of the drug in the coprecipitates. For reference, PXRD patterns of piroxicam, PVP, and their physical mixtures are paralleled in Fig 6-4.

Piroxicam has three polymorphic forms and a monohydrate. As-received piroxicam characteristic peaks at 8.99, 15.76, 23.02, and 25.85° corresponding to cubic form of piroxicam, which is also the most stable form.<sup>151</sup> The PXRD patterns in physical mixtures were similar to that of raw piroxicam indicating lack of drug-polymer interaction because of no distinct crystallinity change of piroxicam in the physical mixtures. In DGA-prepared coprecipitates, however, significant changes in PXRD patterns were observed with varying D/P, showing modification of solid state properties after the DGA treatment. A loss of crystallinity was found with weight ratio greater than 1:2 and drug was presumably converted into either amorphous phase or nanoparticles dispersed in the polymer, depending on the extent and intensity of the drug-polymer interaction.<sup>142</sup> Because precipitation of piroxicam by itself from methylene chloride produced acicular particles, the involvement of PVP K25 could be responsible for this observation through inhibiting the growth of piroxicam crystals. This is compatible with former reports that the interaction of drug with PVP molecules prevented the packing of drug molecules in their preferable orientation.<sup>152</sup> Moreover, between the weight ratio of 1:1 and 1:2, there could be a threshold value of weight ratio when interaction sites are saturated. Above this threshold, the dispersion amount and state of the API could be further adjusted.

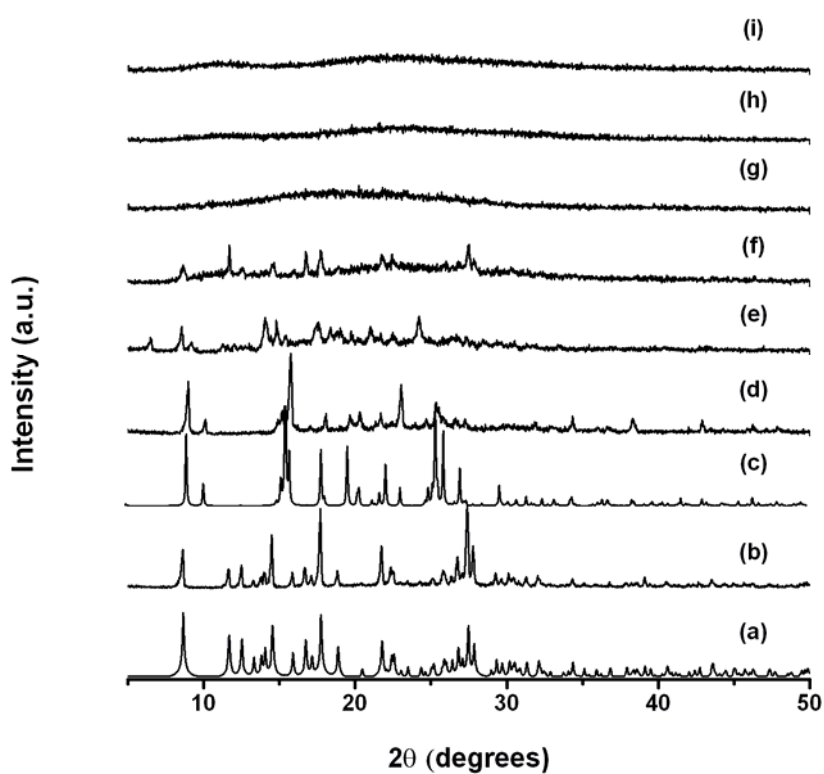


Figure 6-4. PXRD patterns of (a) simulated form I piroxicam (Px), (b) Raw Px, (c) simulated form II Px, (d) DGA-processed Px, (e) spray-dried (SD) Px, (f) physical mixture (PM) with drug-to-polymer weight ratio of 1:4, (g) DGA coprecipitate (starting drug to polymer weight ratio = 1:4), (h) spray-dried solid dispersion (starting drug to polymer weight ratio = 1:4), and (i) as-received PVP K25.

#### 6.3.4 Thermal analysis

DSC measurements were carried out on piroxicam, PVP K25, their physical mixture, and coprecipitates to evaluate the thermal properties of the solid dispersions.

As shown in Fig. 6-5, the endotherm around 475 K is the melting peak for the cubic form of piroxicam. With increasing content of PVP, this endotherm shifted to lower temperature in physical mixtures. Similar phenomenon was seen with the DGA coprecipitates. In both physical mixtures and DGA coprecipitates, the endotherm between 423-473 K was assigned to different states of piroxicam. Because physical mixing with PVP could not change the crystallinity of the API as discussed in the former section, the greater heat of fusion with lower weight ratios indicates appearance of different phases. Nevertheless, the disappearing of melting endotherms in their DSC curves could also be induced by the drug-polymer interaction developed during the heating.<sup>153</sup>

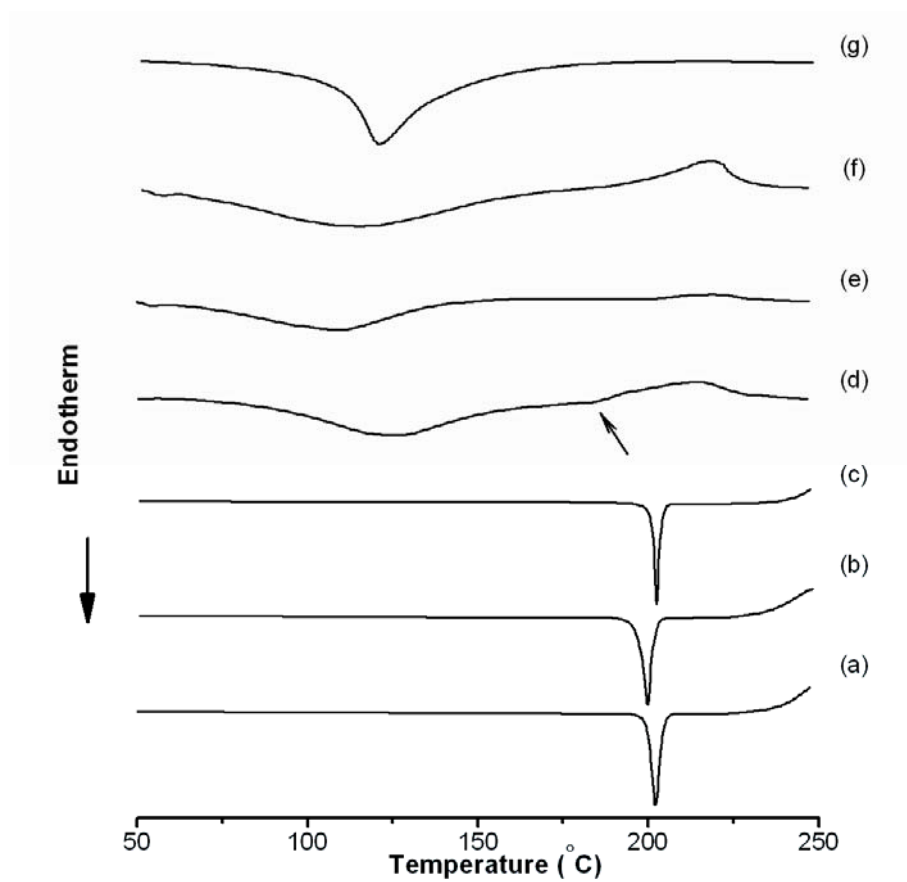


Figure 6-5. DSC curves of (a) as-received Px, (b) DGA-processed Px, (c) spray-dried Px, (d) PM, (e) DGA coprecipitate, (f) spray-dried solid dispersion, and (g) as-received PVP K25.

### 6.3.5 FT-IR analysis

The interactions between drug and polymeric carrier in the solid state were probed by Fourier transform infrared spectrometrical studies. If the drug and PVP interact, then the functional groups in the FT-IR spectra will show band shifts and broadening compared with the spectra of the pure drug and PVP.<sup>136</sup>

The hydrogen donor (-OH and -NH) on piroxicam has a characteristic absorption bands  $\nu_{\text{O-H}}$  at  $3339\text{ cm}^{-1}$  for form I and  $3381\text{ cm}^{-1}$  for form II [Fig. 6-6(a) and (b)]. The spectra shown in Fig. 6-6(d) were simple summations of pure drug and PVP K25, indicating no structure change of the polymer and API and therefore absence of interaction. As can be seen in Fig. 6-6(e), the FT-IR spectra for the solid dispersions are significantly different from their PM counterparts. With lower D/P, a small peak at  $3381\text{ cm}^{-1}$  emerged, and the samples should be mixture of solid dispersions and excess form II piroxicam, which is compatible with the PXRD patterns and SEM observations. With higher D/P, the characteristic absorption bands at  $3339\text{ cm}^{-1}$  disappeared, this can be attributed to the relatively smaller portion of drug in those samples and therefore not quite informative. However, characteristic carbonyl bands between  $1600\text{-}1700\text{ cm}^{-1}$  slightly shifted to higher wave numbers with these solid dispersion systems, probably because of interaction between the hydroxyl group of piroxicam and carbonyl group of PVP K25. Such interactions in drug-PVP solid dispersions were previously reported.<sup>143</sup>

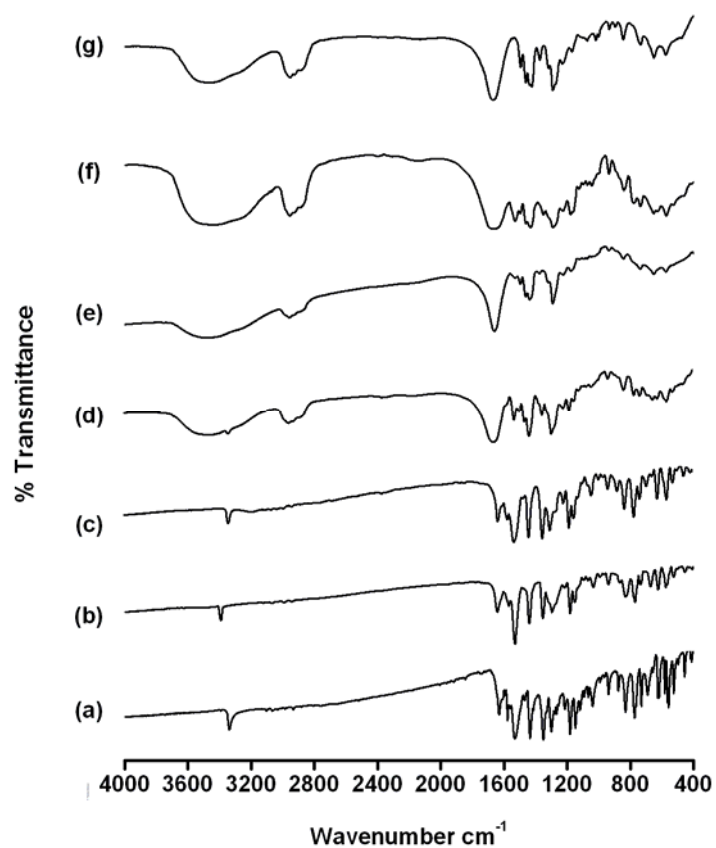


Figure 6-6. FT-IR spectra of (a) as-received Px, (b) DGA-processed Px, (c) spray-dried Px, (d) PM, (e) DGA coprecipitate, (f) spray-dried solid dispersion, and (g) as-received PVP K25.

### 6.3.6 Drug loading

The drug contents in the coprecipitate samples were determined by UV-spectroscopy and the results are listed in Table 3.

Based on earlier discussions, it is clear that drug loading with samples of low D/P would be misleading because of the incomplete encapsulation, so we focused on the drug content of D/P higher than 1:1. DGA-prepared solid dispersions contained less piroxicam than the theoretical value, suggesting the methylene chloride-CO<sub>2</sub> mixture extracted more piroxicam than the polymer, which was reported by Bleich et al when piroxicam and PLA were coprecipitated by DGA processing.<sup>154</sup> However, Muhrer et al reported reverse situation with phenytoin loadings in PVP K30 after DGA coprecipitation.<sup>124</sup> Currently, the phase behavior of carbon dioxide/drug/polymer system with complex interactions among the components complicates DGA technique as a controlled formulation technique. Nonetheless, a quantitative prediction of the drug loading could be made with solubility data of pharmaceuticals and polymers in carbon dioxide under relevant conditions.

### 6.3.7 Dissolution studies

Dissolution rates of as-received piroxicam, physical mixtures of piroxicam with PVP K25, and various DGA-processed coprecipitates are compared in Fig. 6-7.

Evidently dissolution of piroxicam in simulated SGF without pepsin was promoted by both addition of PVP K25 and DGA processing. With DGA-processed solid dispersions, the enhancement effect was the most prominent, especially with higher PVP content. Moreover, over 95% of the API was dissolved within 15 min for 1:4 and 1:9 DGA coprecipitates, suggesting a more than twenty times faster dissolution of raw drug within the first 15 minutes. These results show that

coprecipitation with PVP will improve the dissolution rate of piroxicam significantly. In addition, further sizing treatments is not necessary because the DGA treatment could serve as a means of micronization.

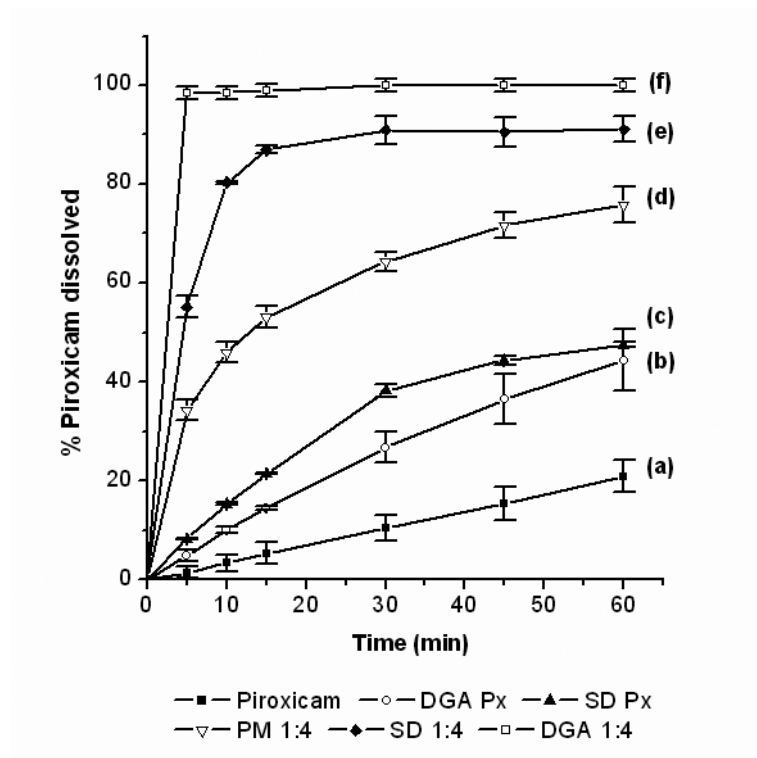


Figure 6-7. Percent drug release profiles of (a) as-received Px, (b) DGA-processed Px, (c) spray-dried Px, (d) PM, (e) DGA coprecipitate, and (f) spray-dried solid dispersion at 37°C.

Table 4. Drug loadings of DGA-prepared solid dispersions.

Initial drug/polymer weight ratio (w/w)	Theoretical loading (%)	Actual loading (%)
1:2	33.3	11.6
1:4	20.0	23.6
1:9	10.0	10.7

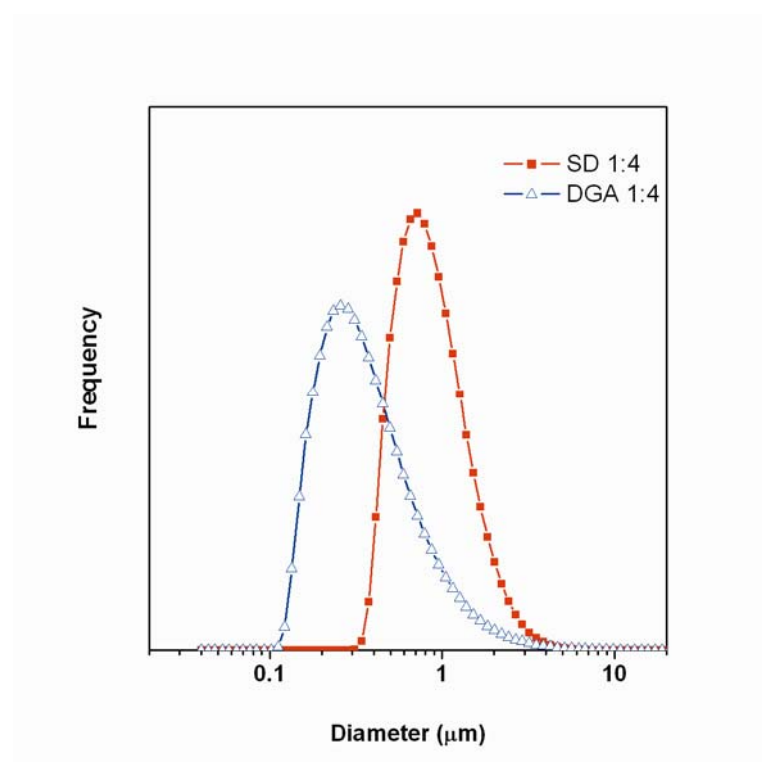


Figure 6-8. Particle size distribution of solid dispersions with drug to polymer weight ratio of 1:4 prepared by DGA and SD process.

## 6.4 Conclusion

Precipitation with compressed carbon dioxide as antisolvent (DGA) was investigated for their potential to prepare fast-dissolving dosage forms of piroxicam, a

poorly water-soluble drug, using PVP K25 as carrier material. We studied the physicochemical properties of the resulted solid dispersions where piroxicam was found dispersed in the polymer with poor crystallinity. FT-IR spectra and thermo-analysis data signaled the existence of hydrogen bonding between the drug and polymer. Comparison of the dissolution profiles of solid dispersions with physical mixtures suggested that loss of crystallinity and particle size reduction are the primary reasons for enhanced dissolution. DGA provided a good example of one-step formation of micronized solid dispersion, whose long-term stability study of is still necessary.

## CHAPTER 7

### CONCLUSION REMARKS

This study investigates the micronization of biodegradable polymers and preparation of solid dispersions of poorly water-soluble drugs and water-soluble polymers by precipitation using dense gas as antisolvent. Due to solubility limitation of RESS, the dense gas antisolvent (DGA) technique is chosen because of its wider applicability. The products of DGA processes will have modified physical or solid state properties. With proper choice of experimental variables, performance of the particulate products is also controllable.

However, further investigations are needed to understand the following issues: the influence of operating parameters on the characteristics of the products (particle size, morphology, and polymorphism, etc.), the fluid dynamics, the nucleation phenomenon, the crystal growth under these specific conditions, the particle agglomeration in the jet, and the method of scaling up, etc.

In summary, dense gas antisolvent techniques have demonstrated great potential in dimension and morphology control of a variety of materials, especially pharmaceutical compounds. Coprecipitation of pharmaceutical compounds with excipients from our study presents an intriguing example of improving the bioavailability of poorly-water soluble APIs using this “green” technique. Utilizing the tunability of the physicochemical properties of dense gas carbon dioxide, this technique is able to provide more opportunities in the development of pharmaceutical formulation with controlled dissolution profiles. Of course, a more comprehensive evaluation of the pros and cons of this technology with others will be necessary in order for its further advancement towards commercialization.

## REFERENCES

1. Shoyele, S. A.; Cawthome, S., Particle engineering techniques for inhaled biopharmaceuticals. *Adv. Drug Delivery Rev.* **2006**, 58, (9-10), 1009-1029.
2. Chow, A. H. L.; Tong, H. H. Y.; Chattopadhyay, P.; Shekunov, B. Y., Particle engineering for pulmonary drug delivery. *Pharm. Res.* **2007**, 24, (3), 411-437.
3. Lobenberg, R.; Amidon, G. L., Modern bioavailability, bioequivalence and biopharmaceutics classification system. New scientific approaches to international regulatory standards. *Eur. J. Pharm. Biopharm.* **2000**, 50, (1), 3-12.
4. Rasenack, N.; Muller, B. W., Micron-size drug particles: Common and novel micronization techniques. *Pharm. Dev. Technol.* **2004**, 9, (1), 1-13.
5. Liu, R., *Water-insoluble drug formulation*. Interpharm: Denver, CO, 2000; Chapter 4.
6. Freiberg, S.; Zhu, X., Polymer microspheres for controlled drug release. *Int. J. Pharm.* **2004**, 282, (1-2), 1-18.
7. Jung, J.; Perrut, M., Particle design using supercritical fluids: Literature and patent survey. *J. Supercrit. Fluids* **2001**, 20, (3), 179-219.
8. Chiou, W. L.; Riegelman, S., Pharmaceutical applications of solid dispersion systems. *J. Pharm. Sci.* **1971**, 60, (9), 1281-1302.
9. Habib, M. J., *Pharmaceutical Solid Dispersion Technology*. Technomic Publishing: 2001; Chapter 2.
10. Serajuddin, A. T. M., Solid dispersion of poorly water-soluble drugs: Early promises, subsequent problems, and recent breakthroughs. *J. Pharm. Sci.* **1999**, 88, (10), 1058-1066.
11. Vasconcelos, T.; Sarmiento, B.; Costa, P., Solid dispersions as strategy to improve oral bioavailability of poor water soluble drugs. *Drug Discovery Today* **2007**, 12, (23-24), 1068-1075.
12. Hannay, J. B.; Hogarth, J., On the solubility of solids in gases. *Proc. R. Soc. London* **1879**, 29, 324-326.
13. Foster, N. R.; Dehghani, F.; Charoenchaitrakool, K. M.; Warwick, B., Application of dense gas techniques for the production of fine particles. *AAPS Pharmsci* **2003**, 5, (2).

14. Bahrami, M.; Ranjbarian, S., Production of micro- and nano-composite particles by supercritical carbon dioxide. *J. Supercrit. Fluids* **2007**, 40, (2), 263-283.
15. McHugh, M. A.; Krukonis, V. J., *Supercritical Fluid Extraction: Principles and Practice*. 2nd ed.; Butterworth-Heinemann: London, 1994; Chapter 1.
16. Francis, A. W., Ternary systems of liquid carbon dioxide. *J. Am. Chem. Soc.* **1954**, 76, (393), 1099-1114.
17. Kawashima, Y.; York, P., Drug delivery applications of supercritical fluid technology. *Adv. Drug Delivery Rev.* **2008**, 60, (3), 297-298.
18. Kompella, U. B.; Koushik, K., Preparation of drug delivery systems using supercritical fluid technology. *Crit. Rev. Ther. Drug* **2001**, 18, (2), 173-199.
19. Shekunov, B. Y.; Chattopadhyay, P.; Seitzinger, J., In *Engineering of composite particles for drug delivery using supercritical fluid technology*; Svenson, S., Ed.; ACS Symposium Series 924, American Chemical Society: Washington, DC, 2006; 234-249.
20. Shekunov, B. Y.; York, P., Crystallization processes in pharmaceutical technology and drug delivery design. *J. Cryst. Growth* **2000**, 211, (1-4), 122-136.
21. Stanton, L. A.; Dehghani, F. B.; Foster, N. R., Improving drug delivery using polymers and supercritical fluid technology. *Aust. J. Chem.* **2002**, 55, (6-7), 443-447.
22. Subramaniam, B.; Rajewski, R. A.; Snively, K., Pharmaceutical processing with supercritical carbon dioxide. *J. Pharm. Sci.* **1997**, 86, (8), 885-890.
23. Reverchon, E., Supercritical antisolvent precipitation of micro- and nanoparticles. *J. Supercrit. Fluids* **1999**, 15, (1), 1-21.
24. Palakodaty, S.; York, P., Phase behavioral effects on particle formation processes using supercritical fluids. *Pharm. Res.* **1999**, 16, (7), 976-985.
25. Marr, R.; Gamse, T., Use of supercritical fluids for different processes including new developments - a review. *Chem. Eng. Process.* **2000**, 39, (1), 19-28.
26. Cooper, A. I., Polymer synthesis and processing using supercritical carbon dioxide. *J. Mater. Chem.* **2000**, 10, (2), 207-234.
27. Rogers, T. L.; Johnston, K. P.; Williams, R. O., Solution-based particle formation of pharmaceutical powders by supercritical or compressed fluid CO<sub>2</sub> and cryogenic spray-freezing technologies. *Drug Dev. Ind. Pharm.* **2001**, 27, (10), 1003-1015.

28. Tan, H. S.; Borsadia, S., Particle formation using supercritical fluids: pharmaceutical applications. *Expert Opin. Ther. Pat.* **2001**, 11, (5), 861-872.
29. Ye, X. G.; Wai, C. M., Making nanomaterials in supercritical fluids: A review. *J. Chem. Edu.* **2003**, 80, (2), 198-204.
30. Yeo, S. D.; Kiran, E., Formation of polymer particles with supercritical fluids: A review. *J. Supercrit. Fluids* **2005**, 34, (3), 287-308.
31. Perrut, M.; Jung, J.; Leboeuf, E., Enhancement of dissolution rate of poorly soluble active ingredients by supercritical fluid processes Part I: Micronization of neat particles. Part II: Preparation of composite particles. *Int. J. Pharm.* **2005**, 288, (1), 3-10.
32. Perrut, M.; Jung, J.; Leboeuf, F., Enhancement of dissolution rate of poorly soluble active ingredients by supercritical fluid processes: Part II: Preparation of composite particles. *Int. J. Pharm.* **2005**, 288, (1), 11-16.
33. Pasquali, I.; Bettini, R.; Giordano, F., Solid-state chemistry and particle engineering with supercritical fluids in pharmaceuticals. *Eur. J. Pharm. Sci.* **2006**, 27, (4), 299-310.
34. Reverchon, E.; Adami, R., Nanomaterials and supercritical fluids. *J. Supercrit. Fluids* **2006**, 37, (1), 1-22.
35. Tandy, A.; Mammucari, R.; Dehghani, F.; Foster, N. R., Dense gas processing of polymeric controlled release formulations. *Int. J. Pharm.* **2007**, 328, (1), 1-11.
36. Byrappa, K.; Ohara, S.; Adschiri, T., Nanoparticles synthesis using supercritical fluid technology - towards biomedical applications. *Adv. Drug Delivery Rev.* **2008**, 60, (3), 299-327.
37. Davies, O. R.; Lewis, A. L.; Whitaker, M. J.; Tai, H. Y.; Shakesheff, K. M.; Howdle, S. M., Applications of supercritical CO<sub>2</sub> in the fabrication of polymer systems for drug delivery and tissue engineering. *Adv. Drug Delivery Rev.* **2008**, 60, (3), 373-387.
38. Martin, A.; Cocero, M. J., Micronization processes with supercritical fluids: Fundamentals and mechanisms. *Adv. Drug Delivery Rev.* **2008**, 60, (3), 339-350.
39. Mishima, K., Biodegradable particle formation for drug and gene delivery using supercritical fluid and dense gas. *Adv. Drug Delivery Rev.* **2008**, 60, (3), 411-432.
40. Okamoto, H.; Danjo, K., Application of supercritical fluid to preparation of powders of high-molecular weight drugs for inhalation. *Adv. Drug Delivery Rev.* **2008**, 60, (3), 433-446.

41. Yasuji, T.; Takeuchi, H.; Kawashima, Y., Particle design of poorly water-soluble drug substances using supercritical fluid technologies. *Adv. Drug Delivery Rev.* **2008**, 60, (3), 388-398.
42. Pasquali, I.; Bettini, R.; Giordano, F., Supercritical fluid technologies: An innovative approach for manipulating the solid-state of pharmaceuticals. *Adv. Drug Delivery Rev.* **2008**, 60, (3), 399-410.
43. Moribe, K.; Tozuka, Y.; Yamamoto, K., Supercritical carbon dioxide processing of active pharmaceutical ingredients for polymorphic control and for complex formation. *Adv. Drug Delivery Rev.* **2008**, 60, (3), 328-338.
44. Pathak, P.; Prasad, G. L.; Meziani, M. J.; Joudeh, A. A.; Sun, Y. P., Nanosized paclitaxel particles from supercritical carbon dioxide processing and their biological evaluation. *Langmuir* **2007**, 23, (5), 2674-2679.
45. Thakur, R.; Gupta, R. B., Formation of phenytoin nanoparticles using rapid expansion of supercritical solution with solid cosolvent (RESS-SC) process. *Int. J. Pharm.* **2006**, 308, (1-2), 190-199.
46. Shinozaki, H.; Oguchi, T.; Suzuki, S.; Aoki, K.; Sako, T.; Morishita, S.; Tozuka, Y.; Moribe, K.; Yamamoto, K., Micronization and polymorphic conversion of tolbutamide and barbitol by rapid expansion of supercritical solutions. *Drug Dev. Ind. Pharm.* **2006**, 32, (7), 877-891.
47. Huang, J. T.; Moriyoshi, T., Fabrication of fine powders by RESS with a clearance nozzle. *J. Supercrit. Fluids* **2006**, 37, (3), 292-297.
48. Chiou, A. H. J.; Cheng, H. C.; Wang, D. P., Micronization and microencapsulation of felodipine by supercritical carbon dioxide. *J. Microencapsul.* **2006**, 23, (3), 265-276.
49. Sun, Y. P.; Meziani, M. L.; Pathak, P.; Qu, L. W., Polymeric nanoparticles from rapid expansion of supercritical fluid solution. *Chem. Eur. J.* **2005**, 11, (5), 1366-1373.
50. Oliveira, J. V.; Pinto, J. C.; Dariva, C., Application of a modified RESS process for polypropylene microparticle production. *Fluid Phase Equilib.* **2005**, 228, 381-388.
51. Moribe, K.; Tsutsumi, S.; Morishita, S.; Shinozaki, H.; Tozuka, Y.; Oguchi, T.; Yamamoto, K., Micronization of phenylbutazone by rapid expansion of supercritical CO<sub>2</sub> solution. *Chem. Pharm. Bull.* **2005**, 53, (8), 1025-1028.
52. Matsuyama, K.; Mishima, K.; Hayashi, K. I.; Ishikawa, H.; Matsuyama, H.; Harada, T., Formation of microcapsules of medicines by the rapid expansion of a supercritical solution with a nonsolvent. *J. Appl. Polym. Sci.* **2003**, 89, (3), 742-752.

53. Gosselin, P. M.; Thibert, R.; Preda, M.; McMullen, J. N., Polymorphic properties of micronized carbamazepine produced by RESS. *Int. J. Pharm.* **2003**, 252, (1-2), 225-233.
54. Gosselin, P.; Lacasse, F. X.; Preda, M.; Thibert, R.; Clas, S. D.; McMullen, J. N., Physicochemical evaluation of carbamazepine microparticles produced by the rapid expansion of supercritical solutions and by spray-drying. *Pharm. Dev. Technol* **2003**, 8, (1), 11-20.
55. Weber, M.; Russell, L. M.; Debenedetti, P. G., Mathematical modeling of nucleation and growth of particles formed by the rapid expansion of a supercritical solution under subsonic conditions. *J. Supercrit. Fluids* **2002**, 23, (1), 65-80.
56. Ksibi, H.; Subra, P., Influence of nozzle design on the nucleation conditions in the RESS process. *Chem. Biochem. Eng. Q.* **1996**, 10, (2), 69-73.
57. Dos Santos, I. R.; Richard, J.; Pech, B.; Thies, C.; Benoit, J. P., Microencapsulation of protein particles within lipids using a novel supercritical fluid process. *Int. J. Pharm.* **2002**, 242, (1-2), 69-78.
58. Wang, Y. L.; Wei, D. G.; Dave, R.; Pfeffer, R.; Sauceau, M.; Letourneau, J. J.; Fages, J., Extraction and precipitation particle coating using supercritical CO<sub>2</sub>. *Powder Technol.* **2002**, 127, (1), 32-44.
59. Wang, T. J.; Tsutsumi, A.; Hasegawa, H.; Mineo, T., Mechanism of particle coating granulation with RESS process in a fluidized bed. *Powder Technol.* **2001**, 118, (3), 229-235.
60. Tsutsumi, A.; Ikeda, M.; Chen, W.; Iwatsuki, J., A nano-coating process by the rapid expansion of supercritical suspensions in impinging-stream reactors. *Powder Technol.* **2003**, 138, (2-3), 211-215.
61. Krober, H.; Teipel, U., Microencapsulation of particles using supercritical carbon dioxide. *Chem. Eng. Process.* **2005**, 44, (2), 215-219.
62. Sun, Y.P.; Atornjitjawat, P.; Meziani, M.J., Preparation of Silver Nanoparticles via Rapid Expansion of Water in Carbon Dioxide Microemulsion into Reductant Solution. *Langmuir* **2001**, 17, (19), 5707-5710.
63. Meziani, M.J.; Pathak, P.; Wang, W.; Desai, T.; Patil, A.; Sun, Y.P., Polymeric Nanofibers from Rapid Expansion of Supercritical Solution. *Ind. Eng. Chem. Res.* **2005**, 44, (13):4594-4598.
64. Pathak, P.; Meziani, M.J.; Desai, T.; Sun, Y.P., Nanosizing Drug Particles in Supercritical Fluid Processing. *J. Am. Chem. Soc.* **2004**, 126, (35), 10842-10843.

65. Meziari, M.J.; Rollins, H.W.; Allard, L.F.; Sun, Y.P., Protein-Protected Nanoparticles from Rapid Expansion of Supercritical Solution into Aqueous Solution. *J. Phys. Chem. B* **2002**, 106, (43), 11178-11182.
66. Thakur R, Gupta RB 2005. Rapid Expansion of Supercritical Solution with Solid Cosolvent (RESS-SC) Process: Formation of Griseofulvin Nanoparticles. *Ind. Eng. Chem. Res.* **2005**, 44, (19), 7380-7387.
67. Thakur, R.; Gupta, R. B., Rapid expansion of supercritical solution with solid cosolvent (RESS-SC) process: Formation of 2-aminobenzoic acid nanoparticle. *J. Supercrit. Fluids* **2006**, 37, (3), 307-315.
68. Muenueklue, P.; Jansens, P. J., Particle formation of an edible fat (rapeseed 70) using the supercritical melt micronization (ScMM) process. *J. Supercrit. Fluids* **2007**, 40, (3), 433-442.
69. Sencar-Bozic, P.; Srcic, S.; Knez, Z.; Kerc, J., Improvement of nifedipine dissolution characteristics using supercritical CO<sub>2</sub>. *Int. J. Pharm.* **1997**, 148, (2), 123-130.
70. Vemavarapu, C.; Mollan, M. J.; Lodaya, M.; Needham, T. E., Design and process aspects of laboratory scale SCF particle formation systems. *Int. J. Pharm.* **2005**, 292, (1-2), 1-16.
71. Hakuta, Y.; Hayashi, H.; Arai, K., Fine particle formation using supercritical fluids. *Curr. Opin. Solid State Mater. Sci.* **2003**, 7, (4-5), 341-351.
72. Knez, Z.; Weidner, E., Particles formation and particle design using supercritical fluids. *Curr. Opin. Solid State Mater. Sci.* **2003**, 7, (4-5), 353-361.
73. Reverchon, E.; Volpe, M. C.; Caputo, G., Supercritical fluid processing of polymers: composite particles and porous materials elaboration. *Curr. Opin. Solid State Mater. Sci.* **2003**, 7, (4-5), 391-397.
74. Shariati, A.; Peters, C. J., Recent developments in particle design using supercritical fluids. *Curr. Opin. Solid State Mater. Sci.* **2003**, 7, (4-5), 371-383.
75. Fages, J.; Lochard, H.; Letourneau, J. J.; Sauceau, M.; Rodier, E., Particle generation for pharmaceutical applications using supercritical fluid technology. *Powder Technol.* **2004**, 141, (3), 219-226.
76. Zhang, Y.; Erkey, C., Preparation of supported metallic nanoparticles using supercritical fluids: A review. *J. Supercrit. Fluids* **2006**, 38, (2), 252-267.
77. Reverchon, E.; Della Porta, G., Particle design using supercritical fluids. *Chem. Eng. Technol* **2003**, 26, (8), 840-845.
78. York, P., Strategies for particle design using supercritical fluid technologies. *Pharm. Sci. Technol. Today* **1999**, 2, (11), 430-440.

79. Date, A. A.; Patravale, V. B., Current strategies for engineering drug nanoparticles. *Curr. Opin. Colloid Interface Sci.* **2004**, 9, (3-4), 222-235.
80. Thakur, R.; Gupta, R. B., Supercritical CO<sub>2</sub> based silica coating of gold nanoparticles using water-in-oil microemulsions. *Ind. Eng. Chem. Res.* **2005**, 44, (9), 3086-3090.
81. Foster, N. R.; Dehghani, F.; Charoenchaitrakool, K. M.; Warwick, B., Application of dense gas techniques for the production of fine particles. *AAPS Pharmsci* **2003**, 5, (2), -.
82. He, W. Z.; Jiang, Z. H.; Suo, Q. L., Progress in generation of fine particles using supercritical fluid precipitation. *Progress Chem.* **2003**, 15, (5), 361-366.
83. Krober, H.; Teipel, U., Particle production using supercritical fluids. *Chem. Ing. Tech.* **2003**, 75, (6), 687-690.
84. Reverchon, E.; Della Porta, G., Supercritical fluids-assisted micronization techniques. Low-impact routes for particle production. *Pure Appl. Chem.* **2001**, 73, (8), 1293-1297.
85. Sacchetti, M.; Van Oort, M. M., In *Spray-drying and supercritical fluid particle generation techniques*; Hickey, A. J., Ed.; Inhalation Aerosols: Physical and Biological Basis for Therapy, 2nd ed.; CRC: Boca Raton, FL, 2007; Vol. 221, pp 307-346.
86. Tong, H. H. Y.; Chow, A. H. L., Control of physical forms of drug particles for pulmonary delivery by spray drying and supercritical fluid processing. *KONA* **2006**, (24), 27-40.
87. Martin, A.; Cocero, M. J., Numerical modeling of jet hydrodynamics, mass transfer, and crystallization kinetics in the supercritical antisolvent (SAS) process. *J. Supercrit. Fluids* **2004**, 32, (1-3), 203-219.
88. Werling, J. O.; Debenedetti, P. G., Numerical modeling of mass transfer in the supercritical antisolvent process. *J. Supercrit. Fluids* **1999**, 16, (2), 167-181.
89. Werling, J. O.; Debenedetti, P. G., Numerical modeling of mass transfer in the supercritical antisolvent process: miscible conditions. *J. Supercrit. Fluids* **2000**, 18, (1), 11-24.
90. de Diego, Y. P.; Wubbolts, F. E.; Jansens, P. J., Modelling mass transfer in the PCA process using the Maxwell-Stefan approach. *J. Supercrit. Fluids* **2006**, 37, (1), 53-62.
91. Dukhin, S. S.; Shen, Y.; Dave, R.; Pfeffer, R., Development in modeling submicron particle formation in two phases flow of solvent-supercritical antisolvent emulsion. *Adv. Colloid Interface Sci.* **2007**, 134-35, 72-88.

92. Bell, P. W.; Stephens, A. P.; Roberts, C. B.; Duke, S. R., High-resolution imaging of the supercritical antisolvent process. *Exp. Fluids* **2005**, 38, (6), 708-719.
93. Reverchon, E.; Caputo, G.; De Marco, I., Role of phase behavior and atomization in the supercritical antisolvent precipitation. *Ind. Eng. Chem. Res.* **2003**, 42, (25), 6406-6414.
94. Rantakyla, M.; Jantti, M.; Aaltonen, O.; Hurme, M., The effect of initial drop size on particle size in the supercritical antisolvent precipitation (SAS) technique. *J. Supercrit. Fluids* **2002**, 24, (3), 251-263.
95. Reverchon, E.; De Marco, I.; Adami, R.; Caputo, G., Expanded micro-particles by supercritical antisolvent precipitation: Interpretation of results. *J. Supercrit. Fluids* **2008**, 44, 98-108.
96. Reverchon, E.; De Marco, I.; Torino, E., Nanoparticles production by supercritical antisolvent precipitation: A general interpretation. *J. Supercrit. Fluids* **2007**, 43, 126-138.
97. Reverchon, E.; De Marco, I., Supercritical antisolvent precipitation of Cephalosporins. *Powder Technol.* **2006**, 164, (3), 139-146.
98. Carretier, E.; Badens, E.; Guichardon, P.; Boutin, O.; Charbit, G., Hydrodynamics of supercritical antisolvent precipitation: Characterization and influence on particle morphology. *Ind. Eng. Chem. Res.* **2003**, 42, (2), 331-338.
99. Mawson, S.; Kanakia, S.; Johnston, K. P., Coaxial nozzle for control of particle morphology in precipitation with a compressed fluid antisolvent. *J. Appl. Polym. Sci.* **1997**, 64, (11), 2105-2118.
100. Jarmer, D. J.; Lengsfeld, C. S.; Randolph, T. W., Manipulation of particle size distribution of poly(L-lactic acid) nanoparticles with a jet-swirl nozzle during precipitation with a compressed antisolvent. *J. Supercrit. Fluids* **2003**, 27, (3), 317-336.
101. Chattopadhyay, P.; Gupta, R. B., Production of antibiotic nanoparticles using supercritical CO<sub>2</sub> as antisolvent with enhanced mass transfer. *Ind. Eng. Chem. Res.* **2001**, 40, (16), 3530-3539.
102. He, W. Z.; Suo, Q. L.; Jiang, Z. H.; Shan, A.; Hong, H. L., Precipitation of ephedrine by SEDS process using a specially designed prefilming atomizer. *J. Supercrit. Fluids* **2004**, 31, (1), 101-110.
103. Abramoff, M. D.; Magelhaes, P. J.; Ram, S. J., Image Processing with ImageJ. *Biophotonics Int.* **2004**, 11, (7), 36-42.
104. Gokhale, A.; Khusid, B.; Dave, R. N.; Pfeffer, R., Effect of solvent strength and operating pressure on the formation of submicrometer polymer particles in supercritical microjets. *J. Supercrit. Fluids* **2007**, 43, (2), 341-356.

105. Lipatova, T. E.; Lipatov, Y. S., Biocompatible polymers for medical application. *Macromol. Symp.* **2000**, 152, 139-150.
106. Kumar, N.; Langer, R. S.; Domb, A. J., Polyanhydrides: an overview. *Adv. Drug Delivery Rev.* **2002**, 54, (7), 889-910.
107. Bourke, S. L.; Kohn, J., Polymers derived from the amino acid L-tyrosine: polycarbonates, polyarylates and copolymers with poly(ethylene glycol). *Adv. Drug Delivery Rev.* **2003**, 55, (4), 447-466.
108. Gopferich, A.; Tessmar, J., Polyanhydride degradation and erosion. *Adv. Drug Delivery Rev.* **2002**, 54, (7), 911-931.
109. Chandra, R.; Rustgi, R., Biodegradable polymers. *Progress Polym. Sci.* **1998**, 23, (7), 1273-1335.
110. Tangpasuthadol, V.; Pendharkar, S. M.; Kohn, J., Hydrolytic degradation of tyrosine-derived polycarbonates, a class of new biomaterials. Part I: Study of model compounds. *Biomaterials* **2000**, 21, (23), 2371-2378.
111. Tangpasuthadol, V.; Pendharkar, S. M.; Peterson, R. C.; Kohn, J., Hydrolytic degradation of tyrosine-derived polycarbonates, a class of new biomaterials. Part II: 3-yr study of polymeric devices. *Biomaterials* **2000**, 21, (23), 2379-2387.
112. James, K.; Levene, H.; Parsons, J. R.; Kohn, J., Small changes in polymer chemistry have a large effect on the bone-implant interface: evaluation of a series of degradable tyrosine-derived polycarbonates in bone defects. *Biomaterials* **1999**, 20, (23-24), 2203-2212.
113. de Diego, Y. P.; Pellikaan, H. C.; Wubbolts, F. E.; Borchard, G.; Witkamp, G. J.; Jansens, P. J., Opening new operating windows for polymer and protein micronisation using the PCA process. *J. Supercrit. Fluids* **2006**, 36, (3), 216-224.
114. de Diego, Y. P.; Pellikaan, H. C.; Wubbolts, F. E.; Witkamp, G. J.; Jansens, P. J., Operating regimes and mechanism of particle formation during the precipitation of polymers using the PCA process. *J. Supercrit. Fluids* **2005**, 35, (2), 147-156.
115. de Diego, Y. P.; Wubbolts, F. E.; Witkamp, G. J.; Jansens, P. J.; de Loos, T. W., Improved PCA process for the production of nano- and microparticles of polymers. *AIChE J.* **2004**, 50, (10), 2408-2417.
116. Lin, C.; Ng, K. M.; Wibowo, C., Producing nanoparticles using precipitation with compressed antisolvent. *Ind. Eng. Chem. Res.* **2007**, 46, (11), 3580-3589.
117. Ertel, S. I.; Kohn, J., Evaluation of a Series of Tyrosine-Derived Polycarbonates as Degradable Biomaterials. *J. Biomed. Mater. Res.* **1994**, 28, (8), 919-930.

118. Bungert, B.; Sadowski, G.; Arlt, W., Separations and material processing in solutions with dense gases. *Ind. Eng. Chem. Res.* **1998**, 37, (8), 3208-3220.
119. Thiering, R.; Dehghani, F.; Foster, N. R., Current issues relating to anti-solvent micronisation techniques and their extension to industrial scales. *J. Supercrit. Fluids* **2001**, 21, (2), 159-177.
120. Teipel, U.; Krober, H.; Krause, H. H., Formation of energetic materials using supercritical fluids. *Propell. Explos. Pyrot.* **2001**, 26, (4), 168-173.
121. Weidner, E.; Petermann, M.; Knez, Z., Multifunctional composites by high-pressure spray processes. *Curr. Opin. Solid State Mater. Sci.* **2003**, 7, (4-5), 385-390.
122. Tomasko, D. L.; Han, X. M.; Liu, D. H.; Gao, W. H., Supercritical fluid applications in polymer nanocomposites. *Curr. Opin. Solid State Mater. Sci.* **2003**, 7, (4-5), 407-412.
123. Won, D. H.; Kim, M. S.; Lee, S.; Park, J. S.; Hwang, S. J., Improved physicochemical characteristics of felodipine solid dispersion particles by supercritical anti-solvent precipitation process. *Int. J. Pharm.* **2005**, 301, (1-2), 199-208.
124. Muhrer, G.; Meier, U.; Fusaro, F.; Albano, S.; Mazzotti, M., Use of compressed gas precipitation to enhance the dissolution behavior of a poorly water-soluble drug: Generation of drug microparticles and drug-polymer solid dispersions. *Int. J. Pharm.* **2006**, 308, (1-2), 69-83.
125. Moneghini, M.; Kikic, I.; Voinovich, D.; Perissutti, B.; Filipovic-Grcic, J., Processing of carbamazepine PEG 4000 solid dispersions with supercritical carbon dioxide: preparation, characterisation, and in vitro dissolution. *Int. J. Pharm.* **2001**, 222, (1), 129-138.
126. Majerik, V.; Horvath, G.; Szokonya, L.; Charbit, G.; Badens, E.; Bosc, N.; Teillaud, E., Supercritical antisolvent versus coevaporation - Preparation and characterization of solid dispersions. *Drug Dev. Ind. Pharm.* **2007**, 33, (9), 975-983.
127. Majerik, V.; Charbit, G.; Badens, E.; Horvath, G.; Szokonya, L.; Bosc, N.; Teillaud, E., Bioavailability enhancement of an active substance by supercritical antisolvent precipitation. *J. Supercrit. Fluids* **2007**, 40, (1), 101-110.
128. Vogt, M.; Derendorf, H.; Krämer, J.; Junginger, H.E.; Midha, K.K.; Shah, V.P.; Stavchansky, S.; Dressman, J.B.; Barends, D.M., Biowaiver monographs for immediate release solid oral dosage forms: Prednisolone. *J. Pharm. Sci.* **2007**, 96, 27-37.

129. Win Loung Chiou, S. R., Increased dissolution rates of water-insoluble cardiac glycosides and steroids *via* solid dispersions in polyethylene glycol 6000. *J. Pharm. Sci.* **1971**, 60, 1569-1571.
130. Sahin, N. O.; Arslan, H., Inclusion complex of prednisolone with skimmed milk part 1: Physicochemical characterization. *Yakugaku Zasshi - J. Pharm. Soc. Jpn.* **2007**, 127, (8), 1255-1261.
131. Meléndez, P. A.; Kane, K. M.; Ashvar, C. S.; Albrecht, M.; Smith, P. A., Thermal inkjet application in the preparation of oral dosage forms: Dispensing of prednisolone solutions and polymorphic characterization by solid-state spectroscopic techniques. *J. Pharm. Sci.* **2007**, 97, 2619-2636.
132. Dean, J. R.; Kane, M.; Khundker, S.; Dowle, C.; Tranter, R. L.; Jones, P., Estimation and Determination of Steroid Solubility in Supercritical Carbon-Dioxide. *Analyst* **1995**, 120, (8), 2153-2157.
133. Subra-Paternault, P.; Roy, C.; Vrel, D.; Vega-Gonzalez, A.; Domingo, C., Solvent effect on tolbutamide crystallization induced by compressed CO<sub>2</sub> as antisolvent. *J. Cryst. Growth* **2007**, 309, 76-85.
134. Veiga, M. D.; Cadorniga, R.; Fonseca, I.; Garcia-Blanco, S., Polymorphism characterization of prednisolone: spectrometric and diffractometric study. *Farm. Ed. Prat.* **1987**, 42, (4), 93-102.
135. Chavez, F.; Debenedetti, P. G.; Luo, J. J.; Dave, R. N.; Pfeffer, R., Estimation of the characteristic time scales in the supercritical antisolvent process. *Ind. Eng. Chem. Res.* **2003**, 42, (13), 3156-3162.
136. Taylor, L. S.; Zografi, G., Spectroscopic characterization of interactions between PVP and indomethacin in amorphous molecular dispersions. *Pharm. Res.* **1997**, 14, (12), 1691-1698.
137. Raghavan, S. L.; Trividic, A.; Davis, A. F.; Hadgraft, J., Crystallization of hydrocortisone acetate: influence of polymers. *Int. J. Pharm.* **2001**, 212, (2), 213-221.
138. Jarmer, D. J.; Lengsfeld, C. S.; Anseth, K. S.; Randolph, T. W., Supercritical fluid crystallization of griseofulvin: Crystal habit modification with a selective growth inhibitor. *J. Pharm. Sci.* **2005**, 94, (12), 2688-2702.
139. Juppo, A. M.; Boissier, C.; Khoo, C., Evaluation of solid dispersion particles prepared with SEDS. *Int. J. Pharm.* **2003**, 250, (2), 385-401.
140. Meure, L. A.; Warwick, B.; Dehghani, F.; Regtop, H. L.; Foster, N. R., Increasing copper indomethacin solubility by coprecipitation with poly(vinylpyrrolidone) using the aerosol solvent extraction system. *Ind. Eng. Chem. Res.* **2004**, 43, (4), 1103-1112.

141. Kulshreshtha, A. K.; Smith, G. G.; Anderson, S. D.; Krukonis, V. J. US Patent 5 803 966, 1998.
142. Karavas, E.; Georgarakis, E.; Sigalas, M. P.; Avgoustakis, K.; Bikiaris, D., Investigation of the release mechanism of a sparingly water-soluble drug from solid dispersions in hydrophilic carriers based on physical state of drug, particle size distribution and drug-polymer interactions. *Eur. J. Pharm. Biopharm.* **2007**, 66, (3), 334-347.
143. Teberekidis, V. I.; Sigalas, M. P., Theoretical study of hydrogen bond interactions of felodipine with polyvinylpyrrolidone and polyethyleneglycol. *Theochem J. Mol. Struct.* - **2007**, 803, (1-3), 29-38.
144. Karavas, E.; Ktistis, G.; Xenakis, A.; Georgarakis, E., Effect of hydrogen bonding interactions on the release mechanism of felodipine from nanodispersions with polyvinylpyrrolidone. *Eur. J. Pharm. Biopharm.* **2006**, 63, (2), 103-114.
145. Bogdanova, S.; Pajeva, I.; Nikolova, P.; Tsakovska, I.; Muller, B., Interactions of poly(vinylpyrrolidone) with ibuprofen and naproxen: Experimental and modeling studies. *Pharm. Res.* **2005**, 22, (5), 806-815.
146. Tajber, L.; Corrigan, O. I.; Healy, A. M., Physicochemical evaluation of PVP-thiazide diuretic interactions in co-spray-dried composites - analysis of glass transition composition relationships. *Eur. J. Pharm. Sci.* **2005**, 24, (5), 553-563.
147. Velaga, S. P.; Berger, R.; Carlfors, J., Supercritical fluids crystallization of budesonide and flunisolide. *Pharm. Res.* **2002**, 19, (10), 1564-1571.
148. Kordikowski, A.; Shekunov, T.; York, P., Polymorph control of sulfathiazole in supercritical CO<sub>2</sub>. *Pharm. Res.* **2001**, 18, (5), 682-688.
149. Van Hees, T.; Piel, G.; Evrard, B.; Otte, X.; Thunus, L.; Delattre, L., Application of supercritical carbon dioxide for the preparation of a piroxicam-beta-cyclodextrin inclusion compound. *Pharm. Res.* **1999**, 16, (12), 1864-1870.
150. Macnaughton, S. J.; Kikic, I.; Foster, N. R.; Alessi, P.; Cortesi, A.; Colombo, I., Solubility of anti-inflammatory drugs in supercritical carbon dioxide. *J. Chem. Eng. Data* **1996**, 41, (5), 1083-1086.
151. Vrečer, F.; Vrbinc, M.; Meden, A., Characterization of piroxicam crystal modifications. *Int. J. Pharm.* **2003**, 256, (1-2), 3-15.
152. Konno, H.; Taylor, L. S., Influence of different polymers on the crystallization tendency of molecularly dispersed amorphous felodipine. *J. Pharm. Sci.* **2006**, 95, 2692-2705.
153. Hasegawa, S.; Furuyama, N.; Yada, S.; Hamaura, T.; Kusai, A.; Yonemochi, E.; Terada, K., Effect of physical properties of troglitazone crystal on the molecular interaction with PVP during heating. *Int. J. Pharm.* **2007**, 336, (1), 82-89.

154. Bleich, J.; Muller, B. W., Production of drug loaded microparticles by the use of supercritical gases with the aerosol solvent extraction system (ASES) process. *J. Microencapsulation* **1996**, 13, (2), 131-139.
155. Reverchon, E.; Della Porta, G., Production of antibiotic micro- and nano-particles by supercritical antisolvent precipitation. *Powder Technol.* **1999**, 106, (1-2), 23-29.
156. Wubbolts, F. E.; Bruinsma, O. S. L.; van Rosmalen, G. M., Dry-spraying of ascorbic acid or acetaminophen solutions with supercritical carbon dioxide. *J. Cryst. Growth* **1999**, 199, 767-772.
157. Magnan, C.; Badens, E.; Commenges, N.; Charbit, G., Soy lecithin micronization by precipitation with a compressed fluid antisolvent - influence of process parameters. *J. Supercrit. Fluids* **2000**, 19, (1), 69-77.
158. Reverchon, E.; Della Porta, G.; Falivene, M. G., Process parameters and morphology in amoxicillin micro and submicro particles generation by supercritical antisolvent precipitation. *J. Supercrit. Fluids* **2000**, 17, (3), 239-248.
159. Badens, E.; Magnan, C.; Charbit, G., Microparticles of soy lecithin formed by supercritical processes. *Biotechnol. Bioeng.* **2001**, 72, (2), 194-204.
160. Chattopadhyay, P.; Gupta, R. B., Production of griseofulvin nanoparticles using supercritical CO<sub>2</sub> antisolvent with enhanced mass transfer. *Int. J. Pharm.* **2001**, 228, (1-2), 19-31.
161. Edwards, A. D.; Shekunov, B. Y.; Kordikowski, A.; Forbes, R. T.; York, P., Crystallization of pure anhydrous polymorphs of carbamazepine by solution enhanced dispersion with supercritical fluids (SEDS<sup>TM</sup>). *J. Pharm. Sci.* **2001**, 90, (8), 1115-1124.
162. Rehman, M.; Shekunov, B. Y.; York, P.; Colthorpe, P., Solubility and precipitation of nicotinic acid in supercritical carbon dioxide. *J. Pharm. Sci.* **2001**, 90, (10), 1570-1582.
163. Reverchon, E.; Della Porta, G.; Pallado, P., Supercritical antisolvent precipitation of salbutamol microparticles. *Powder Technol.* **2001**, 114, (1-3), 17-22.
164. Cocero, M. J.; Ferrero, S., Crystallization of beta-carotene by a GAS process in batch - Effect of operating conditions. *J. Supercrit. Fluids* **2002**, 22, (3), 237-245.
165. Krober, H.; Teipel, U., Materials processing with supercritical antisolvent precipitation: process parameters and morphology of tartaric acid. *J. Supercrit. Fluids* **2002**, 22, (3), 229-235.

166. Reverchon, E.; De Marco, I.; Della Porta, G., Rifampicin microparticles production by supercritical antisolvent precipitation. *Int. J. Pharm.* **2002**, 243, (1-2), 83-91.
167. Warwick, B.; Dehghani, F.; Foster, N. R.; Biffin, J. R.; Regtop, H. L., Micronization of copper indomethacin using gas antisolvent processes. *Ind. Eng. Chem. Res.* **2002**, 41, (8), 1993-2004.
168. Krober, H.; Teipel, U., Micronization of organic materials by crystallization with compressed gases. *Eng. Life Sci.* **2003**, 3, (3), 137-140.
169. Yeo, S. D.; Kim, M. S.; Lee, J. C., Recrystallization of sulfathiazole and chlorpropamide using the supercritical fluid antisolvent process. *J. Supercrit. Fluids* **2003**, 25, (2), 143-154.
170. Fusaro, F.; Mazzotti, M.; Muhrer, G., Gas antisolvent recrystallization of paracetamol from acetone using compressed carbon dioxide as antisolvent. *Cryst. Growth Des.* **2004**, 4, (5), 881-889.
171. Reverchon, E.; De Marco, L., Supercritical antisolvent micronization of Cefonicid: thermodynamic interpretation of results. *J. Supercrit. Fluids* **2004**, 31, (2), 207-215.
172. Subra, P.; Berroy, P.; Vega, A.; Domingo, C., Process performances and characteristics of powders produced using supercritical CO<sub>2</sub> as solvent and antisolvent. *Powder Technol.* **2004**, 142, (1), 13-22.
173. Breitenbach, A.; Mohr, D.; Kissel, T., Biodegradable semi-crystalline comb polyesters influence the microsphere production by means of a supercritical fluid extraction technique (ASES). *J. Controlled Release* **2000**, 63, (1-2), 53-68.
174. Yeo, S. D.; Lee, J. C., Crystallization of sulfarnethizole using the supercritical and liquid antisolvent processes. *J. Supercrit. Fluids* **2004**, 30, (3), 315-323.
175. Chen, K. X.; Zhang, X. Y.; Pan, J.; Yin, W. H., Recrystallization of andrographolide using the supercritical fluid antisolvent process. *J. Cryst. Growth* **2005**, 274, (1-2), 226-232.
176. Kalogiannis, C. G.; Pavlidou, E.; Panayiotou, C. G., Production of amoxicillin microparticles by supercritical antisolvent precipitation. *Ind. Eng. Chem. Res.* **2005**, 44, (24), 9339-9346.
177. Liu, X. W.; Li, Z. Y.; Han, B.; Yuan, T. L., Supercritical antisolvent precipitation of microparticles of quercetin. *Chinese J. Chem. Eng.* **2005**, 13, (1), 128-130.
178. Subra, P.; Laudani, C.-G.; Vega-Gonzalez, A.; Reverchon, E., Precipitation and phase behavior of theophylline in solvent-supercritical CO<sub>2</sub> mixtures. *J. Supercrit. Fluids* **2005**, 35, (2), 95-105.

179. Bakhbakhi, Y.; Charpentier, P. A.; Rohani, S., Experimental study of the GAS process for producing microparticles of beclomethasone-17,21-dipropionate suitable for pulmonary delivery. *Int. J. Pharm.* **2006**, 309, (1-2), 71-80.
180. Kikic, I.; Alessi, P.; Eva, F.; Moneghini, M.; Perissutti, B., Supercritical antisolvent precipitation of atenolol: The influence of the organic solvent and of the processing approach. *J. Supercrit. Fluids* **2006**, 38, (3), 434-441.
181. Miguel, F.; Martin, A.; Gamse, T.; Cocero, M. J., Supercritical anti solvent precipitation of lycopene - Effect of the operating parameters. *J. Supercrit. Fluids* **2006**, 36, (3), 225-235.
182. Niu, F. H.; Roby, K. F.; Rajewski, R. A.; Decedue, C.; Subramaniam, B., In *Paclitaxel nanoparticles: Production using compressed CO<sub>2</sub> as antisolvent: Characterization and animal model studies*; Svenson, S., Ed.; ACS Symposium Series 924, American Chemical Society: Washington, DC, 2006; 262-277.
183. Park, S. J.; Jeon, S. Y.; Yeo, S. D., Recrystallization of a pharmaceutical compound using liquid and supercritical antisolvents. *Ind. Eng. Chem. Res.* **2006**, 45, (7), 2287-2293.
184. Sacha, G. A.; Schmitt, W. J.; Nail, S. L., Identification of critical process variables affecting particle size following precipitation using a supercritical fluid. *Pharm. Dev. Technol* **2006**, 11, (2), 187-194.
185. Sacha, G. A.; Schmitt, W. J.; Nail, S. L., Identification of physical-chemical variables affecting particle size following precipitation using a supercritical fluid. *Pharm. Dev. Technol* **2006**, 11, (2), 195-205.
186. Thakur, R.; Gupta, R. B., Production of hydrocortisone micro- and nanoparticles using supercritical anti-solvent with enhanced mass transfer. *Chem. Eng. Commun.* **2006**, 193, (3), 293-305.
187. Kim, M. S.; Lee, S.; Park, J. S.; Woo, J. S.; Hwang, S. J., Micronization of cilostazol using supercritical antisolvent (SAS) process: Effect of process parameters. *Powder Technol.* **2007**, 177, (2), 64-70.
188. Martin, A.; Gutierrez, L.; Mattea, F.; Cocero, M. J., Precipitation of mandelic acid with a supercritical antisolvent process: Experimental and theoretical analysis, optimization, and scaleup. *Ind. Eng. Chem. Res.* **2007**, 46, (5), 1552-1562.
189. Park, H. J.; Kim, M. S.; Lee, S.; Kim, J. S.; Woo, J. S.; Park, J. S.; Hwang, S. J., Recrystallization of fluconazole using the supercritical antisolvent (SAS) process. *Int. J. Pharm.* **2007**, 328, (2), 152-160.
190. Tenorio, A.; Gordillo, M. D.; Pereyra, C.; de la Ossa, E. J. M., Controlled submicro particle formation of ampicillin by supercritical antisolvent precipitation. *J. Supercrit. Fluids* **2007**, 40, (2), 308-316.

191. Tenorio, A.; Gordillo, M. D.; Pereyra, C. M.; de la Ossa, E. J. M., Relative importance of the operating conditions involved in the formation of nanoparticles of ampicillin by supercritical antisolvent precipitation. *Ind. Eng. Chem. Res.* **2007**, 46, (1), 114-123.
192. Vatanara, A.; Najafabadi, A. R.; Gilani, K.; Asgharian, R.; Darabi, M.; Rafiee-Tehrani, M., A Plackett-Burman design for screening of the operation variables in the formation of salbutamol sulphate particles by supercritical antisolvent. *J. Supercrit. Fluids* **2007**, 40, (1), 111-116.
193. Adami, R.; Reverchon, E.; Jarvenpaa, E.; Huopalahti, R., Supercritical AntiSolvent micronization of nalmefene HCl on laboratory and pilot scale. *Powder Technol.* **2008**, 182, (1), 105-112.
194. Cardoso, M. A. T.; Monteiro, G. A.; Cardoso, J. P.; Prazeres, T. J. V.; Figueiredo, J. M. F.; Martinho, J. M. G.; Cabral, J. M. S.; Palavra, A. M. F., Supercritical antisolvent micronization of minocycline hydrochloride. *The J. Supercrit. Fluids* **2008**, 44, (2), 238-244.
195. Chang, Y.-P.; Tang, M.; Chen, Y.-P., Micronization of sulfamethoxazole using the supercritical anti-solvent process. *J. Mater. Sci.* **2008**, 43, (7), 2328-2335.
196. Franceschi, E.; Kunita, M. H.; Tres, M. V.; Rubira, A. F.; Muniz, E. C.; Corazza, M. L.; Dariva, C.; Ferreira, S. R. S.; Oliveira, J. V., Phase behavior and process parameters effects on the characteristics of precipitated theophylline using carbon dioxide as antisolvent. *J. Supercrit. Fluids* **2008**, 44, 8-20.
197. Kim, J.-S.; Kim, M.-S.; Park, H. J.; Jin, S.-J.; Lee, S.; Hwang, S.-J., Physicochemical properties and oral bioavailability of amorphous atorvastatin hemi-calcium using spray-drying and SAS process. *Int. J. Pharm.* **2008**, 359, (1-2), 211-219.
198. Kim, M.-S.; Jin, S.-J.; Kim, J.-S.; Park, H. J.; Song, H.-S.; Neubert, R. H. H.; Hwang, S.-J., Preparation, characterization and in vivo evaluation of amorphous atorvastatin calcium nanoparticles using supercritical antisolvent (SAS) process. *Eur. J. Pharm. Biopharm.* **2008**, 69, (2), 454-465.
199. Kim, Y. H.; Shing, K. S., Supercritical fluid-micronized ipratropium bromide for pulmonary drug delivery. *Powder Technol.* **2008**, 182, (1), 25-32.
200. Sanganwar, G. P.; Gupta, R. B., Enhancement of Shelf Life and Handling Properties of Drug Nanoparticles: Nanoscale Mixing of Itraconazole with Silica. *Ind. Eng. Chem. Res.* **2008**, 47, (14), 4717-4725.
201. Tavares Cardoso, M. A.; Geraldies, V.; Cabral, J. M. S.; Palavra, A. M. F., Characterization of minocycline powder micronized by a supercritical antisolvent (SAS) process. *J. Supercrit. Fluids* **2008**, 46, (1), 71-76.

202. Tenorio, A.; Gordillo, M. D.; Pereyra, C. M.; de la Ossa, E. J. M., Screening design of experiment applied to supercritical antisolvent precipitation of amoxicillin. *J. Supercrit. Fluids* **2008**, 44, (2), 230-237.
203. Li, D.; Han, B. X.; Liu, Z. M., Grafting of 2-hydroxyethyl methacrylate onto isotactic poly(propylene) using supercritical CO<sub>2</sub> as a solvent and swelling agent. *Macromol. Chem. Phys.* **2001**, 202, (11), 2187-2194.
204. Reverchon, E.; Della Porta, G.; De Rosa, I.; Subra, P.; Letourneur, D., Supercritical antisolvent micronization of some biopolymers. *J. Supercrit. Fluids* **2000**, 18, (3), 239-245.
205. Sarkari, M.; Darrat, I.; Knutson, B. L., Generation of microparticles using CO<sub>2</sub> and CO<sub>2</sub>-philic antisolvents. *AIChE J.* **2000**, 46, (9), 1850-1859.
206. Elvassore, N.; Baggio, M.; Pallado, P.; Bertucco, A., Production of different morphologies of biocompatible polymeric materials by supercritical CO<sub>2</sub> antisolvent techniques. *Biotechnol. Bioeng.* **2001**, 73, (6), 449-457.
207. Park, Y. K.; Curtis, C. W.; Roberts, C. B., Formation of nylon particles and fibers using precipitation with a compressed antisolvent. *Ind. Eng. Chem. Res.* **2002**, 41, (6), 1504-1510.
208. Song, K. H.; Lee, C. H.; Lim, J. S.; Lee, Y. W., Preparation of L-PLA submicron particles by a continuous supercritical antisolvent precipitation process. *Korean J. Chem. Eng.* **2002**, 19, (1), 139-145.
209. Vega-Gonzalez, A.; Domingo, C.; Elvira, C.; Subra, P., Precipitation of PMMA/PCL blends using supercritical carbon dioxide. *J. Appl. Polym. Sci.* **2004**, 91, (4), 2422-2426.
210. Choi, S.; Lee, K.; Kwon, S.; Kim, H., Preparation of fine particles of poly(N-vinyl-2-pyrrolidone-co-2-methylene-1,3-dioxepane) using supercritical antisolvent. *J. Supercrit. Fluids* **2006**, 37, (3), 287-291.
211. Duarte, A. R. C.; Gordillo, M. D.; Cardoso, M. M.; Simplicio, A. L.; Duarte, C. M. M., Preparation of ethyl cellulose/methyl cellulose blends by supercritical antisolvent precipitation. *Int. J. Pharm.* **2006**, 311, (1-2), 50-54.
212. Jarmer, D. J.; Lengsfeld, C. S.; Randolph, T. W., Scale-up criteria for an injector with a confined mixing chamber during precipitation with a compressed-fluid antisolvent. *J. Supercrit. Fluids* **2006**, 37, (2), 242-253.
213. Kim, M. Y.; Lee, Y. W.; Byun, H. S.; Lim, J. S., Recrystallization of poly(L-lactic acid) into submicrometer particles in supercritical carbon dioxide. *Ind. Eng. Chem. Res.* **2006**, 45, (10), 3388-3392.
214. Adami, R.; Osseo, L. S.; Huopalahti, R.; Reverchon, E., Supercritical AntiSolvent micronization of PVA by semi-continuous and batch processing. *J. Supercrit. Fluids* **2007**, 42, (2), 288-298.

215. Chang, S. C.; Lee, M. J.; Lin, H. M., Nanoparticles formation for metallocene catalyzed cyclic olefin copolymer via a continuous supercritical anti-solvent process. *J. Supercrit. Fluids* **2007**, 40, (3), 420-432.
216. Chen, A. Z.; Pu, X. M.; Kang, Y. Q.; Liao, L.; Yao, Y. D.; Yin, G. F., Study of poly(L-lactide) microparticles based on supercritical CO<sub>2</sub>. *J. Mater. Sci. - Mater. Med.* **2007**, 18, (12), 2339-2345.
217. Costa, M. S.; Duarte, A. R. C.; Cardoso, M. M.; Duarte, C. M. M., Supercritical antisolvent precipitation of PHBV microparticles. *Int. J. Pharm.* **2007**, 328, (1), 72-77.
218. Kim, M.; Yoo, K.-P.; Lim, J., Preparation of poly(L-lactic acid) submicron particles in aerosol solvent extraction system using supercritical carbon dioxide. *Korean J. Chem. Eng.* **2007**, 24, (5), 860-865.
219. Obrzut, D. L.; Bell, P. W.; Roberts, C. B.; Duke, S. R., Effect of process conditions on the spray characteristics of a PLA plus methylene chloride solution in the supercritical antisolvent precipitation process. *J. Supercrit. Fluids* **2007**, 42, (2), 299-309.
220. De Marco, I.; Reverchon, E., Supercritical antisolvent micronization of cyclodextrins. *Powder Technol.* **2008**, 183, (2), 239-246.
221. Young, T. J.; Johnston, K. P.; Mishima, K.; Tanaka, H., Encapsulation of lysozyme in a biodegradable polymer by precipitation with a vapor-over-liquid antisolvent. *J. Pharm. Sci.* **1999**, 88, (6), 640-650.
222. Ghaderi, R.; Artursson, P.; Carlfors, J., A new method for preparing biodegradable microparticles and entrapment of hydrocortisone in DL-PLG microparticles using supercritical fluids. *Eur. J. Pharm. Sci.* **2000**, 10, (1), 1-9.
223. Elvassore, N.; Bertucco, A.; Caliceti, P., Production of insulin-loaded poly(ethylene glycol)/poly(l-lactide) (PEG/PLA) nanoparticles by gas antisolvent techniques. *J. Pharm. Sci.* **2001**, 90, (10), 1628-1636.
224. Elvassore, N.; Bertucco, A.; Caliceti, P., Production of protein-loaded polymeric microcapsules by compressed CO<sub>2</sub> in a mixed solvent. *Ind. Eng. Chem. Res.* **2001**, 40, (3), 795-800.
225. Taki, S.; Badens, E.; Charbit, G., Controlled release system formed by supercritical anti-solvent coprecipitation of a herbicide and a biodegradable polymer. *J. Supercrit. Fluids* **2001**, 21, (1), 61-70.
226. Corrigan, O. I.; Crean, A. M., Comparative physicochemical properties of hydrocortisone-PVP composites prepared using supercritical carbon dioxide by the GAS anti-solvent recrystallization process, by coprecipitation and by spray drying. *Int. J. Pharm.* **2002**, 245, (1-2), 75-82.

227. Martin, T. M.; Bandi, N.; Shulz, N.; Roberts, C. B.; Kompella, U. B., Preparation of Budesonide and Budesonide-PLA Microparticles Using Supercritical Fluid Precipitation Technology. *AAPS PharmSciTech* **2002**, 3, (3), 1-11.
228. Tu, L. S.; Dehghani, F.; Foster, N. R., Micronisation and microencapsulation of pharmaceuticals using a carbon dioxide antisolvent. *Powder Technol.* **2002**, 126, (2), 134-149.
229. Boutin, O.; Badens, E.; Carretier, E.; Charbit, G., Co-precipitation of a herbicide and biodegradable materials by the supercritical anti-solvent technique. *J. Supercrit. Fluids* **2004**, 31, (1), 89-99.
230. Caliceti, P.; Salmaso, S.; Elvassore, N.; Bertucco, A., Effective protein release from PEG/PLA nano-particles produced by compressed gas anti-solvent precipitation techniques. *J. Controlled Release* **2004**, 94, (1), 195-205.
231. Salmaso, S.; Elvassore, N.; Bertucco, A.; Lante, A.; Caliceti, P., Nisin-loaded poly-L-lactide nano-particles produced by CO<sub>2</sub> anti-solvent precipitation for sustained antimicrobial activity. *Int. J. Pharm.* **2004**, 287, (1-2), 163-173.
232. Jun, S. W.; Kim, M. S.; Jo, G. H.; Lee, S.; Woo, J. S.; Park, J. S.; Hwang, S. J., Cefuroxime axetil solid dispersions prepared using solution enhanced dispersion by supercritical fluids. *J. Pharm. Pharmacol.* **2005**, 57, (12), 1529-1537.
233. Thote, A. J.; Gupta, R. B., Formation of nanoparticles of a hydrophilic drug using supercritical carbon dioxide and microencapsulation for sustained release. *Nanomed. Nanotechnol. Bio. Med.* **2005**, 1, (1), 85-90.
234. Zhou, H. Y.; Zhang, Y. L.; Biggs, D. L.; Manning, M. C.; Randolph, T. W.; Christians, U.; Hybertson, B. M.; Hg, K. Y., Microparticle-based lung delivery of INH decreases INH metabolism and targets alveolar macrophages. *J. Controlled Release* **2005**, 107, (2), 288-299.
235. Kalogiannis, C. G.; Michailof, C. M.; Panayiotou, C. G., Microencapsulation of Amoxicillin in poly(L-lactic acid) by supercritical antisolvent precipitation. *Ind. Eng. Chem. Res.* **2006**, 45, (25), 8738-8743.
236. Lee, S.; Kim, M. S.; Kim, J. S.; Park, H. J.; Woo, J. S.; Lee, B. C.; Hwang, S. J., Controlled delivery of a hydrophilic drug from a biodegradable microsphere system by supercritical anti-solvent precipitation technique. *J. Microencapsulation* **2006**, 23, (7), 741-749.
237. Mammucari, R.; Dehghani, F.; Foster, N. R., Dense gas processing of micron-sized drug formulations incorporating hydroxypropylated and methylated beta-cyclodextrin. *Pharm. Res.* **2006**, 23, (2), 429-437.
238. Moneghini, M.; Perissutti, B.; Kikic, I.; Grassi, M.; Cortesi, A.; Princivalle, F., Preparation of theophylline-hydroxypropylmethylcellulose matrices using

- supercritical antisolvent precipitation: A preliminary study. *Drug Dev. Ind. Pharm.* **2006**, 32, (1), 39-52.
239. Toropainen, T.; Matilainen, L.; Velaga, S.; Heikkila, T.; Jarho, P.; Carlfors, J.; Lehto, V. P.; Jarvinen, T.; Jarvinen, K., Preparation of solid budesonide/Y-cyclodextrin complexes with a novel single-step supercritical fluid process (SEDS). *Eur. J. Pharm. Sci.* **2006**, 28, S17-S17.
  240. Wang, Y. L.; Wang, Y. P.; Yang, J.; Pfeffer, R.; Dave, R.; Michniak, B., The application of a supercritical antisolvent process for sustained drug delivery. *Powder Technol.* **2006**, 164, (2), 94-102.
  241. Yasuji, T.; Haslam, J.; Kajiyama, A.; McIntosh, M. P.; Rajewski, R. A., Preliminary evaluation of polymer-based drug composite microparticle production by coacervate desolvation with supercritical carbon dioxide. *J. Pharm. Sci.* **2006**, 95, (3), 581-588.
  242. He, W. Z.; Suo, Q. L.; Hong, H. L.; Shan, A.; Li, C. P.; Huang, Y. C.; Li, Y. X.; Zhu, M. D., Production of natural carotene-dispersed polymer microparticles by SEDS-PA co-precipitation. *J. Mater. Sci.* **2007**, 42, (10), 3495-3501.
  243. Jun, S. W.; Kim, M. S.; Kim, J. S.; Park, H. J.; Lee, S.; Woo, J. S.; Hwang, S. J., Preparation and characterization of simvastatin/hydroxypropyl-beta-cyclodextrin inclusion complex using supercritical antisolvent (SAS) process. *Eur. J. Pharm. Biopharm.* **2007**, 66, (3), 413-421.
  244. Martin, A.; Mattea, F.; Gutierrez, L.; Miguel, F.; Cocero, M. J., Co-precipitation of carotenoids and bio-polymers with the supercritical anti-solvent process. *J. Supercrit. Fluids* **2007**, 41, (1), 138-147.
  245. Barrett, A.; Dehghani, F.; Foster, N., Increasing the Dissolution Rate of Itraconazole Processed by Gas Antisolvent Techniques using Polyethylene Glycol as a Carrier. *Pharm. Res.* **2008**, 25, (6), 1274-1289.
  246. Kang, Y.; Wu, J.; Yin, G.; Huang, Z.; Liao, X.; Yao, Y.; Ouyang, P.; Wang, H.; Yang, Q., Characterization and Biological Evaluation of Paclitaxel-Loaded Poly(L-lactic acid) Microparticles Prepared by Supercritical CO<sub>2</sub>. *Langmuir* **2008**, 24, (14), 7432-7441
  247. Lee, L. Y.; Wang, C. H.; Smith, K. A., Supercritical antisolvent production of biodegradable micro- and nanoparticles for controlled delivery of paclitaxel. *J. Controlled Release* **2008**, 125, (2), 96-106.
  248. Lee, S.-Y.; Jung, I.-I.; Kim, J.-K.; Lim, G.-B.; Ryu, J.-H., Preparation of itraconazole/HP-[beta]-CD inclusion complexes using supercritical aerosol solvent extraction system and their dissolution characteristics. *J. Supercrit. Fluids* **2008**, 44, (3), 400-408.

## **APPENDICES**

Table A-1. Pharmaceutical substances micronized with the dense gas antisolvent process (1999 - present).

Substrates	Solvents	Acronym	Morphology	Year	References
Griseofulvin	NMP	SAS	0.6-0.8 $\mu\text{m}$ aggregates of tetracycline	1999	Reverchon <sup>155</sup>
ampicillin	DMSO				
amoxicillin	EtOH				
tetracycline	DCM				
ascorbic acid	EtOH	PCA	2 $\mu\text{m}$ crystals	1999	Wubbolts <sup>156</sup>
acetaminophen		SAS			
soy lecithin	EtOH	SAS	1-40 $\mu\text{m}$ spherical aggregates	2000	Magnan <sup>157</sup>
amoxicillin	NMP	SAS	0.25-1.2 $\mu\text{m}$ spherical particles	2000	Reverchon <sup>158</sup>
	DMSO				
soy lecithin	EtOH	SAS	1-40 $\mu\text{m}$ spherical aggregates	2001	Badens <sup>159</sup>
Griseofulvin	THF	SAS-EM	130 nm nanoparticles	2001	Chattopadhyay <sup>160</sup>
	DCM				
tetracycline	THF	SAS-EM	125 nm nanoparticles	2001	Chattopadhyay <sup>101</sup>
carbamazepine	MeOH	SEDS	different polymorphs	2001	Edwards <sup>161</sup>
	DCM				
sulfathiazole	MeOH	SEDS	different polymorphs	2001	Kordikowski <sup>148</sup>
	Ace				
nicotinic acid	MeOH	SEDS	1-5 $\mu\text{m}$	2001	Rehman <sup>162</sup>
salbutamol	DMSO	SAS	1-3 $\mu\text{m}$ x 0.2-0.35 $\mu\text{m}$ rods	2001	Reverchon <sup>163</sup>
	MeOH				
	EtOH/H <sub>2</sub> O				
$\beta$ -carotene	EtAc	GAS	<1 $\mu\text{m}$ crystals	2002	Cocero <sup>164</sup>
	DCM				

Substrates	Solvents	Acronym	Morphology	Year	References
tartaric acid	Ace EtOH	PCA	10-60 $\mu\text{m}$ needles or plate-like crystals	2002	Krober <sup>165</sup>
rifampicin	MeOH/EtOH DMSO NMP MeOH EtAc	SAS	0.4-1 $\mu\text{m}$ nanoparticles; 2.5-5 $\mu\text{m}$ microparticles	2002	Reverchon <sup>166</sup>
budesonide	Ace	SEDS	different polymorphs	2002	Velaga <sup>147</sup>
flunisolide	MeOH				
Copper indomethacin	DMF	GAS ASES	8 $\mu\text{m}$ from ASES	2002	Warwick <sup>167</sup>
Copper indomethacin	DMF	ASES	<5 $\mu\text{m}$ microspheres; 20-50 $\mu\text{m}$ porous particles	2003	Foster <sup>13</sup>
paracetamol	MeOH	PCA	microcrystals and microspheres	2003	Krober <sup>168</sup>
tartaric acid	EtOH Ace DMF MeOH/EtOH				
sulfathiazole	Ace	SAS	microcrystals with changed crystal habit	2003	Yeo <sup>169</sup>
chlorpropamide	MeOH EtAc				
paracetamol	Ace	GAS	50-250 $\mu\text{m}$ crystals	2004	Fusaro <sup>170</sup>
cefonicid	DMSO	SAS	0.2-50 $\mu\text{m}$ spheres	2004	Reverchon <sup>171</sup>
cholesterol	DCM	SAS	10s-100s $\mu\text{m}$ particles	2004	Subra <sup>172</sup>
flunisolide	Ace MeOH	SEDS	different polymorphs	2004	Velaga <sup>173</sup>

Substrates	Solvents	Acronym	Morphology	Year	References
sulfamethizole	Ace DMF	SAS	1s-100s $\mu\text{m}$ with different crystal habits	2004	Yeo <sup>174</sup>
ahdrographolide	EtOH	SAS	different crystallinity and size	2005	Chen <sup>175</sup>
amoxicillin	DMSO	SAS	0.2-1.6 $\mu\text{m}$ spherical particles	2005	Kalogiannis <sup>176</sup>
	EtOH/DMSO				
quercetin	EtOH	SAS	1-6 $\mu\text{m}$ spherical particles	2005	Liu <sup>177</sup>
theophylline	EtOH/DCM	SAS	15-500 $\mu\text{m}$ plate-like aggregates	2005	Subra <sup>178</sup>
beclomethasone-17,21-dipropionate	Ace MeOH EtOH	GAS	1.8 $\mu\text{m}$ on average	2006	Bakhabkhi <sup>179</sup>
atenolol	MeOH EtOH i-PrOH	SAS	10s $\mu\text{m}$ particles	2006	Kikic <sup>180</sup>
lycopene	DCM	SAS	10-80 $\mu\text{m}$ particles	2006	Miguel <sup>181</sup>
phenytoin	Ace Ace/EtOH	GAS PCA	1s-10s $\mu\text{m}$ with different aspect ratios	2006	Muhrer <sup>124</sup>
paclitaxel	Ace	PCA	0.6-0.64 $\mu\text{m}$	2006	Niu <sup>182</sup>
sulfabenzamide	Ace MeOH EtOH EtAc	SAS	1s-10s $\mu\text{m}$ with different aspect ratios	2006	Park <sup>183</sup>
cefuroxime	DMSO	SAS	0.1-14 $\mu\text{m}$ spherical pariticles and 3-50 $\mu\text{m}$ balloons	2006	Reverchon <sup>97</sup>
cefoperazone					
methylprednisolone acetate	THF	SAS	10s $\mu\text{m}$ particles	2006	Sacha <sup>184</sup>

Substrates	Solvents	Acronym	Morphology	Year	References
methylprednisolone acetate methylprednisolone hemisuccinate Prednisolone Prednisolone acetate Prednisolone hemisuccinate hydrocortisone acetate hydrocortisone cilostazol	THF Chloroform Ace MeOH DCM EtOH MeOH DCM Acetic acid	SAS SAS-EM SAS	10s $\mu\text{m}$ particles 180 nm nanoparticles 0.9-4.5 $\mu\text{m}$ particles	2006 2006 2007	Sacha <sup>185</sup> Thakur <sup>186</sup> Kim <sup>187</sup>
salicylic acid mandelic acid fluconazole tolbutamide	EtOH Ace EtAc DCM Ace EtAc Ace/EtOH Ace/diethyl ether Ace/H <sub>2</sub> O	PCA SAS SAS SAS SAS	100 nm nanoparticles 30-200 $\mu\text{m}$ prismatic or needlelike particles different polymorphs different polymorphs	2007 2007 2007 2007 2007	Lin <sup>116</sup> Martin <sup>188</sup> Park <sup>189</sup> Subra-Paternault <sup>133</sup>
ampicillin	NMP DMSO EtOH	SAS	0.26 $\pm$ 0.08 $\mu\text{m}$ spherical particles	2007	Tenorio <sup>190</sup>
ampicillin salbutamol sulphate nalmefene hydrochloride minocycline hydrochloride	NMP MeOH EtOH EtOH	SAS SAS SAS SAS	99-395 nm 10s $\mu\text{m}$ particles 0.5-2 $\mu\text{m}$ spheres and 10-20 $\mu\text{m}$ balloons 0.1-1 $\mu\text{m}$ particles	2007 2007 2007 2008	Tenorio <sup>191</sup> Vatanara <sup>192</sup> Adami <sup>193</sup> Cardoso <sup>194</sup>

Substrates	Solvents	Acronym	Morphology	Year	References
sulfamethoxazole	Ace	GAS SAS	10s $\mu\text{m}$ foR GAS; 1s $\mu\text{m}$ for SAS	2008	Chang <sup>195</sup>
theophylline	EtOH/DCM	PCA	3-70 $\mu\text{m}$ platelike particles	2008	Franceschi <sup>196</sup>
atorvastatin hemi-calcium	Ace	SAS	68.7 $\pm$ 15.8 nm from Ace; 95.7 $\pm$ 12.2 nm from THF	2008	Kim <sup>197</sup>
atorvastatin hemi-calcium	THF	SAS	152-863 nm	2008	Kim <sup>198</sup>
ipratropium bromide	MeOH	ASES	0.6-3.0 $\mu\text{m}$	2008	Kim <sup>199</sup>
	DMF				
	EtOH				
	EtOH/Ace				
itraconazole	DCM	SAS-EM	flakes with thickness <150 nm	2008	Sanganwar <sup>200</sup>
minocycline	EtOH	SAS	250 nm particles	2008	Cardoso <sup>201</sup>
amoxicillin	NMP	SAS	182-450 nm particles	2008	Tenorio <sup>202</sup>
chelerythrine	MeOH	SEDS-PA	0.1-1 $\mu\text{m}$	2008	Hong

Note:

1. 1s  $\mu\text{m}$ : 1-10  $\mu\text{m}$
2. 10s  $\mu\text{m}$ : 10-100  $\mu\text{m}$

Table A-2. Polymeric materials prepared with the dense gas antisolvent process (2000 – present).

Polymer	Solvent	Acronym	Morphology	Year	References
L-PLA	DCM	ASES	microspheres	2000	Breitenback <sup>173</sup>
DSS(8)-L-PLA			foams		
PVA(15)-L-PLA			balloons		
poly(ethylene terephthalate)	Phenol	GAS	agglomerated flakes	2000	Li <sup>203</sup>
			cobwebs		
			fibers		
dextran	DMSO	SAS	microparticles with different degree of	2000	Reverchon <sup>204</sup>
L-PLA	DCM		agglomeration		
HPMA					
Inulin					
PVA					
PCA					
L-PLA	DCM	PCA	0.5-2.5 $\mu\text{m}$ particles	2000	Sakari <sup>205</sup>
	Chloroform				
hyaluronic	acid-derived	DMSO	SAS	2001	Elvassore <sup>206</sup>
polymers			microspheres		
			threads		
			fibers		
			networks/sponges		
nylon 6/6	formic acid	PCA	microspheres	2002	Park <sup>207</sup>
			fibers		
			films		
L-PLA	DCM	SAS	0.1-1 $\mu\text{m}$	2002	Song <sup>208</sup>
L-PLA	DCM	PCA	0.19-1.43 $\mu\text{m}$	2003	Jarmer <sup>100</sup>
dextran	DMSO	PCA	microparticles	2004	Perez <sup>115</sup>

Polymer	Solvent	Acronym	Morphology	Year	References
PMMA/PCL	DCM	SAS	fibrous networks	2004	Vega-Gonzalez <sup>209</sup>
L-PLA	DCM	PCA	5-50 $\mu\text{m}$ particles	2005	de Diego <sup>114</sup>
poly(NVP-co-MDOP)	DCM	ASES	0.1-2 $\mu\text{m}$ fibers 0.18-0.26 $\mu\text{m}$ particles	2006	Choi <sup>210</sup>
N-trimethylchitosan	DMSO DMSO+H <sub>2</sub> O	PCA	1-10 $\mu\text{m}$ particles	2006	de Diego <sup>113</sup>
ethyl cellulose/methyl cellulose	DCM+DMF	SAS	5-30 $\mu\text{m}$ particles	2006	Durate <sup>211</sup>
L-PLA	DCM	PCA	around 1 $\mu\text{m}$ particles	2006	Jarmer <sup>212</sup>
L-PLA	DCM	ASES	submicronic particles	2006	Kim <sup>213</sup>
PVA	THF 1,4-dioxane DMSO	GAS SAS	GAS: 0.4-2 $\mu\text{m}$ SAS: 50-250 nm	2007	Adami <sup>214</sup>
m(COC)	Toluene o-Xylene m-Xylene p-Xylene THF	SAS	nanoparticles	2007	Chang <sup>215</sup>
L-PLA	DCM+Ace	SEDS	0.64-6.64 $\mu\text{m}$ particles	2007	Chen <sup>216</sup>
PHBV	DCM	SAS	3-9 $\mu\text{m}$	2007	Costa <sup>217</sup>
PVP	DCM DCM+Ace	SAS	nanoparticles	2007	Gokhale <sup>104</sup>

Polymer	Solvent	Acronym	Morphology	Year	References
L-PLA	DCM	ASES	submicronic particles	2007	Kim <sup>218</sup>
L-PLA	DCM	SAS	0.25-5.5 $\mu\text{m}$	2007	Obrzut <sup>219</sup>
$\alpha$ -cyclodextrin	DMSO	SAS	0.1-11 $\mu\text{m}$	2008	De Marco <sup>220</sup>
$\beta$ -cyclodextrin					

Note:

1. m(COC): metallocene catalyzed cyclic olefin copolymer
2. PHBV: poly(3-hydroxybutyrate-co-3-hydroxyvalerate)

Table A-3. Composite particles prepared using dense gas antisolvent processes (1999 - present).

Substrates	Polymers	Solvent	Acronym	Morphology (μm)	Year	References
lysozyme	L-PLA	DCM	DGA	5-70 μm particles	1999	Young <sup>221</sup>
hydrocortisone	l-PLGA	DCM	SEDs	2.4-140 μm particles	2000	Ghaderi <sup>222</sup>
	L-PLA	EtAc	(CO <sub>2</sub> + N <sub>2</sub>			
	d,L-PLA	Ace	as			
	PCL	Hexane	antisolvent			
		i-PrOH	)			
		EtOH				
insulin	PEG/L-PLA	DCM/DMSO	ASES	400-600 nm nanospheres	2001	Elvassore <sup>223</sup>
insulin	PLA	DCM/DMSO	SAS	0.5-2 μm microspheres	2001	Elvassore <sup>224</sup>
carbamazepine	PEG	Ace	GAS	different morphogy and size	2001	Moneghini <sup>125</sup>
diluron	L-PLA	DCM	SAS	1s μm particles	2001	Taki <sup>225</sup>
hydrocortisone	PVP	EtOH	SAS	microcrystals	2002	Corrigan <sup>226</sup>
budesonide	PLA	DCM	DGA	1s μm particles	2002	Martin <sup>227</sup>
p-HBA	L-PLA	MeOH	ASES	microspheres and	2002	Tu <sup>228</sup>
(parahydroxybenzoic acid)		DMSO		nanospheres		
lysozyme		DCM				

Substrates	Polymers	Solvent	Acronym	Morphology (µm)	Year	References
2,6-dimethyl-8-(2-ethyl-6-methylbenzylamino)-3-hydroxymethylimidazo-[1,2-a]pyridine mesylate	mannitol eudragit E100	Ace MeOH DMSO	SEDS	irregular particles	2003	Juppo <sup>139</sup>
diluron	L-PLA ethyl cellulose PMMA	DCM THF	SAS	aggregates fibers spongy solid	2004	Boutin <sup>229</sup>
insulin	PLA/PEG	DCM/DMSO	DGA	nanoparticles	2004	Caliceti <sup>230</sup>
copper	PVP	DMF	ASES	50 nm-40 µm spheres	2004	Meure <sup>140</sup>
indomethacin	L-PLA	DMSO/DCM	DGA	200-400 nm particles	2004	Salmaso <sup>231</sup>
nisin	PSA	DCM	DGA	modified morphology	2004	Jarmer <sup>138</sup>
griseofulvin	HPMC 2910/PVPK30	DCM/EtOH	SEDS	200-300 nm	2005	Jun <sup>232</sup>
cefuroxime axetil	PLGA	MeOH	SAS-EM	150-200 nm	2005	Thote <sup>233</sup>
dexamethasone phosphate	HPMC/ Poloxamer 188 Poloxamer 407 Polyoxyethylene (60) hydrogenated castor oil	EtOH/DCM	SAS	200-250 nm	2005	Won <sup>123</sup>
felodipine	L-PLA	DCM	DGA	1-3 µm particles	2005	Zhou <sup>234</sup>
isoniazid	L-PLA	DCM/DMSO	SEDS	~1 µm particles	2006	Kalogiannis <sup>235</sup>
methanesulfonate						
amoxicillin						

Substrates	Polymers	Solvent	Acronym	Morphology (µm)	Year	References
bupivacaine	d,l-PLGA	EtOH/DCM	SAS	4-10 µm particles	2006	Lee <sup>236</sup>
hydrochloride	L-PLA					
naproxen	HPBCD	DMSO/Ace	ASES	<3 µm particles	2006	Mammucari <sup>237</sup>
	MBCD	EtOH				
theophylline	HPMC E5	Ace				
	HPMC K100	MeOH	SAS	N/A	2006	Moneghini <sup>238</sup>
		EtOH				
		Ace				
phenytoin	PVP	DCM/EtOH				
		EtOH/Ace	GAS;DGA	aggregates needles	2006	Muhrer <sup>124</sup>
budesonide	γ-CD	EtOH	SEDS	aggregates	2006	Toropainen <sup>239</sup>
hydrocortisone	PLGA	Ace	SAS	irregular particles	2006	Wang <sup>240</sup>
		MeOH				
		DCM				
phenytoin	PVP	EtOH	SAS	microparticles	2006	Yasuji <sup>241</sup>
		EtOH/Hexane				
carotene	PEG	DCM	SEDS-PA	irregular particles	2007	He <sup>242</sup>
simvastatin	HPBCD	EtOH/DCM	SAS	aggregated particles	2007	Jun <sup>243</sup>
oxeglitazar	Poloxamer 188	EtOH	SAS	irregular particles	2007	Majerik <sup>127</sup>
	Poloxamer 407	THF				
	PEG 8000	DCM				
	PVP K17	Chloroform				
		NMP				
		DMSO				
		EtOH/THF				
		EtOH/Chloroform				

Substrates	Polymers	Solvent	Acronym	Morphology (μm)	Year	References
oxeglitazar	PVP K17 Poloxamer 407	DCM	SAS	irregular particles	2007	Majerik <sup>126</sup>
β-carotene lutein	PEG	DCM	DGA	aggregated particles	2007	Martin <sup>244</sup>
itraconazole	PEG	DMF THF DCM	ASES	6.9 μm particles	2008	Barrett <sup>245</sup>
paclitaxel	L-PLA	DCM	SEDS	1s μm particles	2008	Kang <sup>246</sup>
paclitaxel	L-PLA	DCM	SAS-EM	370-820 nm particles	2008	Lee <sup>247</sup>
itraconazole	HPBCD	EtOH/DCM	ASES	aggregated nanoparticles	2008	Lee <sup>248</sup>

Table A-4. Vendor information of dense gas antisolvent equipment and accessories.

<b>Item</b>	<b>Vendors</b>
Gas cylinders	GTS-Welco
CO <sub>2</sub> cylinder regulator	Messer
HPLC syringe pump	Teledyne,
Tubing/fittings/valves	Swagelok
High pressure view cells	NE controls
Back pressure regulators	Tescom
Pressure gauge	Winters
Heat band	Omega
Rotameter	Dwyer
Coaxial nozzle	Sonotek
Air booster	Haskel
Chiller	Restek
Filter unit/element	Swagelok
Capillary nozzle	Varian

Table A-5. Summary of dense gas antisolvent precipitation of PVP.

PVP	$C_{total}$ [% (w/v)]	Solvent	$T$ (K)	$P$ (MPa)	Mean particle size ( $\mu\text{m}$ )	SEM
K29/32	1.0	DCM	298	9.66	0.6	Fig. 2-6(a)
K29/32	1.0	DCM	298	11.0	-	not shown
K29/32	1.0	DCM	298	12.4	-	not shown
K29/32	1.0	DCM	298	13.8	-	not shown
K29/32	3.0	DCM	293	9.66	1.6	Fig. 2-3(b)
K29/32	3.0	DCM	303	9.66	2.8	Fig. 2-3(d)
K29/32	3.0	DCM	298	9.66	1.5	Fig. 2-3(c) Fig. 2-5(a) Fig. 2-6(b)
K29/32	3.0	DCM	298	11.0	0.8	Fig. 2-5(b)
K29/32	3.0	DCM	298	12.4	1.8	Fig. 2-5(c)
K29/32	3.0	DCM	298	13.8	2.2	Fig. 2-5(d)
K29/32	5.0	DCM	298	9.66	2.0	Fig. 2-6(c)
K29/32	5.0	DCM	298	11.0	-	not shown
K29/32	5.0	DCM	298	12.4	-	not shown
K29/32	5.0	DCM	298	13.8	-	not shown
K29/32	8.0	DCM	298	9.66	2.5	Fig. 2-6(d)
K29/32	8.0	DCM	298	11.0	-	not shown
K29/32	3.0	DCM + Ace (v/v = 1:4)	298	9.66	-	not shown
K25	1.0	DCM	298	9.66	-	not shown
K25	5.0	DCM	308	9.66	-	not shown
K25	3.0	DCM	293	9.66	1.5	Fig.2-4(b)
K25	3.0	DCM	308	9.66	4.5	Fig.2-4(d)
K25	3.0	DCM	298	9.66	2.0	Fig.2-4(c)
K90	3.0	DCM	298	9.66	0.7	Fig. 2-7(a)
360K	3.0	DCM	298	9.66	0.8	Fig. 2-7(b)

Table A-6. Summary of dense gas antisolvent precipitation of poly(DTE carbonate).

<b>Solvent</b>	<b><math>C_{total}</math> [% (w/v)]</b>	<b><math>T</math> (K)</b>	<b><math>P</math> (MPa)</b>	<b><math>Q</math> (mL/min)</b>	<b>SEM</b>
DCM	0.5	306	10.34	1	Fig. 3-4(b)
DCM	1.0	293	8.97	1	not shown
DCM	1.0	293	9.66	1	not shown
DCM	1.0	293	12.41	1	not shown
DCM	1.0	298	9.66	1	not shown
DCM	1.0	293	10.34	1	Fig. 3-3(a)
DCM	1.0	298	11.03	1	Fig. 3-2(b)
DCM	1.0	298	11.72	1	not shown
DCM	1.0	303	8.97	1	not shown
DCM	1.0	303	9.66	1	not shown
DCM	1.0	303	10.34	1	not shown
DCM	1.0	303	11.03	1	not shown
DCM	1.0	303	11.72	1	not shown
DCM	1.0	303	12.41	1	not shown
DCM	1.0	303	13.79	1	not shown
DCM	1.0	306	8.97	1	not shown
DCM	5.0	306	10.34	1	Fig. 3-4(a)
DCM	1.0	306	10.34	0.5	not shown
DCM	1.0	308	10.34	1	Fig. 3-2(b)
DCM	1.0	306	11.03	1	not shown
DCM	1.0	306	11.72	1	not shown

Table A-7. Summary of dense gas antisolvent precipitation of PVP and Prd from solutions of methylene chloride.

Substance(s)	D/P	$C_{total}$ [% (w/v)]	$P$ (MPa)	$Q$ (mL/min)	Mean particle size ( $\mu\text{m}$ )	SEM
Prd + PVP K29/32	1:5	1.5	9.66	1	2.0	Fig. 4-3(a)
Prd + PVP K29/32	1:5	1.5	11.0	1	-	not shown
Prd + PVP K29/32	1:5	1.5	12.4	1	-	not shown
Prd + PVP K29/32	1:5	1.5	13.8	1	-	not shown
Prd + PVP K29/32	1:5	3.0	9.66	0.5	-	not shown
Prd + PVP K29/32	1:5	3.0	9.66	1	2.5	Fig. 4-3(b)
Prd + PVP K29/32	1:5	3.0	9.66	2	-	not shown
Prd + PVP K29/32	1:5	3.0	9.66	3	-	not shown
Prd + PVP K29/32	1:5	3.0	11.0	1	1.2	Fig. 4-4(b)
Prd + PVP K29/32	1:5	3.0	12.4	1	1.6	Fig. 4-4(c)
Prd + PVP K29/32	1:5	3.0	13.8	1	1.0	Fig. 4-4(d)
Prd + PVP K29/32	1:5	5.0	9.66	1	2.2	Fig. 4-3(c)
Prd + PVP K29/32	1:5	5.0	11.0	1	-	not shown
Prd + PVP K29/32	1:5	5.0	12.4	1	-	not shown
Prd + PVP K29/32	1:5	5.0	13.8	1	-	not shown
Prd + PVP K29/32	1:5	8.0	9.66	1	1.0	Fig. 4-3(d)
Prd + PVP K29/32	1:5	8.0	11.0	1	-	not shown
Prd + PVP K29/32	1:5	8.0	12.4	1	-	not shown
Prd + PVP K29/32	1:5	8.0	13.8	1	-	not shown
Prd + PVP K29/32	1:9	5.0	9.66	1	-	not shown
Prd + PVP K29/32	1:4	3.0	9.66	1	-	not shown
Prd + PVP K 25	1:5	3.0	9.66	1	2.0	Fig. 4-5(a)
Prd + PVP K 90	1:5	3.0	9.66	1	-	not shown
Prd + PVP K29/32	1:5	1.5	9.66	1	-	not shown

Table A-8. Summary of dense gas antisolvent precipitation of PVP and PrAc.

Substance(s)	Solvent	$C_{total}$ [% (w/v)]	$T$ (K)	$P$ (MPa)	SEM image
PrAc	DCM/Ace (1:4, v/v)	0.6	298	9.66	Fig. 5-2(b)
PrAc	Ace	0.5	298	9.66	Fig. 5-2(c)
PrAc	Ace	0.5	313	9.66	Fig. 5-2(d)
PrAc + PVP (1:5, w/w)	DCM/Ace (9:1, v/v)	2.4	298	9.66	Fig. 5-4(a)
PrAc + PVP (1:5, w/w)	DCM/Ace (8:2, v/v)	2.4	298	9.66	Fig. 5-4(b)
PrAc + PVP (1:5, w/w)	DCM/Ace (6:4, v/v)	2.4	298	9.66	not shown
PrAc + PVP (1:5, w/w)	DCM/Ace (5:5, v/v)	2.4	298	9.66	Fig. 5-4(d)
PrAc + PVP (1:5, w/w)	DCM/Ace (4:6, v/v)	2.4	298	9.66	Fig. 5-4(c)
PrAc + PVP (1:5, w/w)	DCM/Ace (2:8, v/v)	2.4	298	9.66	Fig. 5-4(e)
PrAc + PVP (1:5, w/w)	DCM/Ace (1:9, v/v)	2.4	298	9.66	Fig. 5-4(f)
PrAc + PVP (1:5, w/w)	DCM/Ace (1:4, v/v)	1.2	298	9.66	Fig. 5-5(a)
PrAc + PVP (1:5, w/w)	DCM/Ace (1:4, v/v)	2.4	298	9.66	Fig. 5-5(b)
PrAc + PVP (1:5, w/w)	DCM/Ace (1:4, v/v)	3.6	298	9.66	Fig. 5-5(c)
PrAc + PVP (1:5, w/w)	DCM/Ace (1:4, v/v)	4.8	298	9.66	Fig. 5-5(d)
PrAc + PVP (1:2, w/w)	DCM/Ace (1:4, v/v)	2.4	298	9.66	not shown
PrAc + PVP (1:3, w/w)	DCM/Ace (1:4, v/v)	2.4	298	9.66	not shown
PrAc + PVP (1:9, w/w)	DCM/Ace (1:4, v/v)	2.4	298	9.66	not shown
PrAc + PVP (1:5, w/w)	DCM/Ace (1:4, v/v)	2.4	298	11.0	Fig. 5-7(b)
PrAc + PVP (1:5, w/w)	DCM/Ace (1:4, v/v)	3.4	298	12.4	Fig. 5-7(c)
PrAc + PVP (1:5, w/w)	DCM/Ace (1:4, v/v)	4.4	298	13.8	Fig. 5-7(d)

Table A-9. Summary of dense gas antisolvent precipitation of PVP and Px.

Substance(s)	D/P	$C_{total}$ [% (w/v)]	Solvent	$T$ (K)	$P$ (MPa)	SEM image
Px	N/A	1.5	Ace	313	9.66	Fig. 6-2(d)
Px	N/A	1.0	ACN:Ace (v/v = 2:1)	298	9.66	not shown
Px	N/A	2.0	DCM	298	9.66	Fig. 6-3(a)
Px	N/A	1.5	DCM	298	11.0	not shown
Px	N/A	1.5	DCM	313	11.0	not shown
Px	N/A	1.5	DCM	313	9.66	not shown
Px	N/A	1.5	DCM	313	12.4	not shown
Px	N/A	1.5	DCM	303	9.66	not shown
Px	N/A	1.2	DCM+EtOH (v/v = 4:1)	298	9.66	not shown
Px	N/A	1.5	DCM+Hexane (v/v = 3:1)	298	9.66	not shown
Px	N/A	1.5	DMF	298	9.66	not shown
Px	N/A	1.5	DMF	313	9.83	not shown
Px	N/A	1.5	DMSO	313	9.66	N/A
Px	N/A	1.0	EtAc	298	9.66	not shown
Px	N/A	1.0	EtAc	313	9.66	not shown
Px + PVP K25	1:1	5.0	DCM	298	9.66	Fig. 6-3(c)
Px + PVP K25	1:2	5.0	DCM	298	9.66	Fig. 6-3(d)
Px + PVP K25	1:4	5.0	DCM	308	9.66	not shown
Px + PVP K25	1:9	5.0	DCM	298	9.66	Fig. 6-3(f)
Px + PVP K25	2:1	5.0	DCM	298	9.66	Fig. 6-3(b)
Px + PVP K90	1:1	5.0	DCM	298	9.66	not shown
Px + PVP K90	1:4	5.0	DCM	298	9.66	Fig. 6-3(e)
Px + PVP K90	1:9	5.0	DCM	298	9.66	not shown
Px <sup>+</sup> PVP K29/32	1:1	5.0	DCM	298	9.66	not shown
Px <sup>+</sup> PVP K29/32	1:9	5.0	DCM	298	9.66	not shown
Px <sup>+</sup> PVP K29/32	1:4	5.0	DCM	298	9.66	not shown

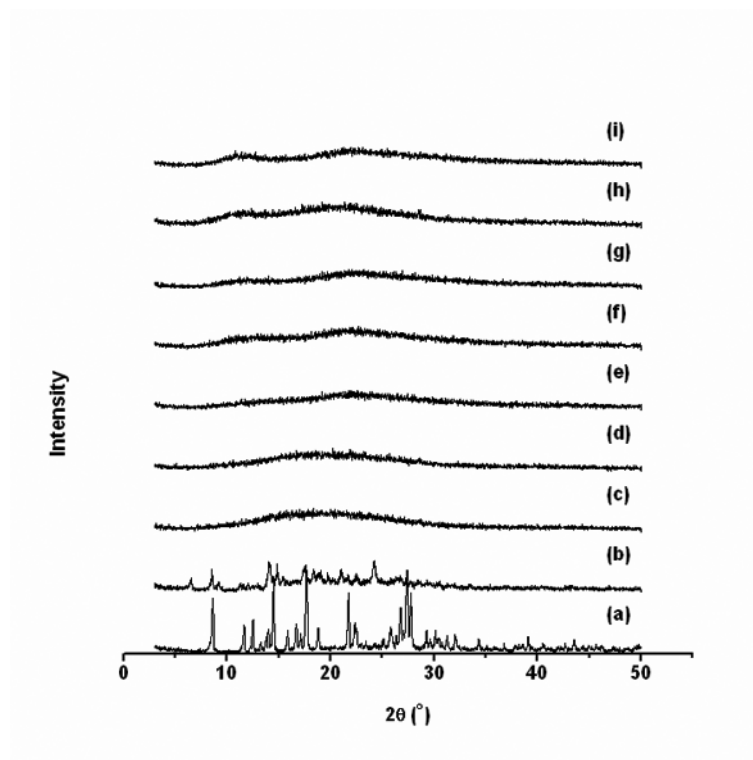


Figure A-1. PXRD patterns of piroxicam before (a) and after (b) spray drying and spray-dried solid dispersions with drug/polymer weight ratio of. (c) 2:1, (d) 1:1, (e) 1:2, (f) 1:4, (g) 1:9; PVP K25 before (h) and after (i) spray drying.

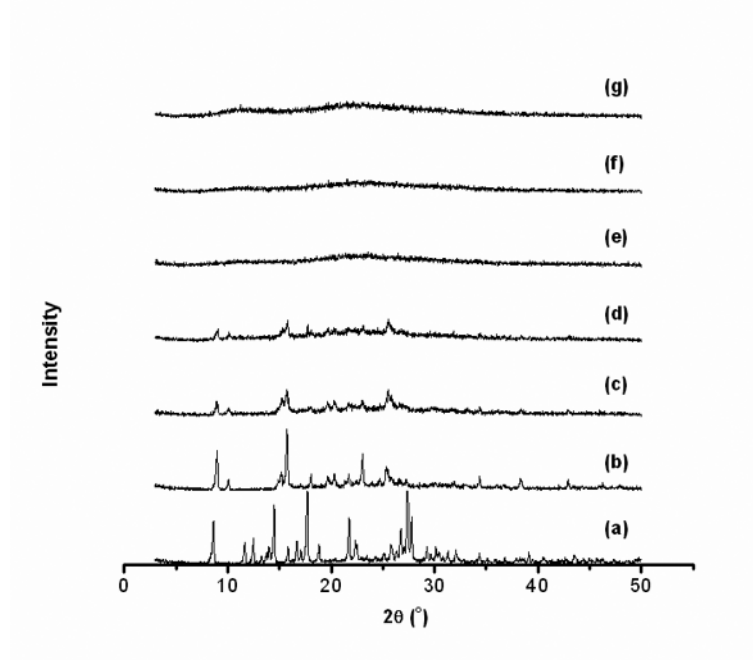


Figure A-2. PXRD patterns of piroxicam before (a) and after (b) DGA processing and DGA-processed solid dispersions with drug/polymer weight ratio of. (c) 2:1, (d) 1:1, (e) 1:2, (f) 1:4, (g) 1:9.

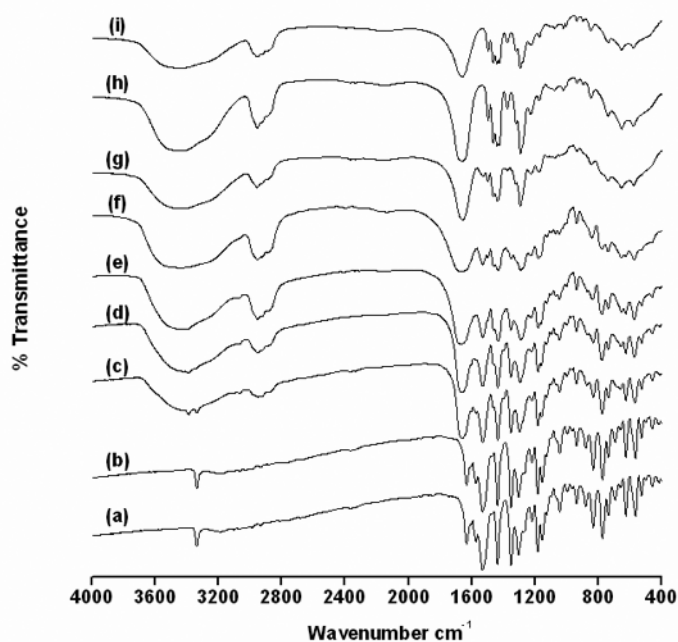


Figure A-3. FT-IR spectra of piroxicam before (a) and after (b) spray drying and spray-dried solid dispersions with drug/polymer weight ratio of. (c) 2:1, (d) 1:1, (e) 1:2, (f) 1:4, (g) 1:9; PVP K25 before (h) and after (i) spray drying.

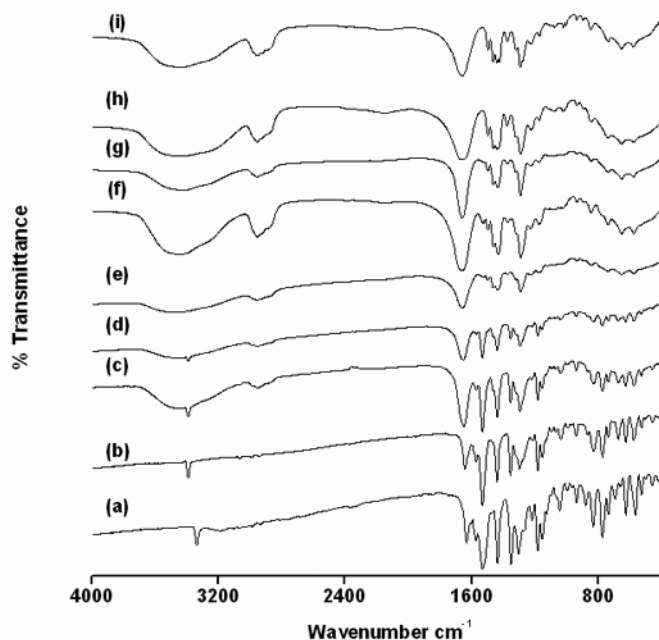


Figure A-4. FT-IR spectra of piroxicam before (a) and after (b) DGA processing and DGA-processed solid dispersions with drug/polymer weight ratio of. (c) 2:1, (d) 1:1, (e) 1:2, (f) 1:4, (g) 1:9; PVP K25 before (h) and after (i) DGA processing.

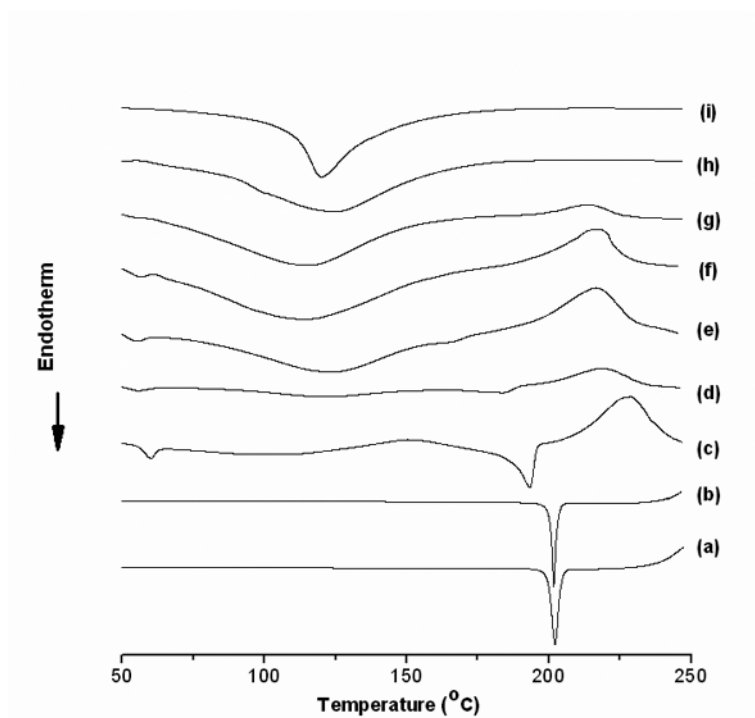


Figure A-5. DSC curves of piroxicam before (a) and after (b) spray drying and spray-dried solid dispersions with drug/polymer weight ratio of. (c) 2:1, (d) 1:1, (e) 1:2, (f) 1:4, (g) 1:9; PVP K25 before (h) and after (i) spray drying.

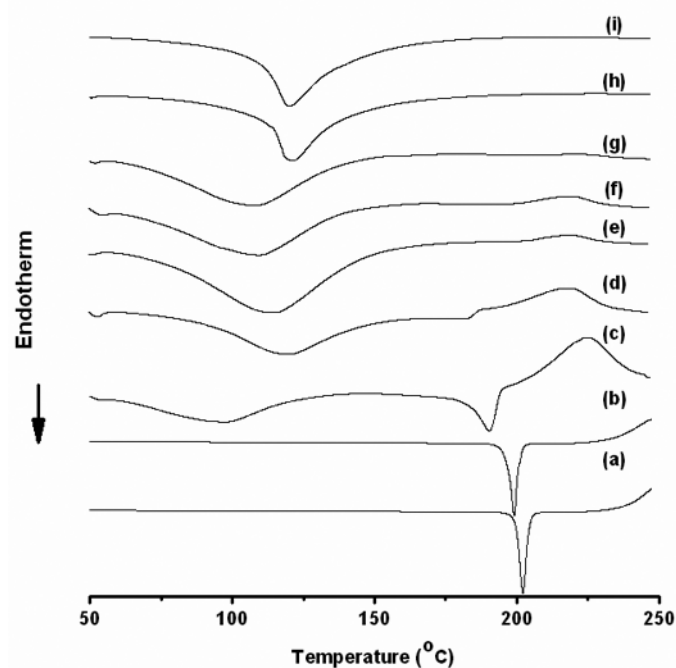


Figure A-6. DSC curves of piroxicam before (a) and after (b) DGA processing and DGA-processed solid dispersions with drug/polymer weight ratio of. (c) 2:1, (d) 1:1, (e) 1:2, (f) 1:4, (g) 1:9; PVP K25 before (h) and after (i) DGA processing.

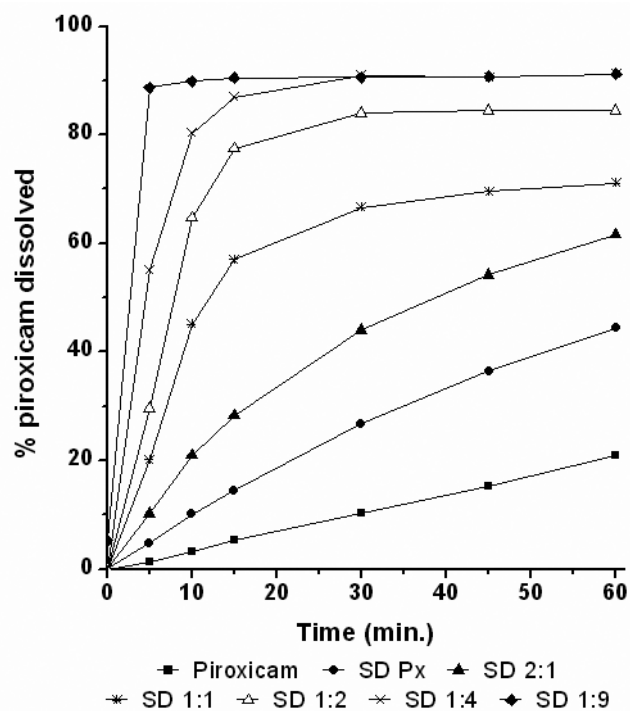


Figure A-7. Dissolution profiles of spray-dried solid dispersion systems. Ratio behind SD is the starting drug/polymer weight ratio.

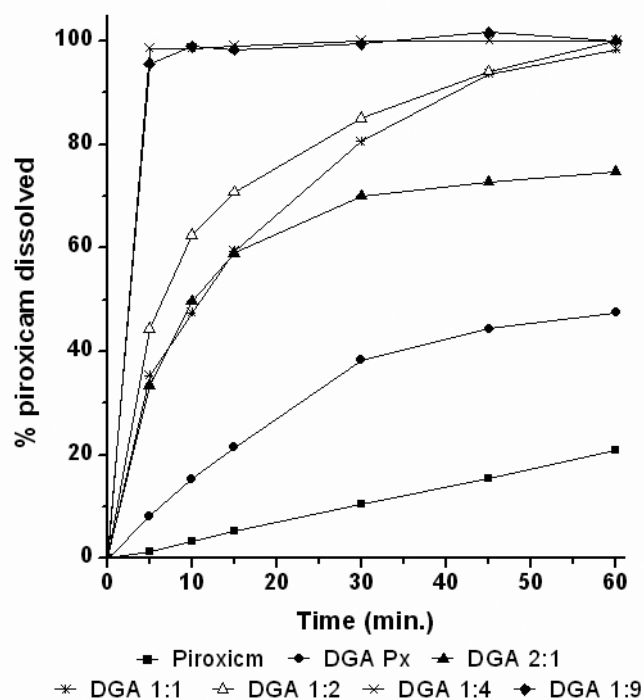


Figure A-8. Dissolution profiles of DGA prepared solid dispersion systems. Ratio behind DGA is the starting drug/polymer weight ratio.

## CURRICULUM VITAE

**Ke Wu**

### Education

Ph.D. in Inorganic Chemistry 2003~2008

Department of Chemistry and Chemical Biology, Rutgers University

Master of Science in Inorganic Chemistry 2002

College of Chemistry and Molecular Science, Wuhan University

Bachelor of Engineering in Fine Chemicals 1999

College of Chemistry and Environmental Science, Henan Normal University

---

### Experience

Graduate/Teaching Assistant 2003~2008

Department of Chemistry and Chemical Biology, Rutgers University

Intern 2007

Johnson & Johnson Pharm. Res. & Development, L.L.C.

Teaching Assistant 2002~2003

Department of Chemistry, Wayne State University

Research assistant 1999~2002

Infrared Materials Laboratory, Wuhan University

---

### Publications

"Formation and characterization of solid dispersions of piroxicam and polyvinylpyrrolidone using spray drying and precipitation with compressed antisolvent", Ke Wu, Jing Li, Wayne Wang, Denita A. Winstead, *J. Pharm. Sci.* (In press)

"Precipitation of a biodegradable polymer using compressed carbon dioxide as antisolvent", Ke Wu, Jing Li, *J. Supercrit. Fluids* **2008**, 46, 211-216.

"Multifunctional microporous MOFs exhibiting gas/hydrocarbon adsorption selectivity, separation capability and three-dimensional magnetic ordering", Kunhao Li, David H. Olson, Jeong Yong Lee, Wenhua Bi, Ke Wu, Tan Yuen, Qiang Xu, and Jing Li, *Advanced Functional Materials*, **2008**, 18, 2205-2214.

"Preliminary study of anti-Stokes fluorescence cooling in fluorozirconate fiber doped with Yb<sup>3+</sup>", Ke Wu, Jiacheng Zhong, Chuqing Gong, Xiao Zhou, Ling Zan, Ling Huang, Chengfang Li, *Wuhan Daxue Xuebao, Lixueban* **2001**, 47, (4), 453-455.